Electrophysiological and cellular analysis of filamin-C mutations causing cardiomyopathy using human iPSC-derived cardiomyocytes

Yaqob Samir A Taleb, M.S.

Clinical Science Research Department

Institute of Cardiovascular Science

University College London (UCL)

A thesis submitted to UCL in conformity with the requirements for the degree of Doctor of Philosophy

April 2023

Declaration

I, Yaqob Samir A Taleb, confirm that the work presented in this thesis is my own. Where information has been derived from other sources, I confirm that this has been indicated in the thesis.

Abstract

Background: Arrhythmogenic Cardiomyopathy (AC) is a genetic cardiac disease resulting from different mutations within proteins constituting the intercalated disc, including desmosomal and non-desmosomal proteins. Recent studies have revealed that mutations in filamin-C (FLNC) may lead to AC. The arrhythmogenesis and electrophysiological effects of FLNC-related AC are incompletely understood. Therefore, the aim of this study is to assess the potential electrophysiological consequences of FLNC loss as occurs in AC in human induced pluripotent stem cell-derived cardiomyocytes (hiPSC-CMs). Specifically, I aimed to characterise abnormal electrical activity and the expression and function of key proteins in cardiac electrical activity such as gap junction protein connexin 43 (Cx43).

Methods: hiPSC-CMs were differentiated and observed by immunofluorescence microscopy. Small interfering RNA (siRNA) transfection was utilised to knockdown the expression of FLNC in hiPSC-CMs. Protein analysis was performed using western blotting to confirm the knockdown efficiency. Electrophysiological properties were recorded using a multielectrode array and manual patch clamping. Optical recording of membrane potential and calcium activity from hiPSC-CMs were also carried out using parameter sensitive dyes.

Results: Silencing of FLNC led to markedly decreased immunofluorescence signals of FLNC, Cx43, desmoplakin, and junctional plakoglobin. No significant reductions were noted in the immunofluorescence signals of voltage-gated sodium channel (Nav1.5) and plakophilin-2 compared with control hiPSC-CMs. Western blotting showed the reduction of FLNC and Cx43 expression following silencing of FLNC. Knockdown of FLNC resulted in disturbances to the recorded action and field potential signals of hiPSC-CMs and arrhythmic like-events. Transfected hiPSC-CMs with siRNA-FLNC were associated with prolongation of calcium transient durations, optical action potential duration, and action potentials measured with patch clamping.

Conclusion: The current findings indicated that loss of FLNC resulted in a complex arrhythmogenic phenotype in hiPSC-CMs.

Impact statement

Human induced pluripotent stem cell-derived cardiomyocytes (hiPSC-CMs) can model inherited myocardial disorders such as arrhythmogenic cardiomyopathy, a leading genetic cause of sudden cardiac death. These cells offer an opportunity to study human heart physiology and pathophysiology at the cellular level, therefore providing a valuable tool to recapitulate the molecular and electrophysiological effects of cardiomyopathies. Studying the genes implicated in the development of arrhythmogenic cardiomyopathy, such as filamin-C, at a more fundamental level is necessary to translate these findings into the practice of precision medicine. This study reveals the potential for elucidating the mechanism of arrhythmogenesis by using a dish model of arrhythmogenic cardiomyopathy caused by filamin-C mutations.

Acknowledgments

education. Thanks for listening to my problems and providing perspective.

To my beloved children, Reem, Zobaidah, Salwa, and Yousef you are the best thing in my life. You provided the inspiration necessary for me to complete this process. Many thanks for tolerating daddy being away from you. I love you!

Table of Contents

List of tables

List of figures

13

Abbreviations

AC	Arrhythmogenic Cardiomyopathy
ALVC	Arrhythmogenic Left Ventricular Cardiomyopathy
AP	Action potential
APD	Action potential duration
ARVC	Arrhythmogenic Right Ventricular Cardiomyopathy
ARVD	Arrhythmogenic Right Ventricular Dysplasia
ATP	Adenosine triphosphate
AV	Atrioventricular
BMP4	Bone Morphogenic Protein 4
BSA	Bovine Serum Albumin
C-Myc	Cellular Myelocytomatosis oncogene transcription factor
CAD	Cellular arrhythmic depolarisations
CaMKII	Calmodulin-dependent protein kinase II
cAMP	Cyclic adenosine monophosphate
CaTD	Calcium transient duration
Cav1.2	L-type calcium channel
CCD	Charged coupled device
CICR	Calcium induced calcium release
CLSM	Confocal laser scanning microscope
CMR	Cardiac magnetic resonance
CRISPR-Cas9	Clustered regularly interspaced short palindromic repeats-associated protein 9
Cx43	Gap junctional protein connexin 43
DAD	Delayed afterdepolarisation
DAPI	4′,6-diamidino-2-phenylindole
DCM	Dilated cardiomyopathy

Di-4-ANEPPS	4-(2-(6-(Dibutylamino)-2-naphthalenyl)ethenyl)-1-(3 sulfopropyl)pyridinium hydroxide inner salt
DMEM	Dulbecco's Modified Eagle Medium
DMSO	Dimethyl Sulfoxide
DNA	Deoxyribonucleic Acid
DNAse II	Deoxyribonuclease II
DSC2	Desmocollin-2
DSG2	Desmoglein-2
DSP	Desmoplakin
dsRNA	Double stranded RNA
E4031	hERG channel blocker
EAD	Early afterdepolarisation
EC coupling	Excitation-contraction coupling
ECG	Electrocardiogram
ECL	Enhanced Chemiluminescence
EGFR	Epidermal growth factor receptor
EGTA	Ethylene glycol-bis(2-aminoethylether)-N,N,N',N'-tetraacetic acid
F-actin	Filamentous actin
FBS	Foetal Bovine Serum
FLNC	Filamin-C
Fluo-4 AM	Fluo-4 acetoxymethyl esters
FP	Field potential
FPD	Field potential duration
GAPDH	Glyceraldehyde-3-phosphate dehydrogenase
GHK	Goldman-Hodgkin Katz
GTP	Guanosine triphosphate
HBSS	Hank's balanced salt solution
HEPES	4-(2-hydroxyethyl)-1-piperazineethanesulphonic acid
hERG	Human Ether-a-go-go-related Gene

hESC	Human embryonic stem cell
hESC-CMs	Human embryonic stem cell-derived cardiomyocytes
hiPSC-CMs	Human induced Pluripotent Stem Cell-derived Cardiomyocytes
HRP	horseradish peroxidase
ICD	Implanted cardioverter defibrillator
IDs	Intercalated discs
IP3	Inositol triphosphate
iPSC	Induced Pluripotent Stem Cell
JUP	Junctional Plakoglobin
KLF4	Kruppel-like factor 4 transcription factor
KY02111	Wnt inhibitor
LI-BPEL	Low insulin, BSA, polyvinylalcohol, essential lipids
LIN-28	Lineage 28 transcription factor
LQT	Long QT interval
LV	Left Ventricular
MEA	Multielectrode array
MRI	Magnetic Resonance Imaging
mRNA	Messenger ribonucleic acid
Nav1.5	Voltage-Gated Sodium Channel
NCX1	Sodium-calcium exchanger
OCT3/4	Octamer-binding 3/4 transcription factor
Opti-MEM	Optimized minimal essential medium
PAGE	Polyacrylamide gel electrophoresis
PBS	Phosphate Buffer Saline
PKP2	Plakophilin-2
PLN	phospholamban
PMCA	plasma membrane calcium-ATPase
PMT	Photomultiplier tube
PSCs	Pluripotent Stem Cells

PVDF	Polyvinylidene difluoride
QRS	Ventricular depolarisation seen in the ECG
RISC	RNA-induced silencing complex
RMP	Resting membrane potential
ROCKi	Rho-associated protein kinase inhibitor
RPMI	Rosewell Park Memorial Institute medium
RV	Right Ventricular
RyRs	Ryanodine receptors
SA	Sinoatrial
SCD	Sudden cardiac death
sCMOS	Scientific complementary metal-oxide semiconductor
SDS	Sodium dodecyl sulfate
SERCA2a	Sarco-endoplasmic reticulum calcium-ATPase 2a
shRNA	Short hairpin RNA
siGLO	Fluorescent-labelled siRNA
siRNA	Small interfering ribonucleic acid
SOX2	SRY(sex determining region Y)-box 2 transcription factor
SR	Sarcoplasmic reticulum
T wave	Marker of ventricular repolarisation seen in the ECG
TBST	Tris buffered saline + tween
TGF-β	Transforming Growth Factor Beta
TryplE	Cell dissociated reagent
Vm	Membrane potential
Wnt	Wingless-related integration site (1)
XAV939	Wnt inhibitor

Chapter 1   : Introduction

1.1 *Arrhythmogenic Cardiomyopathy*

Arrhythmogenic Cardiomyopathy (AC) is a genetic cardiac disease, characterised by pathological damage of ventricular myocardium and fibrofatty replacement leading to a number of serious and potentially life-threatening conditions such as ventricular arrhythmias, systolic dysfunction, heart failure and sudden cardiac death (SCD). Although AC is originally described as right ventricular disease, there is now evidence that AC can be presented with both biventricular and left ventricular-dominant disease. This condition is rare and known to be heritable due to mutations in different genes that encode intercalated disc (ID) proteins (Figure 1. 1), including desmosomal and non-desmosomal proteins (2). Despite the high prevalence of desmosomal gene mutations in AC cases such as plakophilin-2, desmoglein-2, and desmoplakin (DSP), mutations of other cellular components in the ID have also been identified to cause AC. Titin, desmin, and filamin-c (FLNC) are considered as intracellular structural proteins and have been linked with AC (3). FLNC belongs to a family of filamins, and its expression occurs mainly in the skeletal and cardiac muscle. More importantly, FLNC plays a fundamental role in structural stability of the actin network as well as cell membrane interactions. To elaborate, FLNC binds to many proteins along the Z-

disc, which defines the lateral borders of the sarcomere, and therefore variants in FLNC have been reported with certain pathological conditions, including skeletal myopathies and cardiomyopathies ([4]). Currently, truncation and missense mutations in FLNC can be associated with the two forms of AC: Arrhythmogenic Right Ventricular Cardiomyopathy (ARVC) and Arrhythmogenic Left Ventricular Cardiomyopathy (ALVC). Prior preclinical investigations revealed that loss of desmosomal integrity causes a decrease in gap junction protein Cx43 and cardiac sodium channel Nav1.5, resulting in electrophysiological abnormalities. Indeed, ID function of Cx43 and Nav1.5 require intact desmosomes ([3], [5]). It is not yet completely understood whether the disruption of FLNC affects Cx43 and sodium channel expression and causes electrophysiological abnormalities in a cellular model.
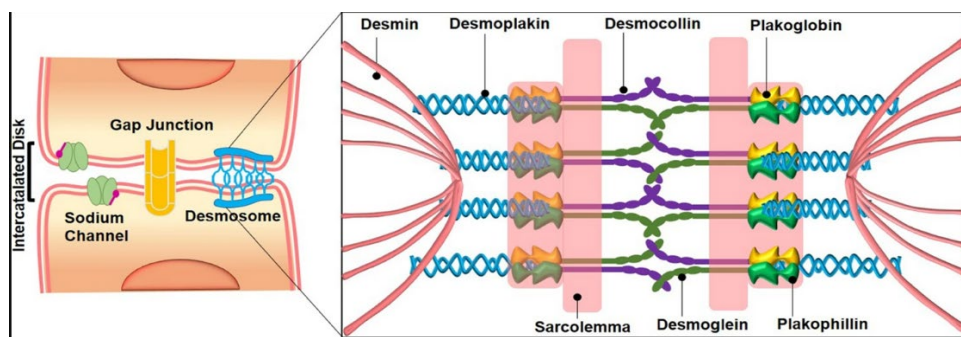
*Figure 1. 1: **structure of intercalated disc**, including desmosomal proteins. The desmosome composed mainly of plakoglobin, desmoplakin, plakophilin-2, desmoglein, and desmocollin. Desmoplakin connects the desmosome complex to the desmin filaments and the desmosomes work together with sodium channels and gap junctions to facilitate mechanical support and electrical coupling of cardiomyocytes. Figure obtained from Yen-Nien Lin et al ([6]).*

This study set out to understand the electrophysiological effects of FLNC-driven AC pathogenesis. To achieve this goal, differentiation protocols were conducted to produce cardiomyocytes from induced pluripotent stem cells (iPSCs). Despite the availability of other human sources to model cardiac disease, for example fresh isolation of human ventricular cardiomyocytes, these are difficult to obtain and often diseased. Perhaps the most serious disadvantage of this method is the limited access of enzymes to isolated cardiomyocytes during cardiac surgery, and low cell yield as well as the risk of hypoxia ([7-9](#)). Thereby the notion of using hiPSC-CMs is frequently considered the most utilisable tool in terms of drug screening and disease modelling. Indeed, these cells offer substantial promise as an alternative to animal models with regard to disease modelling, specifically arrhythmic disorders caused by mutations in ion channel-related proteins, structural and modulatory proteins ([10](#)).

1.1.1 *Aetiology of Arrhythmogenic Cardiomyopathy*

AC can result from different causes, including: genetic, systemic, infectious, and inflammatory disorders. The underlying aetiology of AC in most cases is due to genetic mutations within the ID components, very commonly in the five desmosomal genes DSP, junctional

plakoglobin, desmoglein-2, plakophilin-2, and desmocollin-2 ([11]). However, it is becoming clear that non-desmosomal protein mutations have also been associated with AC, which comprises adherens junction proteins, cytoskeleton proteins, ion transport proteins, calcium-handling proteins, and cytokine signalling proteins ([3], [12]).

1.1.2 *Epidemiology of Arrhythmogenic Cardiomyopathy*

The estimated prevalence rate of AC is approximately 1 in 2000 to 1 in 5000, depending on regional incidence ([13]). For example, it has been reported that the population prevalence of AC in Italy and Germany is higher and estimated to affect around 1:2000 people ([2]). Another important point is that particular gene mutations of AC have been found frequently in specific nations such as junctional plakoglobin in Greece, phospholamban in the Netherlands, and transmembrane protein 43 in Newfoundland and Canada ([14]).

1.1.3 *Pathogenic and Genetic Mechanisms in AC*

In most AC cases, the pattern of inheritance is an autosomal dominant ([15]) and the fibrofatty replacement of cardiomyocytes is the histopathological hallmark ([16]). Originally, AC was known as

arrhythmogenic right ventricular dysplasia (ARVD) because it was thought to be a congenital defect due to abnormal development of the RV. Later, it was discovered to result from a gene mutation in the desmosome and classified as a cardiomyopathy ([15](#)). However, due to the presence of fibrofatty replacement not only in RV but also LV, or biventricular myocardium, it has now been renamed as AC ([2](#)). Furthermore, recent studies suggested a significant contribution of inflammation to AC pathogenesis and it can be either as active driver or as modulator of the disease phenotype ([17](#)). Apoptosis and adipogenesis are all known to be involved in AC pathology as well ([3](#)). The majority of AC patients have desmosomal gene mutations with varying frequencies. For example, in plakophilin-2 (20-46%), desmoglein-2 (3-20%), DSP (3-15%), desmocollin-2 (1-15%), and junctional plakoglobin (0-1%). Nevertheless, non-desmosomal mutations have also been associated with AC and emerged in various proteins such as αT catenin (0-2%), cadherin-2 (0-2%), Phospholamban (0-4%), Transmembrane Protein 43 (0-2%), Nav1.5 (2%), lamin A/C (0-4%), desmin (0-2%), titin (0-10%), and (FLNC; 0-3%) ([12](#), [14](#)). While these mutations are rare, efforts are needed to understand their pathological roles and mechanisms in AC.

1.1.4 *Diagnosis of Arrhythmogenic Cardiomyopathy*

AC can be diagnosed by using the appropriate clinical tests outlined by a Task Force Criteria in 1994, which was then updated in 2010. The criteria encompass multiple factors such as tissue characterisation, structure/function assessment, ventricular arrhythmias, repolarisation and/or depolarisation ECG abnormalities, as well as family history. In 2020, however, the new Padua criteria were proposed by Corrado et al ([18]), suggesting a modification in the original ARVC diagnostic criteria to include the left-sided AC phenotype. Yet the diagnostic challenges reported by clinicians still exist, such as variable disease expression and incomplete penetrance among individuals. Recently, considerable advances have been made in the improvement of risk stratification by developing prediction models for ventricular arrhythmias caused by different genetic variants, and hence aid to subclassifying AC patients into phenotypic groups ([5], [11]).

1.1.5 *Treatment of Arrhythmogenic Cardiomyopathy*

Clinical management of AC are focused on symptomatic relief as well as preventing disease progression and SCD since there is currently no cure for this disease. Treatment consists of primarily placement of

an implanted cardioverter-defibrillator (ICD), and prescribing some medications, particularly beta-blockers and antiarrhythmic drugs (sotalol and amiodarone), which are effective in reducing lethal tachyarrhythmias. In severe cases, for example sustained monomorphic ventricular tachycardia, catheter ablation may be used when patients are intolerant or the medications are ineffective. In selected patients who have lethal arrhythmias and advanced heart failure due to cardiomyopathy, heart transplantation may be needed (5, 11, 19, 20).

1.2 *Electrical activity of the heart*

1.2.1 <u>*Overview of cardiac electrophysiology*</u>

The electrical signal of the heart in healthy individuals initiates in specialised cells (Sinoatrial (SA) node) located in the right atrium that depolarise in a spontaneous manner. This signal subsequently propagates throughout the entire heart from cell to cell with each cell exhibiting an action potential (AP). Thus, the AP spreads through conducting pathways and in the atria and ventricle causes contraction. The APs are categorised based on the upstroke speed into slow AP, originating from sinoatrial and atrioventricular (AV) nodes, and fast AP in atrial myocytes, Purkinje fibers, and ventricular myocytes. The cells in SA node have intrinsic pacemaker activity and are able to depolarise spontaneously. At rest, these cells generate action potentials at a regular pace with intrinsic rate of approximately 70 beat per minute. The pacemaker activity can be regulated by sympathetic and parasympathetic responses. The resting membrane potential of SA node cells is approximately -60 mV. Nevertheless, the cells undergo spontaneous depolarisation as consequence of inward and outward current movements. In general, both Na^+ and Ca^{+2} are inward currents while outward activity carried by K^+ current. Upon reaching to threshold,

the firing of AP occurs due to Nav1.5 that activates opening of L-type (T-type may also be contributed) Ca^{2+} channels. Conversely, closing of Ca^{2+} channels and high K^+ conductance causes repolarisation and that the pacemaker cycle is fully completed. The impulse then reaches the AV node cells in the atrial septum. The importance of AP in the heart is that during excitation contraction coupling, in which the propagation of AP must be timed to synchronised ventricular contraction in order to eject the blood effectively ([21]).

1.2.2 *Cardiac ion channels*

The myocardial cell membrane, known as sarcolemma, consists of phospholipids that, by itself, acts as barrier and is highly impermeable to ions. In addition, the sarcolemma is composed of specialised integral membrane proteins, including ion channels, passive cotransporters, and active transporters. These are important to accommodate multiple cellular functions, particularly maintaining the ion concentration gradients and distribution of charges between the inside and outside of the myocardial cells. Normally, the concentrations of sodium and calcium are greater outside the cell, whilst the potassium concentration is much higher inside the cell. Specific ions can across the sarcolemma and constitute the basis of cardiac action potential ([22]). These ions must

pass through specific channels in order to generate the electrical signal in the heart.

Many cardiac ion channels are voltage-gated channel; in which their gates open or close depending on the alterations in membrane potential. As soon as the cell reaches threshold potential, activation gates of Na^+ channels are open to permit the influx of Na^+ across the membrane, causing the upstroke of the AP and then inactivation gates close the sodium channels to end the upstroke. The sodium channel is inactivated until the end of repolarisation underpinned by the opening of potassium channels when the cell returns to the resting membrane potential. Of note, action potentials vary between different regions of the heart in terms of resting membrane potential, AP peak, and AP duration, as these determined by the number and type of ion channels ([23]). The importance of these ion channels is elucidated below with particular stress on ventricular electrical activity in the myocardium.

1.2.2.1   *Voltage-gated sodium channels (Nav1.5)*

Nav1.5 channel has unique physiological functions upon activation since it facilitates the rapid rise of action potential. There are several voltage-gated Na^+ channels that have been expressed in

cardiomyocytes though they cannot compensate for the important physiological role of Nav1.5 in the myocardium. Recent studies have revealed that Nav1.5 resides in distinct complexes at two different subcellular domains of the cardiomyocyte, one localised at the lateral membrane with the dystrophin/syntrophin complex, and the other is locating at the IDs, specifically with the MAGUK protein SAP97. In addition, Nav1.5 can be associated with other regulatory proteins at the IDs that are involved in stabilisation and targeting (Ankyrin-G), electrical coupling (Cx43), and cell adhesion (Plakophilin-2). These Nav1.5 channels consist of a primary alpha subunits that may interact with auxiliary beta subunits as well. The expression of alpha and beta subunits was studied in the heart tissue and identified Nav1.1α, Nav1.5α, β1, and β2. Other group of researchers identified the existence of Nav1.3 and Nav1.6 in cardiomyocytes. Although the α subunit was found to be associated with both β1 and β2, only β1 subunit has shown a modulatory effect on electrophysiological characteristics of Nav1.5 (24). The alpha-subunit of Nav1.5 forms an ion-conducting pore and voltage-dependent gating. It consists of an intracellular N-terminus and C-terminus as well as four homologous domains (DI-DIV), with each domain containing six transmembrane segments (S1-S6). The distinct cytoplasmic linker region between segments 5 and 6 of all four domains

forms the P segment channel pore, which regulates the selectivity and permeation of ions ([24-26](#)). Positively charged residues on S4 segments serve as voltage sensors to increase channel permeability, resulting in rapid activation of the Na^+ channel when membrane potential (Vm) is depolarised. The voltage gated Na^+ channel is characterised by activation and inactivation gates that determine whether the channel is open or closed, with each state corresponding to a different transmembrane protein conformation ([21](#)). In the resting membrane (phase 4), most ion channels (but not all) are in a closed state and even if the inactivation gate is open, sodium ions cannot pass through due to the closure of the activation gate. However, as soon as Vm is rapidly depolarised (phase 0), the membrane voltage becomes less negative, leading to the opening of both activation and inactivation gates and the entry of Na^+ ions. The slow inactivation that occurs over hundreds of milliseconds has been attributed to the late sodium current (I_{NaLate}), which represent a sustained depolarising current during phase 2, therefore play a key role to maintain the relatively long plateau of the AP ([25](#)). Given the spontaneous closure of the inactivation gate, the Na^+ current ceases and the channel cannot reopen directly from this inactive state due to the conformational change that maintains a closed pore, thereby preventing any flow of sodium ions. On the other hand, when

membrane voltages return to a high negative level during cellular repolarisation (phase 3), the channels recover from the inactivated to the closed resting state. Resting potential of most cells is negative to zero because more K^+ channels are open than Na^+ channels at rest ([22]). Overall, Nav1.5 is the essential channel due to the capability to initiate the cardiac action potential as well as the subsequent propagation throughout the heart ([24], [27], [28]). However, mutations that disrupt Nav1.5 function are known to be associated with life-threating arrhythmias in the heart such as familial atrial fibrillation, Brugada syndrome, cardiac conduction diseases, long QT syndrome (LQT3), arrhythmogenic and dilated cardiomyopathy ([24], [26]).

1.2.2.2 *Voltage-gated calcium channel*

Through voltage-gated L-type calcium channels, calcium enters the cardiomyocyte and plays a central role in myocardial contractility. In principle, voltage-gated calcium channels are vitally important in signal transduction of electrical excitability, which in turns link membrane depolarisation to intracellular Ca^{2+} transients ([29]). The calcium channels may be classified on the basis of their current type into L-type, T-type, N-type, P/Q-type, and R-type ([30]). Among these types, only L-type (long

lasting) and T-type (transient-type) calcium channels are involved in cardiac function. L-type calcium channel (Cav1.2) is highly expressed and has an important physiological role in the heart during excitation-contraction coupling and in the plateau phase of the action potential as well. L-type calcium channel conducts current through the pore forming alpha 1 subunit encoded by CACNA1C gene, and it can co-assembles with the extracellular alpha 2 and intracellular beta 2 subunits in cardiac tissue that modulate kinetics, gating and trafficking properties of the channel. Inward current of L-type calcium channel has a rapid activation and is specifically essential for excitation contraction coupling, since it acts as a trigger for the calcium-induced calcium release from the sarcoplasmic reticulum. The inactivation kinetics of L-type calcium current are depending on both Vm and intracellular calcium concentration, which is dynamically changing during the action potential. The recovery from inactivation is complex and mainly depends on voltage. In addition, L-type calcium current can be modulated by cAMP dependent phosphorylation and other factors, such as intracellular levels of calcium. Also, Calmodulin has been shown to support both inactivation and facilitation of L-type calcium current ([25], [31]). Genetic mutations of this channel have been found to associate with

two forms of cardiac channelopathies: Timothy syndrome (LQT8), and a form of Brugada syndrome ([21]).

1.2.2.3 *Potassium channel*

Potassium channels in the heart are divided into three categories: voltage-gated channels, inward rectifier channels, and the background currents ([31]). With regard to voltage-gated ion channels, potassium channels are considered the largest and most diverse family and there are at least 79 distinct genes in the humans ([21]). These potassium channels consist of both α-subunits and accessory β-subunits, which essentially regulate the transform in the cardiac AP configuration in response to changes in heart rate. Mutations in cardiac K^+ channels are linked to several forms of long QT syndrome and short QT syndrome as well as atrial fibrillation ([21], [22]). The table below is adapted from previous studies ([21], [25], [31], [32]), and summarises the genes encoding the K^+ channel subunits (primarily α-subunits) which compose the cardiac membrane currents that are voltage gated and time dependent:

Current	Description	AP phase	Activation mechanism	Channel protein/Gene	Common cardiac disorders
$I_{to, f}$	Transient outward current, fast	Phase 1	Voltage repolarisation	K_V4.2/KCND2 K_V4.3/KCND3/KCNIP2	Heart failure
$I_{to, s}$	Transient outward current, slow	Phase 1	Voltage, repolarisation	K_V1.4/KCNA4 K_V1.7/KCNA7 K_V3.4/KCNC4	Heart failure
I_{kur}	Delayed rectifier, ultrarapid	Phase 1	Voltage, repolarisation	K_V1.5/KCNA5 K_V3.1/KCNC1	Atrial fibrillation
I_{Kr}	Delayed rectifier, fast	Phase 3	Voltage, repolarisation	K_V11.1(HERG)/KCNH2 KCNE2	LQT2, short QT1 LQT6
I_{Ks}	Delayed rectifier, slow	Phase 3	Voltage, repolarisation	K_V7.1(KVLQT1)/KCNQ1 KCNE1	LQT1, short QT2, familial atrial fibrillation LQT5
I_{K1}	Inward rectifier	Phase 3 & 4	Voltage, repolarisation	Kir2.1/KCNJ2 Kir2.2/KCNJ12	LQT7, Short QT3
I_{KATP}	ADP activated K+ current	Phase 1 & 2	[ADP] / [ATP] ↑	Kir6.2/KCNJ11	Myocardial ischemia
I_{KAch}	Muscarinic-gated K+ current	Phase 4	Acetylcholine	Kir3.1/KCNJ3 Kir3.4(GIRK4)/KCNJ5	LQT13
I_{KP}	Background current	All phases	Metabolism, stretch	TWK1/KCNK1 TWK2/KCNK6 TASK1/KCNK3 TRAAK/KCNK4	hypokalaemia (33) Atrial fibrillation

1.2.3 *The human cardiac ventricular action potential*

In brief, the cardiac ventricular action potential is divided into five phases (Figure 1. 2). Phase 0 is the rapid depolarisation triggered by sodium influx and represented by the upstroke velocity. Phase 1 is characterised by a brief current repolarisation carried by the outward potassium current. Phase 2 is relying on the balance of inward of calcium and potentially sodium currents versus outward potassium current, therefore causing a plateau phase. During this plateau phase, L-type calcium channels located in the t-tubules start opening and lead to calcium influx through this channel, resulting in activation the nearby ryanodine receptor (RyR2) within dyadic clefts. Consequently, this calcium entry triggers the release of even more calcium from the sarcoplasmic reticulum (SR) in a complex process called Ca^{2+}-induced Ca^{2+} release (CICR) detailed in the section below 1.2.4. Phase 3 is a repolarisation phase where the delayed rectifier or slow K^+ channels open, causing K^+ conductance to predominates while Ca^{2+} conductance decreases due to closing of L-type Ca^{2+} channels, leading to a large outward K^+ current, which in turns allow the membrane potential to return toward diastolic levels. Phase 4 is a resting membrane potential and the ion concentrations that were changed by the firing action potential are restored to resting levels by the sodium-potassium

ATPase, sodium-calcium exchanger, and ATP-dependent Ca^{2+} pump

(10, 21, 23, 25).
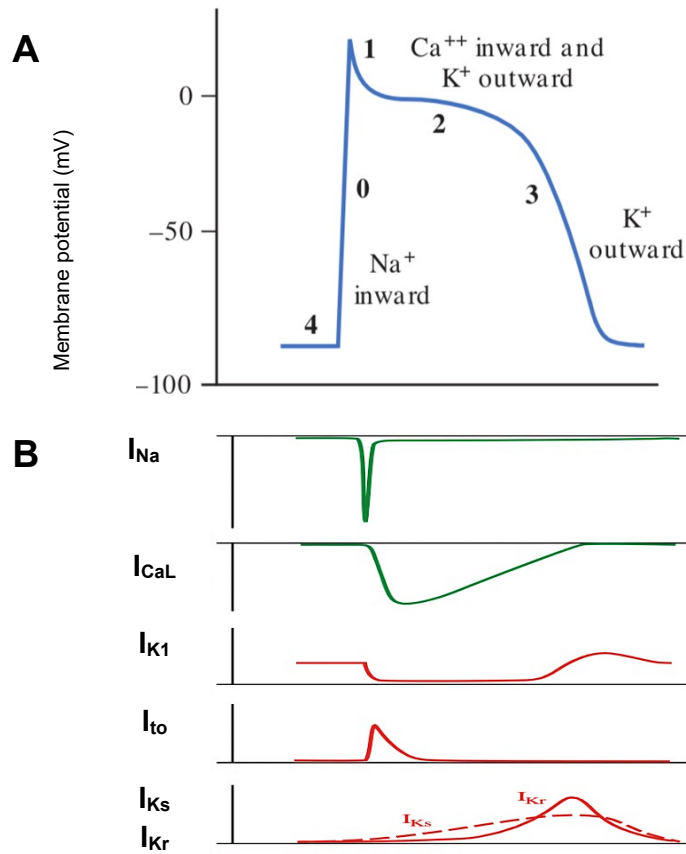
*Figure 1. 2. **Action potential profile (A) and representative ionic currents (B)**. In ventricular myocytes, the AP profile is influenced by opening and closing gates of specific ion channels that governed by time and voltage-dependent amplitudes ([10]).The rapid phase 0 that produces fast conduction of the wave of depolarisation occurs when the cells reach threshold and Nav1.5 channels (I_{Na} / SCN5A) open, leading to a decreased in potassium conductance. Phase 1 is rapid repolarisation to the plateau caused by inactivation of sodium channels and simultaneously opening of voltage-sensitive K^+ channels (I_{to} / KCND3), causing a transient outward potassium current. Phase 2 is plateau generated by fine balance of inward current of calcium ($I_{Ca,L}$ / CACNA1C) and slow outward current of potassium. Eventually $I_{Ca,L}$ become inactivated and in Phase 3 the activation of potassium channels occurs, producing mainly slow and rapid repolarisation due to outward current of potassium (I_{Ks} / KCNQ1 and I_{Kr} / KCNH2). Phase 4 is the resting membrane potential (I_{K1} / KCNJ2), where ion concentrations that were altered by AP firing are returned to resting levels by the sodium-potassium ATPase, sodium-calcium exchanger, and ATP-dependent calcium pump ([23], [34]). Figures taken from Leonard S. Lilly ([34]).*

1.2.4 *Role of calcium in cardiomyocytes*

During the cardiac ventricular action potential, under normal conditions, the concentration of sodium and potassium are maintained hence high potassium inside the cell and low potassium outside and high sodium outside the cell and low sodium inside the cell (Figure 1. 3). To elaborate, sodium is moving inside the cell during depolarisation whilst potassium current is moving outward to drive repolarisation. These cellular ion gradients are maintained due to presence of specific pumps and exchangers. For example, the Na^+-K^+ pump is essential to maintain the membrane potential, where it moves 3 Na^+ ions outside the cell for every 2 K^+ inside, and that requires ATP energy due to moving these ions against their concentration gradient, and therefore the charge transfer becomes more positive outside as well ([34]). Acting in the opposite direction, NCX1 transports 3 Na^+ ions into the cytoplasm in exchange for 1 Ca^{2+} extruded out. NCX1 is therefore one of the main mechanisms of Na^+ influx in cardiac cells ([35]). More importantly, calcium contributes to regulation of ventricular cardiomyocytes function via voltage-gated calcium channel, calcium pumps/transporters as well as activation of ryanodine receptors (RyR2 in the heart) ([36]).
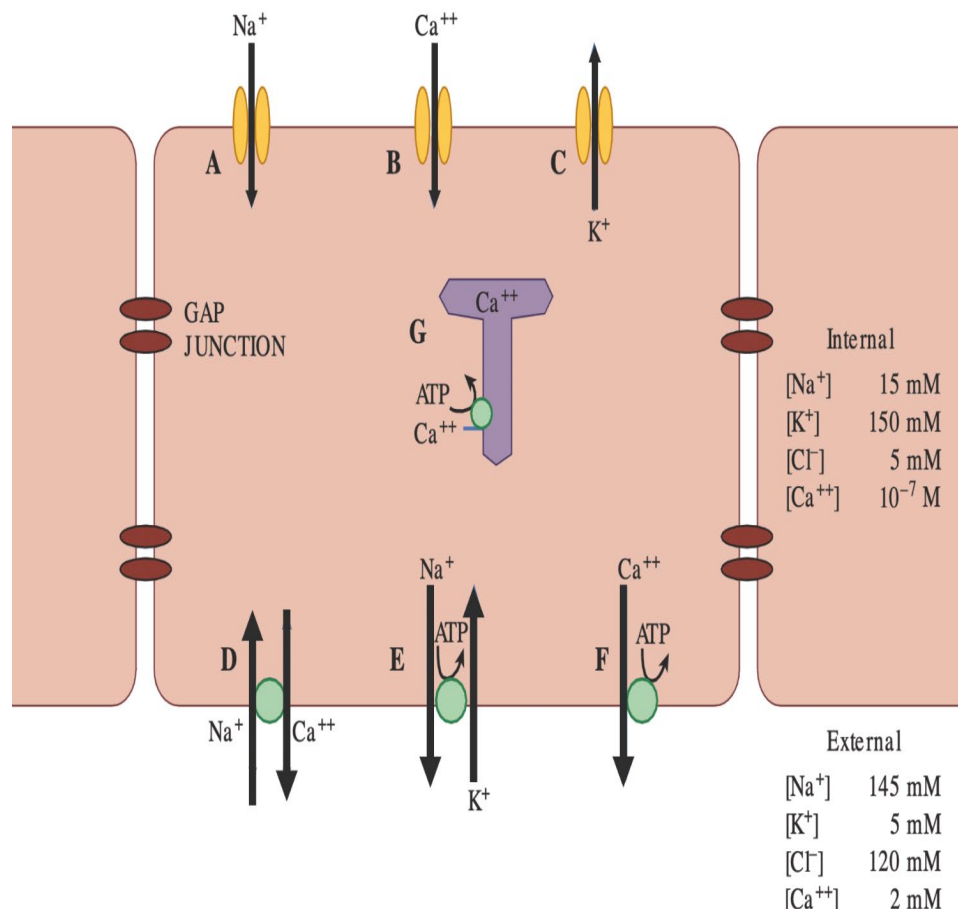
*Figure 1. 3: **Ion channels and ion transporters of the cardiomyocytes**. Figure obtained from Leonard S. Lilly ([34](#)). (A) sodium entry through the fast Na⁺ channel is responsible for phase 0 of the cardiac ventricular action potential. (B) Ca²⁺ enters the cell via L-type Ca²⁺ channel during phase 2. (C) K⁺ exits via different K⁺ Channels to repolarise the cell. Opening K⁺ channels contribute to the resting potential (Phase 4). (D) Na⁺-Ca²⁺ exchanger (NCX1) transports Ca²⁺ from low intracellular concentration to high extracellular concentration in order to maintain the low intracellular Ca²⁺ concentration. This achieved by moving 3 Na⁺ ions into the cell and extruding one Ca²⁺ ion, using electrochemical gradient for Na⁺ as an energy source for transport, hence NCX produces an inward or depolarising current. (E) Na⁺-K⁺pump maintains concentration gradients for these ions by moving 2 K⁺ ions into the cell for every 3 Na⁺ ions that it transports out of the cell, using ATP as an energy source. Therefore, this pump produces an outward or hyperpolarising current ([21](#)). (F) & (G) Active Ca²⁺ transporters help removal of Ca²⁺ to the external environment and into the sarcoplasmic reticulum, respectively.*

Calcium is a key player that links excitation to contraction. Indeed, cardiac contraction is generated by a transient surge in intracellular Ca^{2+} concentration induced by depolarisation of the membrane potential in a process known as excitation-contraction coupling (EC coupling). During the cardiac ventricular AP, the propagation spreads along the T-tubules and the membrane depolarisation causes the L-type calcium channel in the cell membrane to open, allowing calcium influx into the dyadic space, which separates the sarcolemma from the closely apposed (~15 nm) junctional SR in ventricular cardiomyocytes (Figure 1. 4). Significant calcium release events from the junctional SR (called Ca^{2+} spark that can be monitored with Ca^{2+}sensitive dye by fluorescence microscopy) are triggered by extracellular influx of calcium, leading to a substantial increase in local $[Ca^{2+}]_i$ and activation of a cluster of RyR2. This process is known as calcium-induced calcium release (CICR). Thus, during cardiac systole, the temporal summation of these local events by the propagating AP produces a regenerative calcium transient, which can be detected by troponin C to induce the sliding of the myosin-actin filaments, cell shortening, and thus an increase in intraventricular pressure and blood ejection. When the heart's chambers begin to refill with blood during diastole, the $[Ca^{2+}]_i$ must fall and mechanical force relaxes rapidly to resting diastolic levels. The myocardial relaxation

occurs when the cytosolic calcium is either extruded across the sarcolemma by Na^+/Ca^{2+} exchanger (NCX1) and plasma membrane calcium-ATPase (PMCA) or sequestered into the SR by a pump called sarco-endoplasmic reticulum calcium-ATPase 2a (SERCA2a). Depending on the phosphorylation state, phospholamban is a key regulator that can either increase or decrease the pumping rate of SERCA2a, hence controlling the Ca^{2+} affinity. For example, during unphosphorylated state, phospholamban binds to SERCA2a and halts the pump's ability to transport Ca^{2+} by decreasing its apparent affinity for Ca^{2+}. On the other hand, when phospholamban is phosphorylated, it relieves the inhibition of SERCA2a, thus enhancing the pump's affinity for Ca^{2+} and promoting relaxation. It is noteworthy that when multiple L-type calcium channels in ventricular cardiomyocytes open simultaneously, the resulting global increase in $[Ca^{2+}]_i$ is a consequence of the spatial and temporal summation of many Ca^{2+} sparks. Given this a global rise in $[Ca^{2+}]_i$ of ventricular cardiomyocytes has a longer duration than the action potential due to the fact that RYR Ca^{2+} release channels remain open for longer periods of time than L-type calcium channels (blue curve below). Because an increase in $[Ca^{2+}]_i$ can initiate the process of cross-bridge cycling, thick filaments slide through thin filaments, resulting in cardiac tension (red curve below). The

42

development of cardiac tension occurs more slowly than the global rise in intracellular Ca^{2+} concentration (Figure 1. 3). There are four mechanisms of Ca^{2+} removal from the cytoplasm: (1) NCX1 and PMCA in the sarcolemma both extrude Ca^{2+} from the cell, (2) SERCA2a pump sequesters Ca^{2+} into SR, (3) uptake of Ca^{2+} from the cytosol into mitochondria, and (4) Ca^{2+} dissociates from troponin C, preventing actin-myosin interaction and causing relaxation of the myocardium ([21], [36-38]).
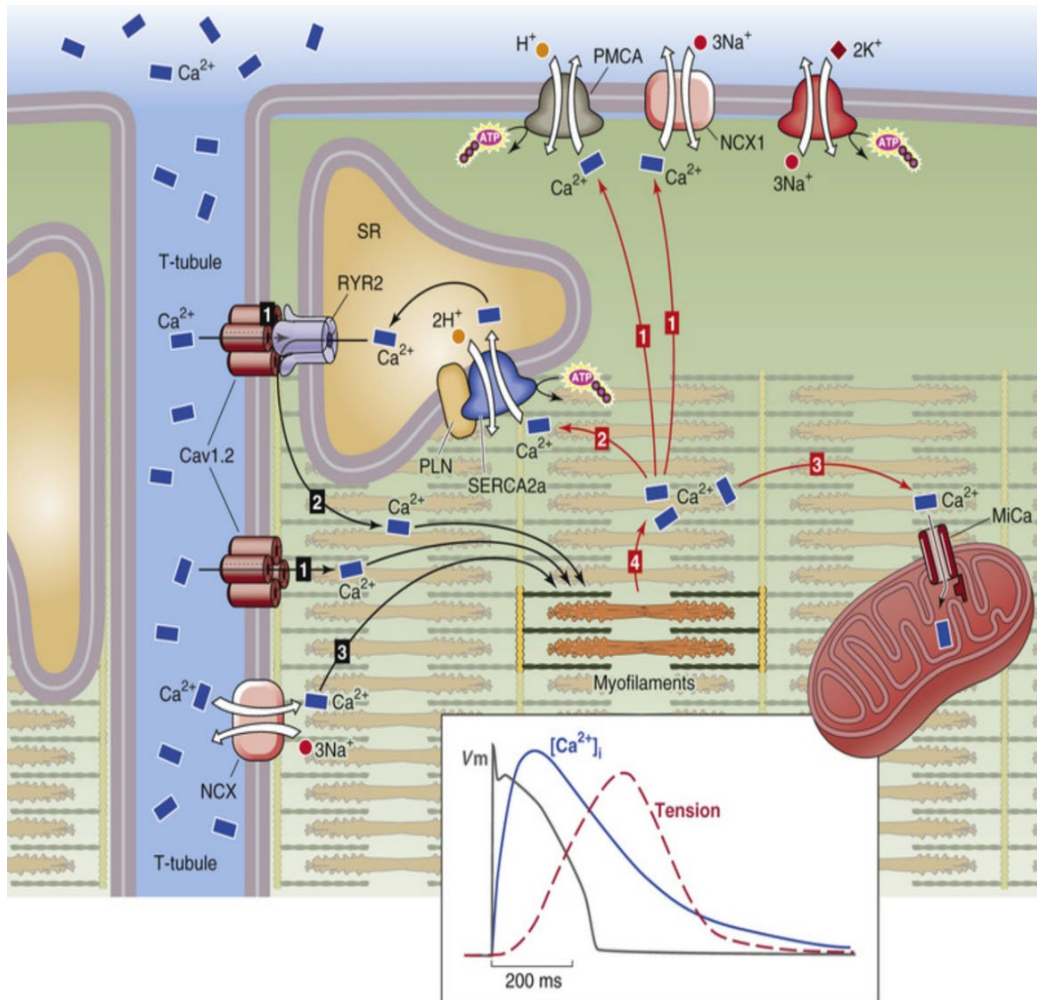
Figure 1. 4. **Role of calcium in myocardial contraction of ventricular cardiomyocytes**. *Membrane depolarisation opens Cav1.2 channels in the cell membrane leading to entry of Ca^{2+} through it, causing an increase in $[Ca^{2+}]_i$ in the vicinity of the RYR2 on the SR. As a result, Ca^{2+} simultaneously activates a neighbouring cluster of RYRs, producing more release of local Ca^{2+} into the cytoplasm. CICR is a robust amplification system whereby the local influx of Ca^{2+} from small clusters of Cav1.2 in the sarcolemma triggers the corresponding release of Ca^{2+} from stores in the SR. Reverse NCX activated by sodium currents may be involved in triggering Ca^{2+} release, although with a small amount of Ca^{2+}, during the initial part of the AP (39). Thus, a global increase in $[Ca^{2+}]_i$ initiates contraction of myocardial cells due to binding of Ca^{2+} with the myofilaments, allowing cross-bridge formation and contraction (1-3 black arrows denote the contraction steps). Ca^{2+} is extruded from the cell via the NCX1 and to a lesser extent via the PMCA or taken up by the SR via SERCA2a. Phosphorylation of PLN accelerates myocardium relaxation. Consequently, fall in $[Ca^{2+}]_i$ leads to unbinding from myofilaments and promote relaxation. (1-4 red arrows denote the relaxation steps). Cav1.2, L-type Calcium channels; RYR2, ryanodine receptor/calcium release channel; SR, sarcoplasmic reticulum; PLN, phospholamban; NCX1, Na^+/Ca^{2+} exchanger; PMCA, Ca^{2+} ATPase; SERCA2a, sarco-endoplasmic reticulum Ca^{2+} ATPase 2a; H^+ protons; MiCa, mitochondrial Ca^{2+} channels. Figure obtained from Boron and Boulpaep (21).*

44

1.2.4.1 *Calcium-mediated signalling cascades in cardiac cells*

Beside its role in EC coupling, different calcium-dependent signalling pathways can be activated during disease and participate in cardiac arrhythmogenesis, including calpain, protein kinase C (PKC), Ca^{2+}/Calmodulin-dependent protein kinase II (CaMKII), and calcineurin/ NFAT signalling pathway. Calpain is involved in the calcium dependent regulation of many different cellular processes. Dysregulation of calpain resulted from calcium handling abnormalities during heart diseases such as, atrial fibrillation, heart failure, or hypertrophy can have a severe effect on cellular function. The PKC signalling pathway is a major target of calpain. PKCs have been involved in cardiac arrhythmias because of their role in the electrical remodelling of the heart. For example, downregulation of PKC could contribute to increase activity of the acetylcholine-activated inward-rectifier potassium current, which shorten the APD and hyperpolarise the resting membrane potential, leading to re-entry and atrial fibrillation promotion. Also, increased PKC-mediated phosphorylation of TnT and TnI were observed during heart failure, which alters the myofilament calcium sensitivity. CaMKII activation is one of the major calcium regulations during heart disease. For example, sympathetic stimulation enhances CaMKII activation via fast heart rate, increased $[Ca^{2+}]i$, and regulation of exchange-protein

activated by cAMP. Active CaMKII can regulates many key components in calcium handing of heart cells, such as RyR2, L-type calcium channel, SERCA2a, and phospholamban. In addition, CaMKII plays a key role in myocardial contraction (through the phosphorylation of myosin binding protein-C and titin), intracellular trafficking, hypertrophy, inflammation, and other mechanisms. The proarrhythmic events associated with CaMKII hyperactivity have been shown in different experimental model. For instance, CaMKII-mediated phosphorylation of Nav1.5 increases late Na current, and causes prolongation of the APD, resulting in calcium handling abnormalities and DADs (40).

1.2.5 *Cellular arrhythmias- Early and Delayed Afterdepolarisation (EAD and DAD) and re-entry*

Cardiac arrhythmias are generally classified as abnormal impulse formation, including early after-depolarisation (EAD), and delayed after-depolarisation (DAD), and abnormal conduction facilitated by re-entry ([41](#)). Under certain conditions, the ventricular AP can originate a triggered activity of abnormal depolarisations that result in a spontaneous abnormal beat or series of beats. High concentrations of intracellular sodium can lead to increases in intracellular calcium concentration via NCX1, therefore provoking arrhythmogenic triggered activity such as EAD and DAD. EAD is characterised by additional depolarisation occurring prior to the end of the preceding AP during the plateau of phase 2 or phase 3 repolarisation. EADs are typically generated when the action potential duration (APD) is abnormally prolonged at relatively slow rates. Consequently, L-type calcium channels which have recovered from inactivation and are now able to reopen, and some of the Ca^{2+} channels carry a calcium window current, generating positive voltage oscillation in membrane potential (Figure 1. 4) during phase 2 and phase 3 ([25](#)). EADs are more likely to develop with certain pathologies or medications that cause calcium loading or reduction in K^+ currents or increasing the late Na^+ current. For example,

ventricular hypertrophy, heart failure, and drugs like β-adrenergic agonist are predisposing factors for the development of EADs ([42]). Nevertheless, EADs can also be triggered by CaMKII phosphorylation which decreases the inactivation time of L-type calcium channels, thereby accelerating the recovery from inactivation and potentially leading to EAD events. Another example of EAD formation is due to activation of NCX current and therefore generating membrane depolarisation caused by an increase in Ca^{2+} transients resulting from elevated $[Ca^{2+}]_i$ whilst Vm is negative to the equilibrium potential for NCX1([38]). On the other hand, DADs are abnormal changes of the V_m that occur after full repolarisation (Figure 1. 5). DAD is likely generated by calcium-sensitive depolarising currents when spontaneous calcium is released from the SR during calcium overload, or CaMKII phosphorylation. DADs are usually induced at fast rates and have been associated with different forms of heart disease such as chronic atrial fibrillation, catecholaminergic polymorphic ventricular tachycardia, heart failure, ischemia or drugs like digitalis. It is now understood that calcium-sensitive current (most commonly NCX) or calcium-sensitive chloride current play an important role in DAD formation ([25]). For example, during diastole, the events of spontaneous Ca^{2+} sparks, which are able to combine to form a sub-sarcolemmal Ca^{2+} wave and cleared by NCX1,

can rise in response to an increase in SR Ca^{2+} leakage. This causes a depolarising (3 Na^+ moving inside: 1 Ca^{2+} moving outside) inward current to flow into the myocardial cells at an inappropriate time, eliciting ventricular arrhythmia. In addition, an increase in CaMKII-dependent phosphorylation contributing to an increase in RYR2-mediated Ca^{2+} leak has also been associated with DADs and arrhythmia. This is certainly true in the case of catecholaminergic polymorphic ventricular tachycardia and heart failure ([37]).

Another mechanism of cardiac arrhythmia is a conduction disturbance caused by re-entry. Re-entry is a self-sustained activity in which a propagating electrical wave can return to tissue in a circus movement pathway. It occurs when an activation wavefront propagates around an anatomic or function obstacle and re-excites the site of origin. Thus all cells take turns in recovering from excitation and so that they are ready to be excited again upon arrival of the next wavefront ([42]). In general, the classical concept of re-entry requires a substrate and a trigger. The substrate can be defined as the structure and electrophysiological activity of the tissue through which the re-entry wave moves. The trigger can be seen as an ectopic beat in ECG and it associated with unidirectional conduction block that forces the wave to move and propagate in a circuitous pathway. However, any interruption

of the re-entrant circuit at any point along its path would terminate the circus movement ([41](#)).

(A) **EAD and EAD-induced triggered activity**   **(B)**   **DAD and DAD-induced triggered activity**
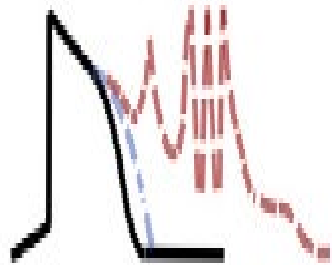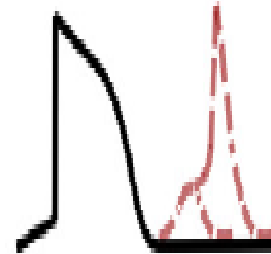
(C)   **Reentry**
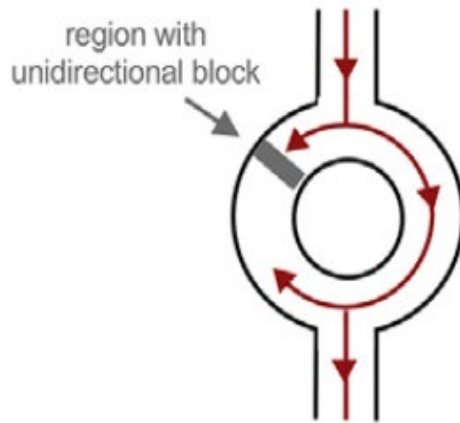
*Figure 1. 5. **Mechanisms of cellular arrhythmia caused by abnormal impulse formation.*** *(A) EAD can be resulted from inward current of L-type calcium channels. Prolongation in APD may leads EAD formation (dashed blue line) followed by a triggered activity started in phase 2 of cardiac ventricular AP (dashed red line). (B) DAD results from several mechanism, including calcium transient inward current associated with NCX1, as well as spontaneous Ca^{2+} release from the SR. Typically, Ca^{2+} handling abnormalities can activate transient-inward NCX1 currents and promote DAD occurrences. The initial rise (dashed red line) illustrates DAD formation, which can then induce a triggered beat. (C) Re-entry is usually caused by a substrate with two pathways for conduction that favour unidirectional block. Then re-entry is triggered by ectopic beat. The re-entrant wave follows an anatomically defined path that surrounds a region of non-conducting tissue. DAD, delayed after-depolarisation; NCX1, sodium-calcium exchanger; SR, sarcoplasmic reticulum; EAD, early after-depolarisation; AP, action potential. Figures is taken from Brenda Yang et al (41).*

1.2.5.1 _Cardiac electrical alternans_

Cardiac alternans that are detected by the ECG characteristically have alternating complexes of differing QRS amplitudes and T wave morphologies. It has been linked to an increased risk of ventricular tachyarrhythmic events and SCD. There are two hypotheses that may explain the cellular mechanisms of cardiac alternans. First, the alternation in cellular sarcolemmal currents (e.g. Calcium and potassium currents), APD, and AP amplitude causes an alternation in $[Ca^{2+}]_i$ on a beat-to-beat basis. Thus, disruptions of intracellular Ca^{2+} homeostasis at the subcellular level result in $[Ca^{2+}]_i$ alternans, which leads to APD and ECG alternans. The second hypothesis proposes that $[Ca^{2+}]_i$ alternans is the primary driver that can lead to changes in AP morphology (43). For example, a study has found that alternans in intracellular Ca^{2+} concentration were correlated with APD alternans in time and magnitude. Also, suppression SR Ca^{2+} release abolished APD alternans in voltage-clamped cardiomyocytes while alteration of the voltage command had no effect on Ca^{2+} alternans. Therefore, perhaps a primary disturbance in Ca^{2+} handling may be responsible for the cellular manifestations of alternans (44, 45).

1.2.6 *Electrical abnormalities of Arrhythmogenic cardiomyopathy*

AC is considered a disease of the ID. The cardiac IDs are composed of gap junctions, desmosomes, adherens junctions, and subsidiary ion channels (Figure 1. 5). All these complexes are necessary for the normal function of cardiomyocytes, specifically electrical and mechanical communication between neighbouring cells (46-48). It is thought that changes in mechanical adhesion ID proteins can affect the functional roles of Nav1.5 and Cx43, leading to disruption of the cardiac electrical signals and arrhythmia (49-51). Nav1.5 is a primary cardiac isoform of the sodium channel and responsible for the rapid upstroke of AP in the cardiomyocytes and normally expressed in the sarcolemma. Cx43 in the ventricle is necessary for gap junctional-mediated intercellular communication and important in controlling of electrical signal passage from one cell to another (52). The estimated size of gap junctional pore is 2.5 nm in the open state, which allows several ions and molecules of less than 1 kDa to move between adjacent cells, including cAMP, IP3, Ca^{2+}, ATP, and other metabolites (53, 54). Thus, the disturbance of Nav1.5 and/or Cx43 can lead to abnormal electrical activity in myocardial cells (Figure 1. 6). Furthermore, some studies have revealed mechanistic insights into the interaction between Cx43 and Nav1.5 expression in that Cx43 may acts

as a regulator for Nav1.5 functions at IDs ([55](#), [56](#)). Indeed, it has been confirmed that Cx43 could modulate Nav1.5 recruitment at ID in hiPSC-CMs, resulting in increased sodium current and upstroke velocities, hence improving the electrical activity ([52](#)). In AC, for instance, both mislocalisation of Cx43 and degradation of Nav1.5 expression at IDs were noted ([49](#), [50](#), [57](#), [58](#)). Also, plakophilin-2 has a role in forward trafficking of Nav1.5 and synapse-associated protein 97 (SAP97) as well was found as a major vehicle protein for incorporation of Nav1.5 in the membrane and it is shown to be majorly downregulated in hearts of AC patients ([3](#)).

A

Intercalated disk

Branched structure of cardiac muscle

Myosin   Actin   Microfibril   Intercalated disk

Z line

Adherens Junction

Perinexal Nav1.5 channel

Desmosome

Mitochondrion

Gap junction

Z line
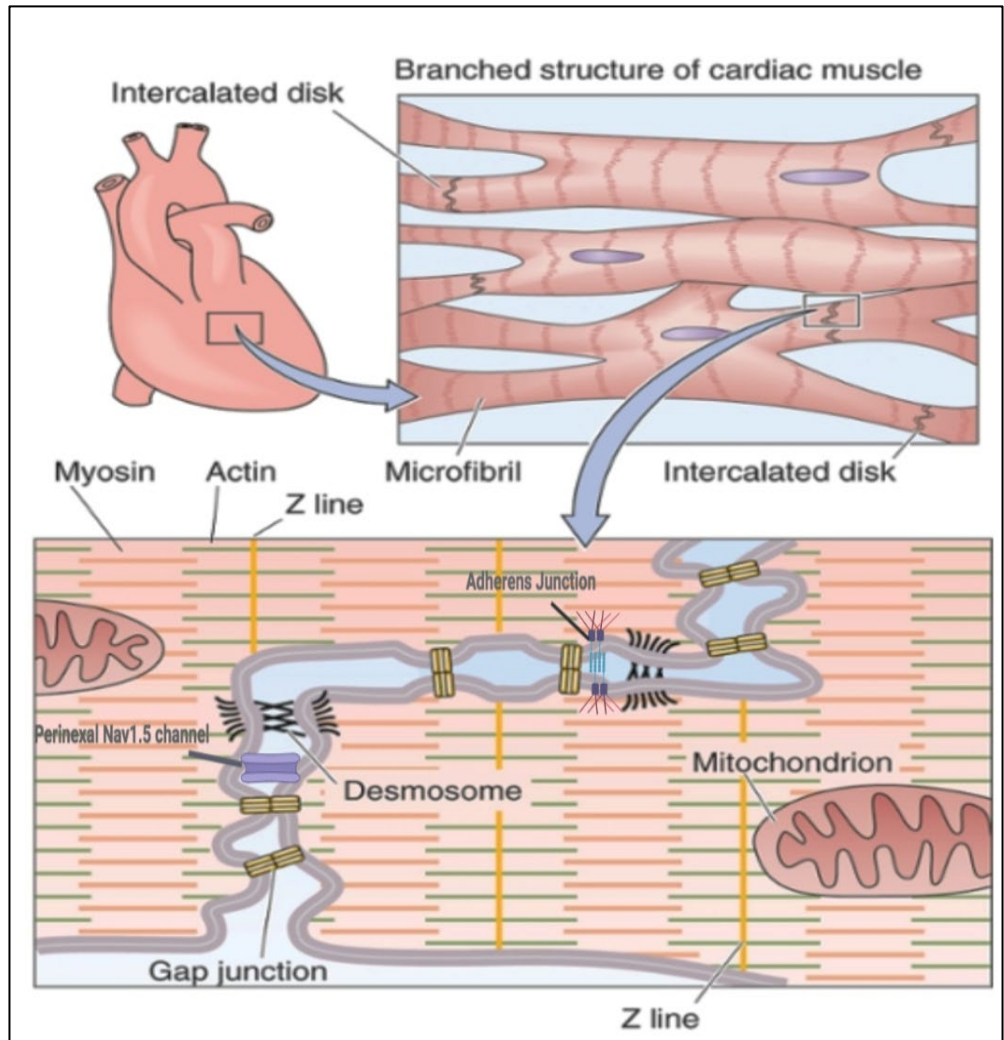
B
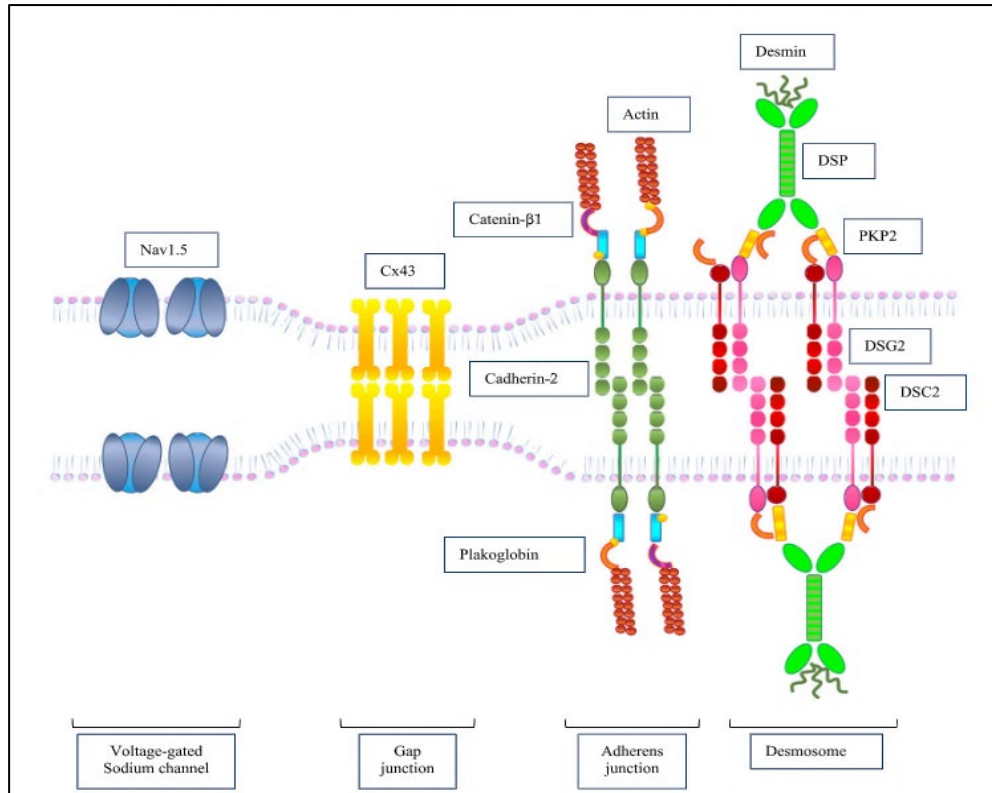
*Figure 1. 6. **Electrical coupling of cardiomyocytes**.(A). The cartoon above is Adapted from Boron & Boulpaep (21) and shows the structural organisation and localisation of Cx43 gap junction and Nav1.5 channels in the intercalated disc. When an action potential is initiated in one cell of myocardium, the current flows via gap junctions and depolarises adjacent cells, generating self-propagating action potentials (51, 55, 59). (B). The cardiac IDs composed of gap junctions, desmosomes, adherens junctions, and voltage-gated sodium channel. Figure obtained from S.costa M. Cerrone Sagunar et al (60). DSP, desmoplakin; DSG2, desmoglein-2; DSC2, desmocollin-2; PKP2, plakophilin-2; Cx43, connexin-43; Nav1.5, voltage gated sodium channel.*

1.3 *Stem Cells*

1.3.1 *Definition*

Stem cells are undifferentiated cells that are capable of self-renewal and can be differentiated to many different types of cells in the human body. They can be used to establish a unique cellular platform to model disease progression. Unlike animal models, stem cells and their derivatives overcome the challenge of species differences. This is evident in the case of gene mutations of AC such as transmembrane protein 43, as it was found that animal models were unable to mimic the human phenotype ([61-63](#)). However, the benefit of using stem cells in disease modelling must not disregard the importance of animal models to understand pathophysiological mechanisms associated with cardiac diseases ([10](#)). The stem cells may be classified on the basis of differentiation potency into pluripotent, multipotent, unipotent, totipotent, and oligopotent stem cells. Given that the capability of these cells to generate all the cell types from ectoderm, endoderm, and mesoderm, they termed as pluripotent stem cells ([64](#)). However, multipotent and unipotent stem cells are restricted to specific tissues or lineages. Multipotent cells develop only in their tissue or cell types and are unable to differentiate into other cell types of different tissue origin under normal

physiological conditions, for example hematopoietic stem cells. Similarly, unipotent cells can only be induced to one cell type (e.g., blast forming unit-erythroid) can be differentiated into erythrocytes (65). Another class of stem cells is totipotent, which derived from fertilised egg, can differentiate into embryonic and placental cell types (66). Oligopotent stem cells can differentiate and renew themselves only into a few cell types, for example a lymphoid stem cell (67). Recently, the human PSCs have been commonly used in disease modelling and drug discovery (68) and are generally categorised into two types: embryonic stem cells (ESCs) and iPSCs. These two classes of stem cells share a number of key features to differentiate in all the derivatives of the three germ layers (64). However, iPSCs-derived cardiomyocytes offer the advantage of obtaining sophisticated cardiac electrophysiological features for elucidating the functions of inherited heart diseases (69). Another shortcoming, human ESCs technique is prohibited in some nations due to ethical and religious concerns (70). Although some ESCs have been examined in cardiac stem cell studies, the emphasis of this work will be mainly on hiPSC-derived cardiomyocytes.

An experimental demonstration of reprogramming factors to generate iPSC was first carried out by Takahashi and Yamanaka at the onset of the 21st century (71). They established murine ESC-like from

mouse embryonic fibroblasts and adult fibroblasts for induction of PSCs by expressing reprogramming factors, which include Oct3/4, Sox2, Klf4, and c-Myc. Subsequently, another study discovered that Nanog and LIN-28 (72) were also able to induce pluripotency in somatic cells (Figure 1. 7). Three years later, functional cardiomyocytes were successfully derived from iPSC using Takahashi protocols, offered a promising start for in vitro models of cardiovascular research applications (73).
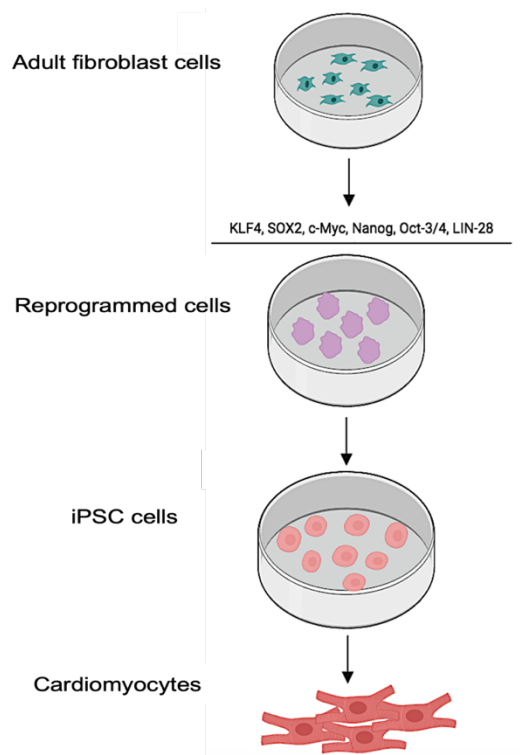
Figure 1. 7. **Generation of hiPSC-CMs from individuals.** *Created with BioRender.com.*

1.3.2 *Adult Cardiomyocytes vs hiPSC-CMs*

The human adult heart is normally composed of fibroblasts, endothelial cells, immune cells, pericytes, smooth muscle cells, and cardiomyocytes (74). Due to the limited availability of human adult cardiac tissue, most of the experimental studies are conducted using in vivo and in vitro models (75). Although it has been difficult to model the complex cellular and molecular characteristics of the heart of cardiomyopathy patients using hiPSC-CMs in vitro due to the variability of cellular compositions under pathological conditions such as fibrosis or inflammation, hiPSC-CMs are still useful for examining the electrophysiological phenotype of the heart cells (62). Another obvious challenge that cannot be ignored is the state of maturity of hiPSC-CMs (*Table 1*), which demonstrates differences compared to adult cardiomyocytes in structural features, metabolism, contractile functions, and electrical properties. Despite this, researchers have been developed several approaches to overcome these shortcomings in many different ways including, biochemical, environmental, and multicellular 3D culture. The following table summarises the significant differences between these two forms of cells (76-79).

Table 1: The major differences between adult CMs and hiPSC-CMs

Properties	Adult cardiomyocytes	hiPSC-CMs
Structure	Elongated, ↑ length: width ratio	Round, ↓ length: width ratio
Sarcomere	Longer, organised	Shorter, unorganised
Banding	I, H, A, M, and Z-discs	Z-discs and I bands
T-tubules	Yes	No
Distribution of gap junctions	Polarised to intercalated discs	Circumferential
Resting membrane potential	≈ -90 mV	≈ -60 mV
Upstroke velocity	~250 V/s	~50 V/s
Amplitude	High	Small
Sodium current (I_{Na})	High	Low
Calcium transients and amplitude	Efficient Increase with pacing	Inefficient Decrease with pacing
Excitation-contraction coupling	Fast	Slow
Contractility	No spontaneous beating Higher force	High spontaneous beating Lower force
Metabolism	Fatty acids, energy production through oxidative phosphorylation	Glucose, lactate, and rare or none fatty acids

1.4 *Filamin C (FLNC) in Arrhythmogenic Cardiomyopathy*

1.4.1 *FLNC structure and function*

The filamins are an assembly of actin-binding proteins that thought to be involved in cell membrane interactions. In the human genome, filamins exist in three forms: filamin-A, filamin-B, and filamin-C. The latter is more prevalent in cardiac and skeletal muscles while filamin-A and filamin-B are widely expressed. Mutations in Filamin-A are found to be associated with central nervous system diseases, skeletal disease, haematological diseases, and respiratory diseases. Nonetheless, certain cardiovascular disorders, such as mitral valve prolapse, patent ductus arteriosus, hypertension, and aortic aneurysm, may result from Filamin-A mutations ([80](#), [81](#)). Filamin-B mutations have been linked to skeletal malformations, for example delay in bone growth and low bone mineral density, as well as apoptosis in chondrocytes, and defects in angiogenesis ([82](#)). Structurally, all these filamins contain an N-terminal actin-binding domain and a C-terminal immunoglobulin-like domain that causes protein dimerisation ([83](#), [84](#)), which in turn support anchors filamentous actin (F-actin) to the cell membrane via specific transmembrane receptors ([85](#)). This interaction of C-terminal domains

and transmembrane receptors provided a clue of association between F-actin cytoskeleton and focal adhesion, which is thought to play a role in mechano-transducing stiffness and biochemical signalling pathways. Due to the involvement of filamins in these mechanisms, they underlie the cell membrane interactions of extracellular matrix receptors such as integrins, as well as signal communication of intracellular proteins (83). Thus, FLNC may not only be necessary for maintaining the mechanical link but also for transmitting signals from plasma membrane proteins (86). The (Figure 1. 9) below obtained from Ortiz Genga (87) illustrates the cellular interactions of FLNC in the heart.

1.4.2 *FLNC mutations and AC*

Pathogenic variants in the FLNC gene are now known to be linked with different subtypes of cardiomyopathies such as restrictive cardiomyopathy (88-91), hypertrophic cardiomyopathy (92, 93), dilated cardiomyopathy (DCM) (94-96), and non-compaction left ventricular cardiomyopathy (97, 98). It is becoming increasingly appreciated that a minority of AC cases (4.4%) arise from FLNC mutations with a predominantly left dominant form (98-100). More recently, Marta Gigli et al (101) studied 85 patients carrying FLNC truncating variants and found

that phenotypes were heterogenous at presentation: 49% DCM, 25% ALVC, and 3% ARVC.

Notably, FLNC-related cardiomyopathy has been associated with different types of genetic mutations, including, missense, nonsense, frameshift, and splicing (102). Missense variants of FLNC were identified in hypertrophic and restrictive cardiomyopathy as well as right atrial cardiomyopathy (103), whereas nonsense variations were associated with arrhythmogenic and dilated cardiomyopathies (104). Autosomal dominant FLNC mutations tend to result in high penetrance (>97%) in carriers aged 40 years or over (100). Prevalence of ventricular arrhythmias and SCD in patients harbouring FLNC truncations was relatively high (82%) in addition to LV fibrosis observed on MRI and histological samples (87). In 2018, Begay and co-authors reported manifestations of FLNC truncating mutations, which demonstrated robust evidence of the relationship between FLNC mutations and AC. These manifestations include fibrofatty infiltration in sub-epicardial myocardium and changes in both sarcomeric structures and adherent junctions, which closely represent AC phenotype. Besides the immunohistochemical study, junctional plakoglobin showed normal signals in myocardium and buccal mucosa whereas DSP and SAP97 signals were reduced. In addition staining for glycogen synthase kinase

3β (GSK3β) revealed that this protein retained intracellularly and did not translocate to the IDs, which previously has shown in ARVC. Staining for Cx43 at ID revealed similar immunoreactive signals in intensity and distribution to the healthy control heart tissues, but diminished immunostaining signal of the buccal mucosa (105).

Moreover, both FLNC and DSP shared some disease features like LV impairment and circumferential scarring (106). According to studies of genotype-phenotype correlations, FLNC and DSP are the two most prevalent disease genes in ALVC (107, 108). Another significant aspect of the similarities between FLNC and DSP is the intercellular connections. Indeed, DSP is a major protein that plays a central role for the intracellular adhesion to the intermediate filaments (Figure 1. 8), thereby it is not surprising that a mutation that impairs the desmin filament network will eventually influence the distribution of DSP at the junctional sites, leading to AC phenotype (37, 109, 110). However, FLNC and DSP were also strongly associated with the DCM phenotype, indicating that DCM and AC may have overlapping phenotypes (105, 111).
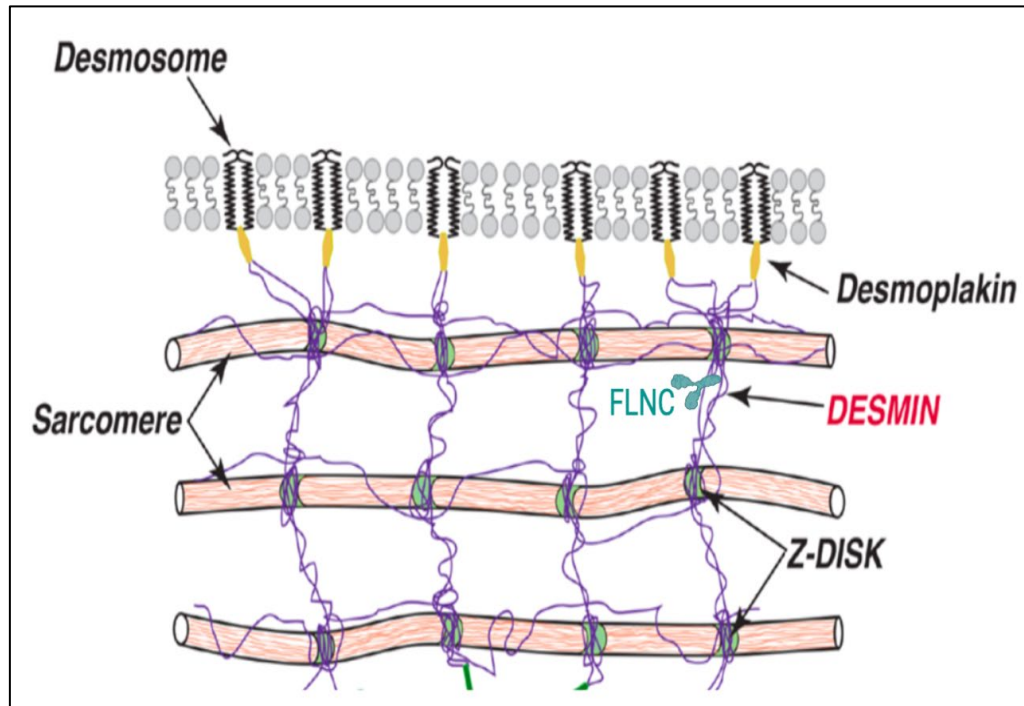
*Figure 1. 8. **Proposed molecular mechanism of FLNC contributing to AC pathogenesis.** Desmin is connected to the desmosome via desmoplakin. Due to the ability of desmin to form a link between the desmosome and cytoskeleton, impaired interaction between these cellular multiprotein complexes may lead to abnormal cellular adhesion (110). A potential consequence of a mutation that alters the desmin filaments network (e.g.FLNC) may change the distribution of desmoplakin at the junctional sites, eventually leading to an Arrhythmogenic cardiomyopathy phenotype. Figure is modified from Mestroni and Sbaizero (109).*

Nonetheless, FLNC truncations were identified in two unrelated families with a predominant phenotype of ARVC ([112](#)). In parallel work, Shimrit Oz and colleagues ([104](#)) reported the reduction in FLNC transcript in three unrelated Ashkenazi Jewish families affected by AC.

Recent published work carried out by Celeghin et al ([99](#)) studied the prevalence of FLNC variants in AC probands and found that eighteen carriers of FLNC variant had a diagnosis of AC (72% males, mean age 45 years) in a cohort of 270 gene-elusive AC probands. The clinical phenotype of FLNC-cardiomyopathy has been characterised by late-onset presentation and typical ECG and CMR features. In ECGs, low QRS voltages and T wave inversion were also detected. SCD has found to be associated with LV fibrosis, but not with severe LV systolic dysfunction. This contrasts with studies published by Akhtar et al ([113](#)) and Kandhari et al ([100](#)) findings, which found that the previously mentioned manifestations were associated with severe LV systolic dysfunction and LV dilation among carriers of truncating variants in FLNC. Additionally, a group of researchers led by Eric D. Carruth et al have recently evaluated the prevalence and associated phenotype of individuals with loss-of-function FLNC variants from MyCode cohort. They found that 10% of FLNC patients have presented with both ventricular dysfunction and arrhythmia- suggestive of ALVC- as

compared to 3% of the remaining variants-negative cohort. Also, they identified through genome screening that those individuals had increased odds of DCM and AC phenotypes, such as decreased LV function during systole as well as frequent ventricular arrhythmias compared to control group (114).

In contrast, in spite of these recent findings about the role of FLNC in AC, Charlotte Hall and other authors (115-117) have highlighted the distinctive phenotype of AC associated with FLNC variants and suggested that the clinical presentation and molecular representation of FLNC- related myocardial disease may demonstrate different appearances of the classical ARVC caused by mutations in the desmosome. In addition, mutations in DSP, FLNC, Nav1.5 or phospholamban can present with an AC phenotype that overlaps with other cardiomyopathies, especially DCM. These findings described above suggest that mutations in FLNC cause diseases with distinct underlying mechanisms. Thus, further investigations and electrophysiological studies with documented arrhythmias at an early stage would be necessary to distinguish AC phenotype from other cardiomyopathies (11).
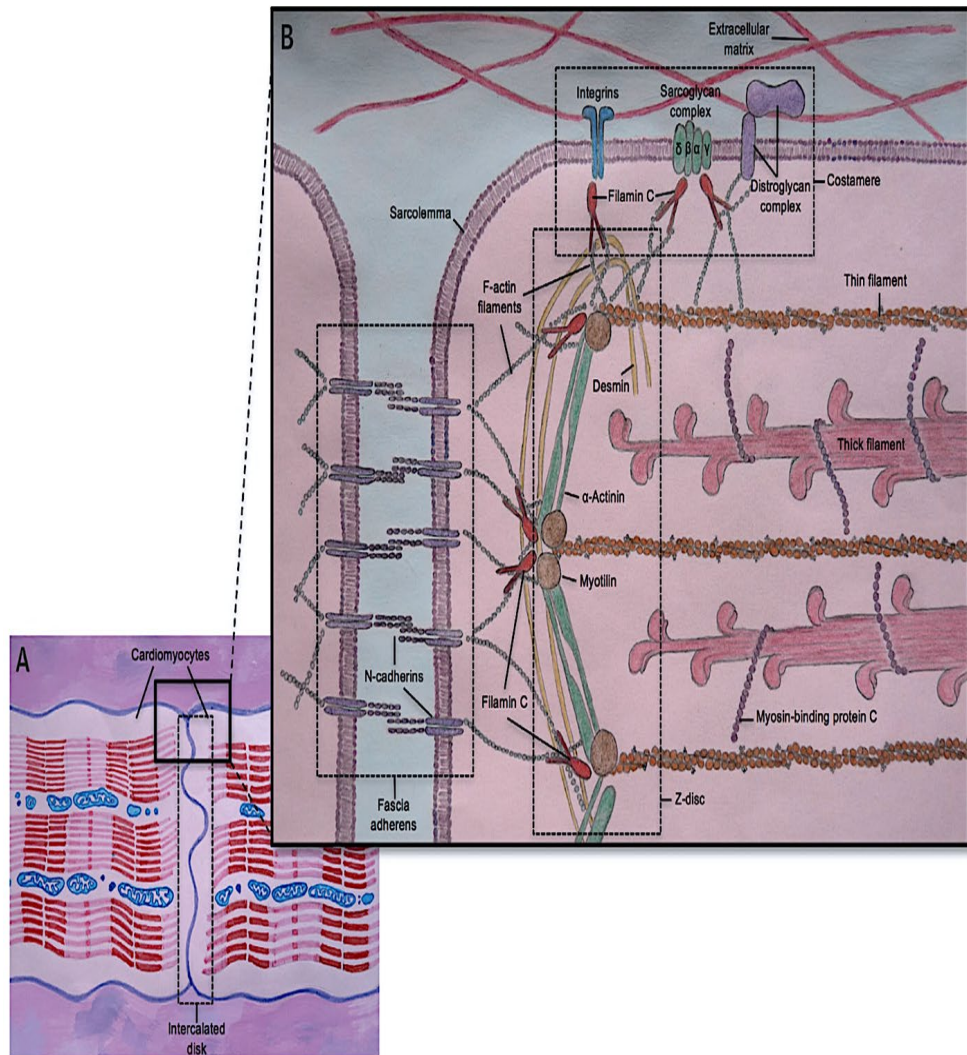
*Figure 1. 9. **Cellular interactions of FLNC at the cardiac IDs**. (A) Cardiomyocytes bind to each other at the IDs. (B) FLNC is primarily localised to Z-discs, where it crosslinks F-actin. FLNC is also involved in interactions with fascia adherens components and costameres. Figure obtained from Ortiz Genga et al (87).*

1.4.3 *__Effects of FLNC mutations on skeletal and cardiac muscle__*

Initially, mutations in FLNC gene were found in families presenting with distal and myofibrillar skeletal muscle disease, which impact the upper and lower limbs resulting in severe muscle weakness and eventually permanent disability ([118](#)). The first mutation described of FLNC by Matthias Vorgerd group used pedigree analysis of a German family and identified a nonsense variant of FLNC associated with myofibrillar myopathy ([119](#)). Two years later, they carried out further investigations and found one-third of those patients with myofibrillar myopathy showed signs of cardiac anomalies comprising left ventricular hypertrophy, diastolic dysfunction, tachycardia, and conduction block ([120](#)). For this reason, FLNC was established as a cause of myopathy and it was apparent that FLNC plays a vital role not only in the structural integrity of skeletal muscle at the myotendinous junction, sarcolemma, and Z-discs but also in cardiac muscle due to its localisation at the IDs of cardiomyocytes ([121](#)).

1.4.4 *FLNC in iPSC-CMs cultures*

The development of iPSCs has provided an opportunity for studying FLNC at cellular levels. To date, four different studies of FLNC have been conducted in both human embryonic stem cells-derived cardiomyocytes (hESC-CMs) and hiPSC-CMs; however, multiple studies have been published in mice, zebrafish, and yeast two-hybrid assays. In addition, other studies have been conducted in patient-derived material as well, including heart samples and buccal cells ([105]).

Despite the key findings of FLNC in iPSC-CMs of Chen et al study, the functional properties were not fully understood and more efforts are needed to investigate the electrical phenotype of FLNC cardiomyopathy ([122]). They identified the disease-specific mechanism of FLNC-related Cardiomyopathy and found a novel link to β-catenin and PDGFRA pathway, which previously observed in human hearts with a DCM and FLNC variants. Also, they found that FLNC-deficient iPSC-CM affected expression levels of desmosomal proteins (desmoplakin, plakoglobin) and caused mis-localisation of connexin43. Electrophysiological properties were assessed using whole-cell patch clamp recordings and abnormal traces were displayed in both mutants FLNC and isogenic FLNC KO$^{-/-}$ iPSC-CMs, specifically beat rate

variations and delayed afterdepolarisations. PDGFRA inhibitor, crenolanib, was used and showed a partial reverse of the pathological gene expression profile, cardiac dysfunction, and electrical instability in FLNC patient-specific CMs. Another study using hiPSC-CMs model, it was found that FLNC cardiomyopathy variants cause protein and lysosome accumulation (123). Agarwal and co-authors suggested that not only FLNC haploinsufficient variants, but also variants that produce misfolded FLNC proteins can cause disease by similar proteotoxic mechanisms in hiPSC-CMs. Complete loss of FLNC (-/-) caused profound sarcomere misassembly, impaired actin-crosslinking and reduced transcription of thin filament genes. Unlike FLNC(-/-) hiPSC-CMs, heterozygous cardiomyopathy variants (FLNC+/-) did not cause sarcomere misassembly, indicating that other mechanisms were involved. Heterozygous FLNC variants caused significant increases in lysosome protein expression and autophagic flux. FLNC(+/-) hiPSC-CMs had increased levels of FLNC binding partners and Z-disc proteins, indicating impaired Z-disc protein turnover. Using hiPSC-CMs, Gabbin (124) generated 2D and 3D models with the goal of developing a new therapeutic approach for RCM patients. He used CRISPR/Cas9 genome editing into healthy control hiPSC-CMs and showed an altered sarcomeric structure of mutants CMs in immunofluorescence assays.

The 3D model of mutant engineered heart tissues showed lower contraction force. One other study has reported the development of hESC-CMs and showed significant reduction of contractility, suggesting an impairment of the contractile apparatus caused by FLNC mutation. No differences in protein expression level and subcellular fraction and FLNC expression was equivalent in both WT and FLNC CMs (125).

However, several studies were conducted in mice to understand the role of FLNC in cardiomyopathy. It was reported that loss of FLNC decreased systolic force development in single CMs and isolated papillary muscles without affecting calcium signalling and twitch kinetics. Electron and immunofluorescence microscopy demonstrated significant abnormalities in Z-disk alignment in knockout mice. Loss of FLNC induced a softening myocytes cortex and structural adaptation at the subcellular level that led to disrupted longitudinal force production in cardiac contraction (126). In addition, mouse model showed that FLNC-deficit myoblasts have changes in cell migration, proliferation, and differentiation as well as dysregulation of Hippo pathway activity (127). Moreover, mouse embryonic CMs with loss of FLNC resulted in foetal death, but in adult CMs showed rapid and severe DCM within 2 weeks. Loss of FLNC was associated with upregulation of different proteins within costamere, ID, and desmin (128). In mice, FLNC mutations affect

the mechanical stability of myofibrillar Z-discs and increased number of lesions upon acute physical exercise, leading to muscle weakness and myofibrillar instability (129). Another study showed that shortly after birth, FLNC deficient mice die due to respiratory failure with severe loss of birth weights and less fibres and primary myotubes, suggesting defects in primary myogenesis (130).

Additional studies used zebrafish to investigate the pathological mechanisms caused by FLNC mutations. Knockdown of FLNC in zebrafish induced systolic dysfunction and severe cardiac phenotype. Sarcomere organisation defects, particularly z-discs irregularity (94). FLNC was found to be an essential for fibre integrity during muscle contraction, but not for muscle specification and loss of FLNC led to muscular failure in zebrafish (131). Progressive degeneration of skeletal muscle in late embryonic stages and myocardial enlargement were detected using Medaka mutant zacro (121). Zac acknowledged as a homozygous nonsense mutation in FLNC and the localisation of FLNC was found at myotendinous junctions, sarcolemma, Z disks in skeletal muscle, and IDs in the myocardium.

Two separated studies were using yeast two hybrid assays to understand the role of FLNC in protein interactions. FLNC was recognised as a putative interactor with KCNE2. The co-localisation of

FLNC and KCNE2 was confirmed within the cell though a physical interaction was only associated with hypoxia ([132](#)). It was also found that Plectin and FLNC organise the cytoskeleton with vital roles in myogenesis, muscle structure, and muscle disease as well. Co-localisation of these proteins was detected at the costameres in adult muscle fibres ([133](#)). Only one study induced depletion of Drosophila by RNAi and showed filamin leads to heart dilatation, impaired systolic function, and sarcomeric disorganisation. Using CRISPR/Cas9 system, three human FLNC missense variants identified in HCM patients showed no impact on cardiac and sarcomere function ([134](#)).

Chapter 2   : Hypothesis and aims of research

Cardiac arrhythmias are a leading cause of death and considerable efforts have been dedicated to develop experimental cell models to study different inherited arrhythmogenic diseases during the past few decades. These models could improve our understanding of the underlying arrhythmia mechanisms and hence translate those understandings into the clinical therapeutic management.

- **Hypothesis**: Lack of filamin-C is highly arrhythmogenic by disrupting gap junction protein connexin 43 (Cx43) and voltage-gated sodium channel (Nav1.5) expression, results in abnormal electrical activity in hiPSC-CMs.

- **The aim of my research**

  o Characterise the expression and subcellular localisation of key desmosomal (Plakophilin-2, desmoplakin, and plakoglobin) and non-desmosomal proteins (FLNC, Cx43, and Nav1.5) following FLNC siRNA administration to knock down FLNC expression in hiPSCs model.

- o Assess the electrophysiological consequences of FLNC downregulation in a cellular model using different functional approaches.

Chapter 3   : Materials and Methods

3.1 *Cell culture*

All cell culture experiments were carried out in a culture hood under sterile conditions and cells were routinely maintained in a humidified incubator at 37°C and 5% CO_2.

3.1.1 <u>*Generation of iPSCs*</u>

Dermal fibroblasts were obtained from healthy donors and some were reprogrammed after several passages and then generated as a control human iPSC cell line - designated HS1M in Professor Andrew Tinker's laboratory at (QMUL) by Duncan C. Miller ([135](#)). Commercial iPS cell lines HPSI0214i-kucg_2 (KG2) and HPSI0214i-wibj_2 (WJ2) purchased from Wellcome Trust Sanger Institute/ HipSci, UK) were gifted to me by my colleague Dr. Aled Rhys Jones at William Harvey Research Institute-Queen Mary University of London and was also used in this study.

3.1.2 <u>*Thawing and maintenance of iPSCs*</u>

The cryo-vial of frozen cells was obtained from the cryogenic store, where samples preserved in a secured liquid nitrogen tank, and instantly warmed in a water bath with 37°C for 90 seconds. Next, the

cells were transferred in a dropwise manner to a 15 mL falcon centrifuge tube containing 9 mL of mTeSR^{TM}1 medium (Stem Cell technologies, Canada) at room temperature. The following step involves centrifugation (Heraeus Labofuge 400R, Thermo Fisher scientific, USA) of the cell suspension at 150 g for 4 minutes, and then the supernatant was removed immediately. Afterwards, the cell pellet was re-suspended with 5 mL mTeSR^{TM}1 and 5μM Y27632 (ROCK-inhibitor, Cambridge bioscience, UK) and placed to a T25 flask. Based on the previous findings of applying Rho-associated protein kinase inhibitors (ROCKi for simplicity), the iPSCs showed an increase in cell survival and cloning efficiency after cryopreservation and therefore ROCKi can be used in post-thawing medium ([136], [137]).The final step for thawing is allowing the cells to settle in T25 followed by an inspection under the microscope to ensure that the cells are attached firmly to the surface. The cells were then incubated and fed with mTeSR^{TM} every 24 hours or mTeSR^{TM} Plus every 48 hours until they become confluent and ready for the first passage. For hiPSC cryopreservation, phosphate buffer saline (PBS) was used to wash the cells and 1 mL of TrypLE, an enzyme for cell dissociation (Gibco #12604013), was added prior to moving for 3 minutes incubation. After that, 9 mL of mTeSR^{TM}1 medium were added to the cells, and subsequent centrifuging at 150g was performed for a

full 4 minutes. Once centrifuged, the supernatant was aspirated and the cell pellets were then re-suspended in adequate amounts of foetal bovine serum (FBS; Gibco #F4135). Afterwards, this suspension was typically aliquoted into three cryo-vials with 0.5 mL of mixture 80% cold FBS and 20% Dimethyl sulfoxide (DMSO, #D2650 Sigma Aldrich, USA) and placed in a special freezing container named Nalgene® Mr. Frosty to store overnight at -80°C and then moved to cryogenic store the following day. A total of 250mL of 2-Propanol (#190764; Sigma-Aldrich, USA) was placed in a Nalgene®Mr. Frosty container, allowing it to undergo five freeze-thaw cycles.

3.1.3 *hiPSC Passaging*

Passaging of hiPSC using TrypLE is an essential step to differentiate iPSCs into cardiomyocytes. Indeed, the successive passage promotes cell proliferation and dilutes out the nonproliferating cells, allowing culture stability with a rapid growth rate. It is worth noting that despite the increase in cell yield during the first and second passage, the senescence may occur at any time, more likely between 30 and 60 cell doublings. Thus, it is not recommended to exceed the fifth passage in continuous cell culture in order to maintain the sufficient

number of cells for freezing. Cells should be used between passages 7 and 15 and should not be used for more than 20 passages ([138](#)).

Cells were routinely grown on Matrigel® (Corning #356230, USA) coated T25 flasks (Sarstedt, Germany). Initially, Matrigel® was moved from -80°C to -20°C freezer to thaw out prior to diluting to $1.25\mu L/cm^2$ in Dulbecco's Modified Eagle Medium (DMEM) and pipetted into T25 flasks for a minimum 45 minutes to allow for polymerisation at room temperature. Geltrex (Thermo Fisher Scientific #A1413301, USA) is another substrate coating and was also used in this study. Due to a delay in delivery from suppliers, Geltrex was used as substitute for Matrigel, despite my preference to use the same substrate to reduce data variability ([139-141](#)). In accordance with our lab protocols, aliquot of Geltrex was thawed immediately at 4°C and then $0.5\mu L/cm^2$ mixed gently and added to the medium DMEM/F-12 (Thermo Fisher Scientific #11320033, USA) in the T25 flasks followed by incubation for at least an hour at 37°C and 5% CO_2. Next, the Geltrex coated T25 flasks were maintained at room temperature until ready to use in the same today or stored at 4°C for up to one week.

Cells underwent a passaging procedure twice in three days by washing once with PBS followed by adding 1ml of TrypLE and placed into 37°C incubator for 3 minutes. Next, 9 mL of mTeSR™1 medium

was added and mixed for detachment of stem cells and then centrifuged for 4 minutes at 150 g. Cells were counted by taking the average of the total number of cells in the four corners squares of haemocytometer. The estimated number of cells is divided by 4 and then multiplied by 10,000 and finally multiplied by 10 in case of splitting one T25 flask. Typically, 1 million cells\ mL was specified for the first passage and 250,000 cells\ mL for the second passage upon differentiation of iPSCs. The supernatant was removed from a centrifuge tube and 2 mL of mTeSR1 was added to dissolve the pellet. After calculating the required media, cells were resuspended in specified volumes of mTeSR1 and Y27632, typically 750,000 (3mL), 1 million (4mL), 1.25 million (5mL), and 1.5 million (6mL) of cells are the ideal numbers of seeding density for the iPSCs cell lines in T25 flasks (Figure 3. 1). Thereafter, coated Matrigel® was removed from T25 flasks and cells were placed into these flasks after washing with PBS. Finally, these T25 flasks were then placed in the incubator at 37°C and the media was changed every day with mTeSR1 or every other day with mTeSR plus. Passaging was carried out between 70% - 80% of cells confluency.

Cells: iPSCs
Substrate: Matrigel/Geltrex
Medium: mTeSR1

cryostore
< -180 °C

cells

Thawing

1st Passaging

37°C

1 million cells per mL

2nd Passaging

37°C

3 mL
4 mL
5 mL
6 mL

250,000 cells per mL

Differentiation

DAY 0 - 6
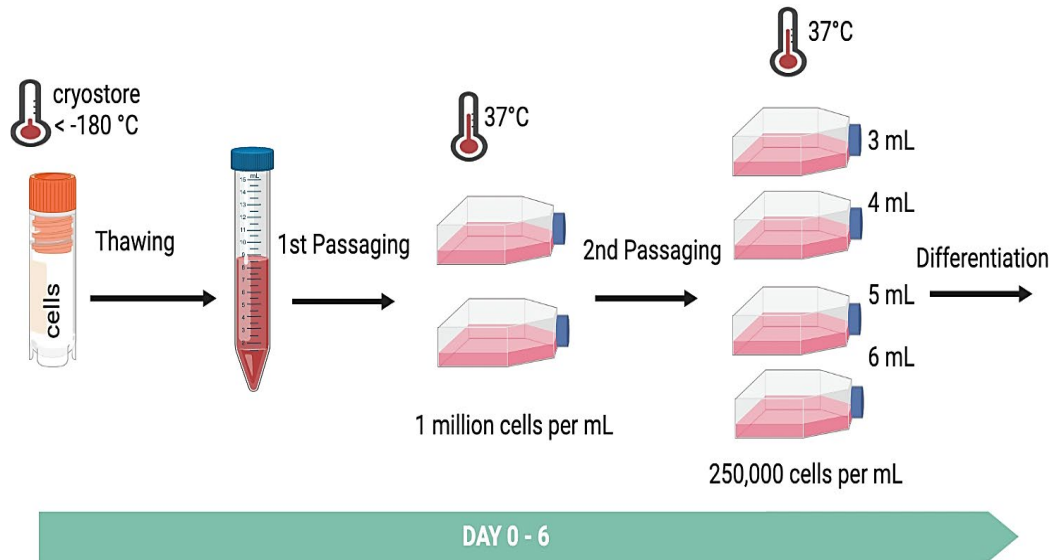
Figure 3. 1. *Schematic of the protocol for hiPSC passaging using TrypLE.* Created with BioRender.com.

3.1.4 *Cardiomyocytes differentiation*

There are several methods for iPSC differentiation into cardiomyocytes, but the main two ways are embryoid body and monolayer based methods.

Preliminary studies used the embryoid body approach, which mimic the early embryonic development by forming small spherical aggregates, to enhance cardiomyocyte differentiation in PSCs (142). Whilst embryoid body culture results in differentiation of PSCs toward beating cardiomyocytes under highly defined conditions (143), such representations are unsatisfactory due to the low efficiency of embryoid bodies to give high cardiomyocyte yield and purity (78, 144). Thus, researchers have developed new techniques in lieu of embryoid body differentiation and proposed PSC monolayer-based differentiation approaches.

Monolayer methods of culturing ESCs and iPSCs have been more effective in inducing differentiation using growth factors and small molecules added to the medium. There are two key characteristics of the monolayer technique: Firstly, iPSCs are grown in a 2D monolayer instead of 3D in embryoid bodies, enabling them to differentiate a large number of cells in a cost-effective manner (142). Secondly, the

cardiomyocytes have been demonstrated to mature phenotype during monolayer differentiation, specifically to ventricular, atrial, or nodal CMs (145). In 2007, Laflamme and colleagues were the first group to report hPSCs differentiation into cardiomyocytes by a confluent monolayer (144). In their experiment, ESCs were cultured on Matrigel® with mouse embryonic fibroblasts until the formation of a cell monolayer was completed and following addition of RPMI medium supplemented with B27. Next, human recombinant Activin-A, followed by a human recombinant Bone Morphogenic Protein 4 (BMP4), a part of transforming growth factor beta (TGF-β) superfamily, were added to the medium to enhance mesodermal formation. The serum-induction model showed that the combined activin/BMP4 had consistently produced more cardiomyocytes in monolayer cultures than in embryoid bodies, according to the reports published by Laflamme and others (144). Subsequently, RPMI supplemented B27 were regularly added to the cells until a spontaneous beating was observed, typically 8 to 12 days after differentiation. During the first five days of differentiation, Lian and co-workers noted that insulin presented in B27 medium supplement halts cardiac differentiation. Therefore, insulin was removed and manufactured as B27 minus insulin. Remarkably improvements were observed in differentiation process of hiPSCs under defined conditions.

Moreover, suppression of Wnt/β-Catenin signalling was also found to play a critical role in cardiac differentiation ([146](#)). Hence, selected studies demonstrated that combination of Wnt inhibitors KY02111 and XAV939 ([147](#), [148](#)) are fundamental to dissect *in vitro* differentiation of hiPSCs to a large number of cardiomyocytes under defined media. Initially cell death is expected during this period due to GSK3β inhibition, but using the correct doses and maintain the defined culture conditions are necessary to induce subsequent cell proliferation.

The cardiac differentiation protocol was adapted from previous studies ([135](#), [149](#)). The hiPSCs were typically differentiated to CMs in 20-30 days using small molecule modulators of Wnt signalling with a chemically defined medium (section 4.1) ([146](#)). The preconditioning step of hiPSC was carried out on Day -1 by diluting 1:100 of Matrigel\Geltrex and 1:10,000 of BMP4 (R&D SYSTEMS #314-BP, USA) in StemPro-34 medium minus serum (Gibco #10639011). About 12-16 hours later, 8 ng/mL Activin A (Life Technologies #PHC9564) and 10 ng/mL BMP4 were mixed together and diluted again in StemPro34 medium to induce cardiac differentiation in stem cells ([150](#)). The hiPSCs were then treated with a Wnt inhibitor, XAV939 and KY02111 (1:1000 dilution; #3748 and #4731; TOCRIS biotechne, USA) in RPMI 1640 medium (Life

Technologies, USA) supplemented with B-27 minus insulin (Thermo fisher Scientific #A1895601, USA) for 48 hours to enhance the cardiac differentiation process (Figure 4. 1). Subsequently, changing the media was achieved with RPMI/B27 plus insulin (Gibco #17504044, Fisher scientific, UK) every other day until day eight of differentiation, at the time that spontaneous beating of cells was typically observed. Additionally, I performed a purification method to enrich hiPSC-CMs by applying 4 mM of sodium lactate (Sigma Aldrich #71718, USA) in RPMI without glucose for six days, thereby removing whichever non-cardiomyocytes, including undifferentiated cells ([151](#)). hPSC-CMs could undergo an optional passage at day 19 using a Collagenase II-based protocol, as described in the previous studies ([152](#)). A brief description of this procedure: washing the cells was done twice with no Ca^{2+} and Mg^{2+} - Hank`s Balanced Salt Solution (HBSS, Life Technologies #14175095). Following that, cardiomyocytes were incubated for 3.5 hours with 2.5 mL collagenase II (Gibco, Life Technologies #17101-015) per T25 flask, supplemented with 1mM 4-(2-hydroxyethyl) piperazine-1-ethanesulfonic acid (HEPES, Sigma #H3375, USA), 10μM Y-27632 (ROCKi) and 30μM N-benzyl-p-toluenesulfonamide (BTS, #SC-202087 Santa Cruz Biotechnology, USA), all diluted 1:1000, and instantly placed at 37°C and 5% CO_2. Thereafter, dissociated cardiomyocytes

were collected from the flasks and washed with RPMI supplemented with 12 mg/ml deoxyribonuclease II (DNAse II – Sigma #D8764, USA) diluted in (1:500), followed by centrifugation at ~100g for 15min. Counting the cells was performed using a haemocytometer following centrifuging again as above. Subsequently, resuspension of the cells was achieved in warm RPMI/B27, ROCKi, 10% FBS and 1% Penicillin/Streptomycin and pipetted slowly into a centrifuge tube. Henceforth, media was replaced by RPMI/B27 in the next day and then every other day until cells become ready for the experiment. Finally, cells were treated with Tri-iodo-L-thyronine (T3, Sigma #T2877, USA) and dexamethasone (Cayman chemical #11015, USA) all diluted 1:10,000, to improve the maturation of T-tubules, Ca-induced Ca release, and ventricular-like excitation-contraction coupling during days 19 to 30 as described before (153).

3.2 *Immunofluorescence staining*

To determine the intracellular localisation and relative expression of IDs proteins, indirect immunofluorescence staining was carried out with specific antibodies against targeted proteins. Using specific antibodies and chemical fluorescent tags, immunofluorescence is a highly sensitive and versatile method for labelling molecular targets within cells and tissue, and has been used widely in diagnosis and research ([154]). This technique permits excellent sensitivity and signal amplification compared with immunohistochemistry ([155]). The immunofluorescence staining is capable of detecting the protein of interest either directly or indirectly ([154]). The latter method is more sensitive because it requires a labelled secondary antibody to detect an unlabelled primary antibody. In contrast, the direct method involves the direct conjugation of a primary antibody to a fluorophore, chemical dye ([156]). The Figure 3. 2 shows a substantial distinction between direct and indirect methods in terms of the amplification of the fluorescents signals due to the ability of many secondary antibodies to identify a single bound primary antibody.
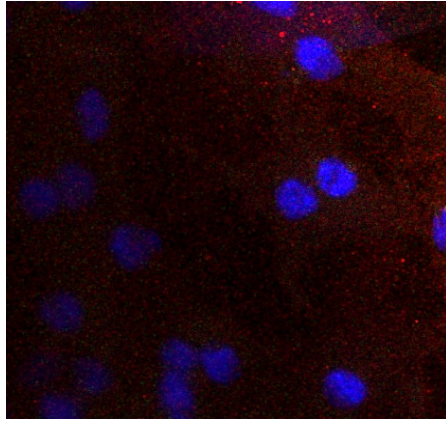
Plakophilin-2 stained only with primary antibody
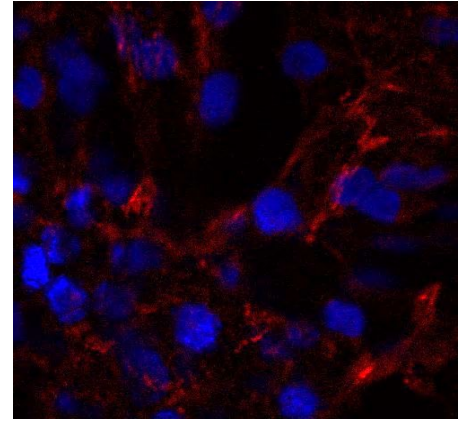
Plakophilin-2 stained with primary and secondary antibody

Figure 3. 2. **Example of antigen detection by using either the direct (A) or indirect (B) labelling method in hiPSC-CMs with confocal microscopy.** *It can be clearly seen that the indirect detection, which involves initial step of applying primary antibodies followed by washing and subsequent using secondary antibodies, produces higher sensitivity due to signal amplification as many secondary antibodies identifying one primary antibody (156).*

Initially, hiPSC were dissociated by adding 3mL of accutase (Fisher scientific #11420705, UK) per T25 flask following incubation for 10-20 minutes at 37°C. The cell pellet was resuspended in 7mL of RPMI/B27, 1% penicillin/streptomycin and 10% FBS and then centrifuged for 4 minutes at 150g. Cells were seeded onto 0.1% gelatin-coated 24-well plate (Thermo Fisher scientific, USA) with 10 mm glass diameter of the coverslips (thickness No. 1, VWR International Ltd, UK) at a density of ~300,000 cells per well. The medium was replaced to RPMI/B27 every 2-3 days until ready for the experiment.

Prior to confocal imaging, cells first rinsed twice with PBS following fixation with ice-cold methanol/acetone (50%/50% mixture) for 10 minutes. The samples were then washed with PBS and blocked at room temperature for minimum 1 hour with PBS containing 5% goat serum (Invitrogen, ThermoFisher scientific, USA) to avoid non-specific binding of the antibodies and support permeabilisation to stain intracellular targets due to inability of these antibodies to penetrate across the cell membrane (154). Once blocking solution was removed from the coverslips, the coverslips were transferred into humidified chamber and primary antibodies were added in 1% goat serum solution prior to incubating overnight in the fridge at 4 °C. In my experiment, I used the following primary antibodies: mouse monoclonal anti plakophilin-2

(1:50; Santa Cruz, USA) anti-DSP (1:50) and anti-plakoglobin (1:20), graciously gifted to us by the David Kelsell lab, anti-connexin 43 (1:200; Millipore, Germany), and anti-cardiac troponin T (1:200; Abcam, UK); rabbit polyclonal antibody anti-filamin C (1:200; sigma-Aldrich, USA), anti-Nav1.5 (1:200; Alomone, Israel). Rabbit polyclonal anti- N-cadherin antibody (1:200; Abcam, UK) was also used. Following day, primary antibodies were removed and immediately three washes of the specimens with PBS were made before incubation with secondary antibodies. The secondary antibodies included Donkey anti-rabbit 555 IgG, and Goat anti-mouse 488 or 568 IgG (Invitrogen Life Technologies, USA) diluted to 1:500 in blocking buffer containing 1% goat serum in PBS, and subsequently incubated at 21°C for minimum 1 hour. These antibodies are summarised in the (*Table 2*) below. The coverslips were washed with PBS three times to remove any remaining antibodies and then incubated for 5 minutes with 100 ng/ml of 4',6-diamidino-2-phenylindole (DAPI, 1:10,000 dilution; ThermoFisher, USA) diluted in PBS. Next, the coverslips were washed twice with PBS and then moved onto 25x75x1mm Polysine adhesion microscopic slides (Epredia, Germany) and mounted with Shandon Immu-Mount (Fisher scientific, UK). Cells were maintained in a dark recipient and stored in the fridge at 4 °C until ready for microscopy.

Table 2 :Primary and secondary antibodies used in immunofluorescence staining

Primary antibody	Dilution	Secondary antibody	Dilution
Mouse monoclonal Anti-DSP antibody (gifted)	1:50	Alexa 488, Goat anti-mouse (Invitrogen, A11001) or Alexa 568, Goat anti-mouse (Invitrogen, A11004)	1:500
Mouse monoclonal Anti-plakoglobin antibody (gifted)	1:20	Alexa 488, Goat anti-mouse (Invitrogen, A11001) or Alexa 568, Goat anti-mouse (Invitrogen, A11004)	1:500
Mouse monoclonal Anti-Plakophilin-2 (Santa Cruz, SC393711)	1:50	Alexa 568, Goat anti-mouse (Invitrogen, A11004)	1:500
Mouse monoclonal Anti-Cx43 antibody (Millipore, MAB3067)	1:200	Alexa 488, Goat anti-mouse (Invitrogen, A11001) or Alexa 568, Goat anti-mouse (Invitrogen, A11004)	1:500
Rabbit polyclonal Anti-FLNC antibody (Sigma-Aldrich, HPA006135)	1:200	Alexa 488, Goat anti-mouse (Invitrogen, A11001) or Alexa 555, Donkey anti-rabbit (Invitrogen, A31572)	1:500
Rabbit polyclonal Anti-Nav1.5 antibody (Alomone, 493511)	1:200	Alexa 488, Goat anti-mouse (Invitrogen, A11001) or Alexa 555, Donkey anti-rabbit (Invitrogen, A31572)	1:500
Rabbit polyclonal Anti-N-cadherin antibody (Abcam, Ab76057)	1:200	Alexa 555, Donkey anti-rabbit (Invitrogen, A31572)	1:500
Mouse monoclonal Anti-Cardiac Troponin T antibody (Abcam, ab8295)	1:200	Alexa 488, Goat anti-mouse (Invitrogen, A11001)	1:500

3.3 *Cell imaging systems*

Imaging techniques of cells can shed light on the fundamental nature of cellular and tissue structure and function. There are several modalities that can be used for cell imaging, including widefield fluorescence, confocal, electron, atomic force microscopy and other systems. In this section, I will provide a summary of the two systems that I used in this study: confocal microscopy and fluorescence microscopy.

3.3.1 *Fluorescence imaging*

Fluorescence imaging has been adapted to interrogate cardiac cellular electrophysiology ([157](#)). The key principle is an indicator will absorb light energy (a photon) before emitting a second photon, just a few nanoseconds later. It should be noted that the emitted photon has less energy than the absorbed photon due to the loss of some energy in this process. More importantly, the energy of light with a short wavelength (towards blue spectral colour) is higher than light with a long wavelength (towards red spectral colour), therefore the emitted light from an indicator normally has a longer wavelength than that of the excited (absorption) light. This change is called the Stokes shift.

Currently, fluorescence microscope of live cells is important in cell biology studies. Indeed, fluorescent protein tags, live cell dyes, and other techniques to fluorescently label proteins of interest provide an opportunity to study practically any biological event under the microscope. This technique has many advantages, including the low cost, simplicity of the system, and the ability to observe the behaviour of specimens in real time using cameras. Some disadvantages exist such as low image resolution and shading artefacts caused by uneven illumination (158). Below is a schematic of the underlying process of fluorescence microscope Figure 3. 3.
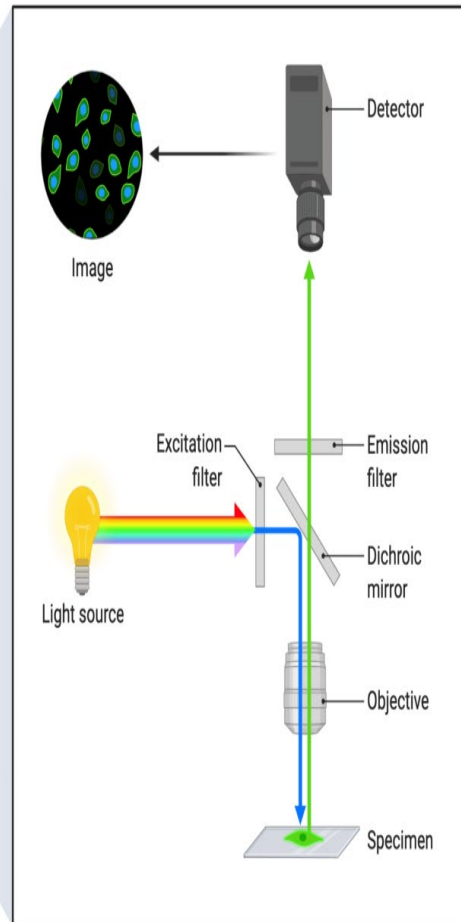
*Figure 3. 3. **Schematic diagram illustrating the fluorescence microscope principle**. The basic light paths into two directions through a fluorescence microscope. Initially, an excitation filter cube containing a dichroic mirror, which first directs excitation light to the specimen and then passes emitted fluorescence to the emission cube for further separation. The filter cubes are essential for aligning filters in the path of excitation and emission lights. Emitted fluorescence is separated by dichroic mirror into two beams. The emission filters can prevent unwanted light (158). Fluorescence was detected by sCMOS camera. Figure created with BioRender.com.*

3.3.2 *<u>Confocal imaging</u>*

The stained cardiomyocytes were imaged using a CLSM710 confocal microscopy (Zeiss, Germany). This instrument facilitates imaging of cellular specimens via laser light emission and helps for co-localisation studies. The specimen in a confocal system is illuminated in a serial manner or point-by-point, and thus physical interaction between the laser light and fluorescence is measured point-by-point. To gather information on the entire specimen, the laser beam must be scanned over the specimen or the specimen must be scanned relative to the laser beam. Comparing to a standard microscope, the confocal aperture (often referred to as a pinhole) positioned in a plane conjugate to the intermediate image plane and, hence, to the object plane of the microscope. The photomultiplier tube (PMT) is a pixelwise detector and can therefore only detect light that passes through the pinhole. Since the laser beam is focused to a diffraction-limited spot, only a single point of the object can be illuminated at once, the point lighted and the point observed (i.e., image and object points) are placed in conjugate planes, therefore they are focused onto each other. Consequently, a confocal beam path is produced. Another essential point is the diameter of the pinhole. Based on the diameter of the pinhole, light originating from object points outside the focal plane is somehow occluded and therefore

not detectable. By varying the pinhole diameter, the degree of confocality can be modified to meet specific needs. The image becomes nonconfocal when the aperture is fully open. The pinhole suppresses stray light, hence enhancing picture contrast (ZEN 2010 Operating manual;https://www.zmbh.uni-heidelberg.de/Central_Services/Imaging_Facility/info/780ZEN2010.pdf).
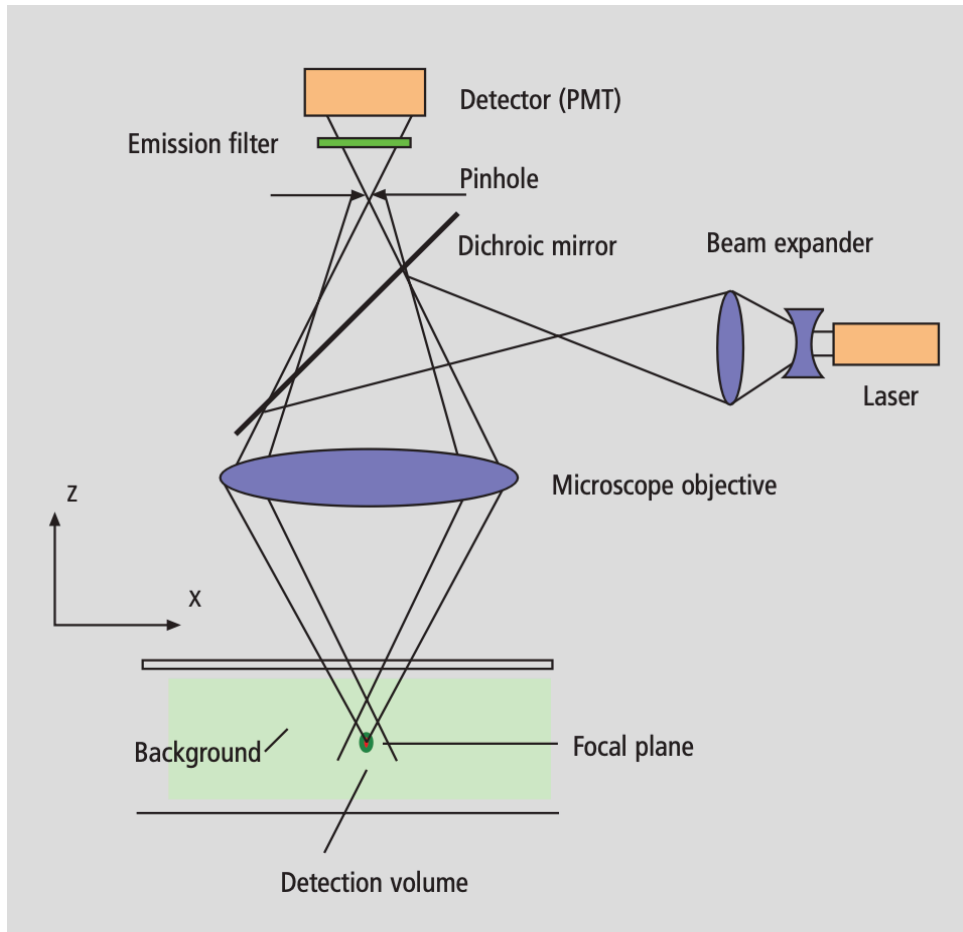
*Figure 3. 4. **Schematic diagram illustrating the path of the beam in a confocal LSM710** (figure obtained from Zen 2010 operating manual). A microscope objective is utilised to focus a laser beam onto a specimen, where it can, excites fluorescence. A dichroic beamsplitter efficiently directs the fluorescent energy captured by the objective onto the detector. The wavelength range of the fluorescence spectrum that is of interest is determined by an emission filter, which also blocks the excitation laser line. The pinhole is positioned in front of the detector on a conjugate plane with the focal plane of the objective. Optical sections are made in different focal planes and produce XYZ image stack, which enable an image to be visualised, processed, and analysed. Light from planes up or down the focal plane is out of focus when it reaches the pinhole, therefore most of it cannot pass through the pinhole and does not play a part in the formation of the image.*

The objective lenses used for this study were: Plan Apochromat 63x/1.4 and 40x/1.3 Oil differential interference contrast (DIC), metric 27-mm objective thread (M27). Before scanning, small drops of immersion oil were placed on the slide just above the coverslips to provide improved resolution while recording the pictures. For green fluorescence, siGLO was excited by the Argon laser at 488nm. DAPI is a blue fluorescent designed for cell nuclei staining and was excited by the Diode laser at 405nm. Finally for red fluorescence, Alexa Fluor 555 and Alexa Fluor 568 were excited by the Helium/Neon laser at 543nm. The relative excitation and emission wavelengths of fluorophores used in this thesis are listed below in Table 3.

Fluorophore	Excitation wavelength	Peak emission	Emission filters
Alexa488/siGLO	488 nm	519 nm	504 – 533 BP
DAPI	405 nm	441 nm	409 – 472 BP
Alexa 555/568	543 nm	620 nm	560 – 680 BP

Table 3: List of fluorescent detection wavelengths with filters used. Nm (nanometre). BP (bandpass) – determine bandwidth of fluorescence emission for the respective channel.

3.3.3 *Quantification of confocal fluorescent images*

The confocal microscopy is useful for quantitative evaluations since the intensity of fluorophores are used as proxy for quantitating the protein expression levels in fixed cell or tissue samples. I adapted the protocol of Shihan et al for the image quantification using ImageJ software ([159](#)). Briefly, I used an automated region of interest selection based on a signal threshold to measure the estimated mean number of fluorescence intensity of a protein of interest. Thresholding technique can separate an image into foreground and background by choosing a value cut-off, therefore the lower pixel values were considered background whilst the greater pixel values are foreground. This can be done automatically by ImageJ. As recommended by authors, mean fluorescence intensity of non-fluorescent area was subtracted from the mean fluorescence intensity of the tissue area (Figure 3. 5).
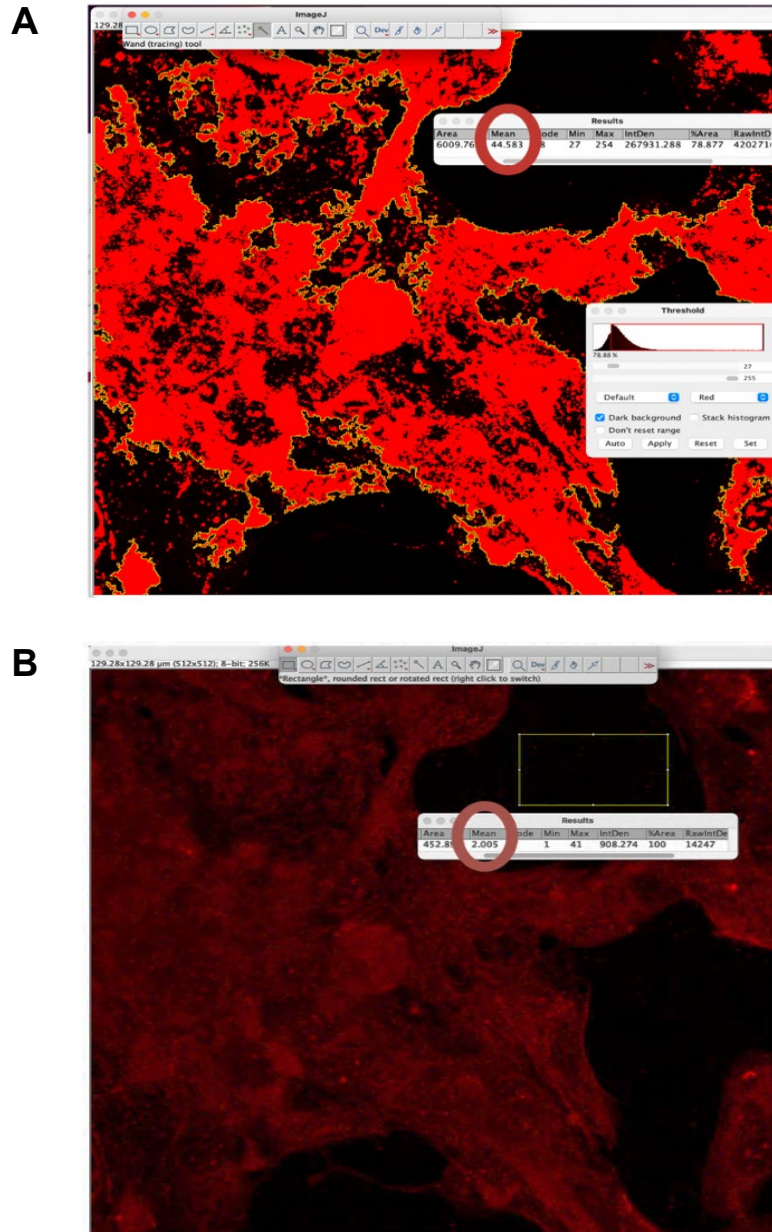
*Figure 3. 5. **Quantification of confocal fluorescent images.** Untreated hiPSC-CMs stained with FLNC serves as an example of the quantification method. (A) Mean fluorescence intensity measurements using a tracing tool selection of an automated region of interest based on a signal threshold. (B) The mean of background of non-fluorescent area was subtracted from the mean of the thresholded area as the background values may affect the quantification. Note: the same amount of selected background should be subtracted from all images when comparing between positive and negative controls.*

3.4 *siRNA Transfection of iPSC-CMs*

Small interfering RNA (siRNA) was carried out to knockdown protein levels of FLNC in iPSC-CMs. This tool can reduce but not generally eliminate the gene expression at the mRNA level, allowing a study of the functional changes and genetic influences on cellular phenotype (160). To elucidate the brief mechanism of synthetic siRNA, short hairpin RNA (shRNA) or long double-stranded RNA (dsRNA) can be processed into small RNA fragments by an enzyme called Dicer. The siRNA duplex will subsequently be incorporated into the complex that composed of argonaut protein and other proteins known as RNA-induced silencing complex (RISC), where only one strand of the siRNA is selected to be bound. Unlike the endogenous siRNA pathways, synthetic siRNA is directly loaded into the RISC complex (Figure 3. 6). The siRNAs consist of two stands, an antisense (or guide) and a sense (or passenger). The latter can be eliminated and the remaining antisense strand of siRNA is loaded into RISC, which then recognises the target complementary mRNA. Hence, argonaut protein in RISC catalyses the cleavage of mRNA and inhibits expression of the protein. The synthetic siRNA is a powerful tool for studying gene function and may be obtained from commercial facilities. There are several delivery methods that synthetic siRNA can be introduced into the cells, including

transfection, electroporation, viral-mediated delivery, and chemically modified siRNA ([161], [162]). The emphasis of this work will be mainly on transfection delivery method (Figure 3. 7).
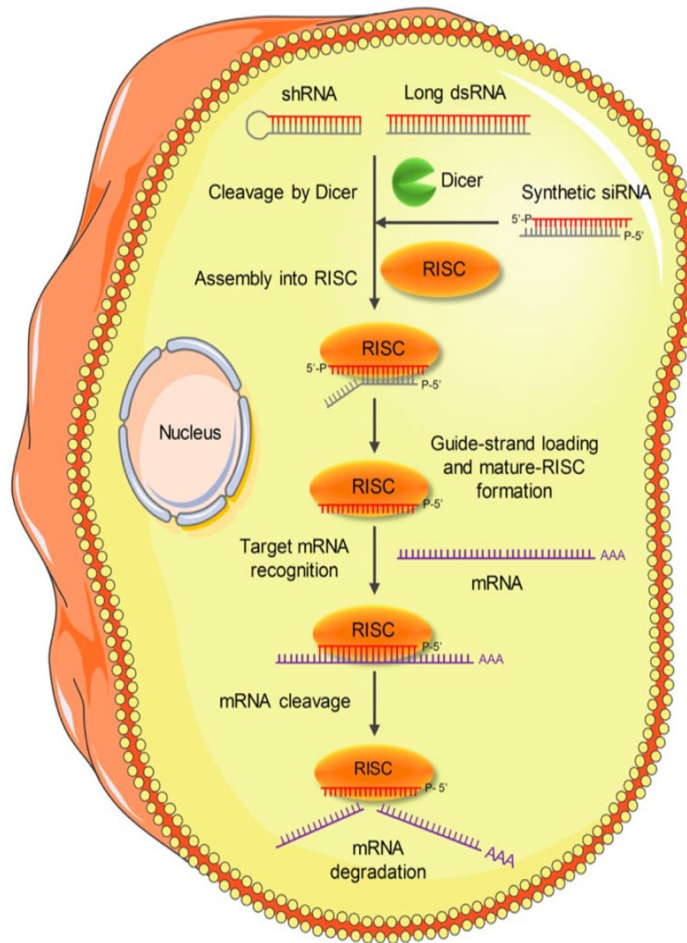
*Figure 3. 6. **Working mechanism of synthetic siRNA**. The long double-stranded RNA binds to Dicer, which in turns cut the RNA into short segments. Synthetic siRNAs instead can be directly loaded into RISC complex. The guide (antisense) strand of the RNA is loaded into RISC complex, where the mRNA is recognised and cleaved, resulting in inhibition of protein translation. Figure taken from Mei Lu et al ([163]).*

siGENOME Human FLNC (2318) siRNA - SMARTpool, 5nmol (M-011272-01-0005) and scrambled non-targeting siRNA Pool #1 & #2 (D-001206-13-05 & D-001206-14-05) were chemically synthesised and modified by Horizon Discovery (Dharmacon, Lafayette, USA). The transfection procedure (Figure 3. 7) was implemented with DharamaFECT reagent and performed on ~300,000 cells/well in 24 well plates or ~3.4 millions of cells/T25 flask in serum culture medium without antibiotic. For 5nmol and a 20µM stock concentration of siRNA, 250µl of RNase-free water was added and aliquoted for 10 µl. The recommended concentrations of the final siRNA to be used for the transfected cells are between 5 and 50 nM.
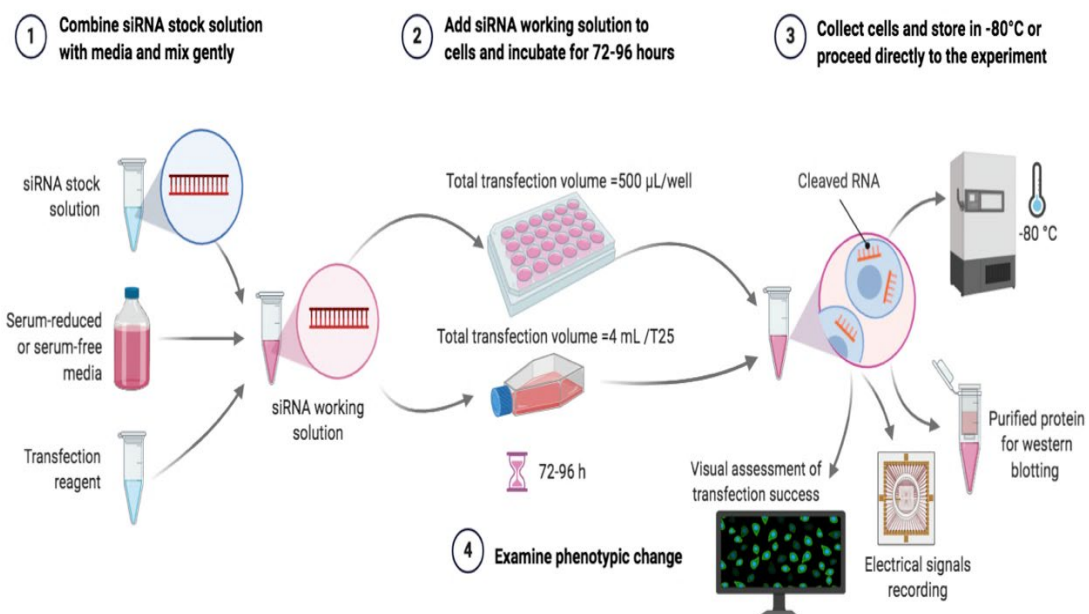
*Figure 3. 7. **Diagram of the transfection workflow.** Delivery of siRNA into the cells using a DharmaFECT^{TM} transfection method. Created with BioRender.com.*

The transfection protocol was adapted from James Cartwright ([164]). Working stocks of 2µM siRNA (1:10) resuspended in RNase-free water were used and diluted for the desired concentration of 40nM in total volume 50 µL per well of 24 well plate or 400 µL per T25 of serum-free Opti-MEM, siRNA and siGLO (Horizon Discovery, Dharmacon, USA). Transfection indicator of siGLO green (1:1 ratio) was used to provide reliable visual assessment of transfection success via confocal microscopy. Also, DharmaFECT transfection reagent-1 was diluted 50 µL Opti-MEM per well or 400 µL Opti-MEM per T25 and pipetted carefully up and down following incubation at room temperature inside the culture hood for 5 minutes. Next, contents of both tubes were gently mixed followed by incubation again at room temperature for an additional 20 minutes. Culture medium was removed from cells and RPMI-B27 without antibiotic (400µL/ well) or (3.2 ml/ T25) was added to the siRNA transfection mixture (100µl/well) or (800µl/T25). Afterwards, the cells were moved to the incubator at 37°C in 5% CO2. The transfection medium was replaced after 24 hours with RPMI-B27 supplemented with 1% penicillin/streptomycin to reduce cytotoxicity. The cells were used experimentally 72 hours following transfection.

3.5 *Western Blot*

Western blot analysis is an effective method for validating immunofluorescence imaging data by measuring the amount of protein expression. Therefore, proteins extracted from cells can be identified using this technique ([165](#)). The hiPSC-CMs were differentiated in a T25 flask and washed twice with cold PBS prior to being lysed on ice for 2 minutes with 300μl of lysis buffer containing 50 mM Tris/HCl (pH 6.8), 10% glycerol, 2% sodium dodecyl sulfate (SDS), ddH$_2$O and protease inhibitor cocktail (1:100 dilution; #87786 Thermo Fisher, USA). The cells were then scraped and collected in 1.5 mL tube and homogenised for 1 minute. The samples were transferred to a dry block heater (Grant – QBD2, UK) for 3 min at 95 °C to denaturant the protein following centrifuging (Centrifuge 5424, Eppendorf UK Limited, UK) at 14,000 rpm for 10 minutes at 4°C. Afterwards, the supernatant was collected and samples placed in ice box prior to calculate protein concentrations using NanoDrop (1000 spectrophotometer, Thermo Fisher scientific, USA). Next, the samples were transferred to a -20°C freezer and stored there until needed. On the experimental day, lysates were thawed on ice and mixed with aliquot of 4x SDS- polyacrylamide gel electrophoresis (PAGE) loading buffer, graciously gifted to me by my colleague Dr.

Alison Thomas, containing: 150mM Tris-HCl pH 7.0, 12% SDS, 0.05% bromophenol blue, 25% glycerol, 6% β-mercaptoethanol and cell lysis buffer. This assembly was heated at 95 °C for 5 minutes and spun at 14,000 rpm for 3 minutes. Running and transfer buffers were prepared as follows: 10xRUNNING buffer, including 30.3g Tris(hydroxymethyl)-aminomethane (#A18494 Alfa Aesar, UK), 144.4g glycine (#G8898, Sigma-Aldrich, USA) 10g SDS (sodium dodecyl sulfate Natriumlaurylsulfat; #62862; Riedel-de Haën, Germany). All were combined and placed in a glass laboratory reagent bottle and filled with 1000ml of ddH2O. Similarly, in a separated bottle, 10x transfer buffer contains (30.3g Tris base, and144 glycine) was filled with 1000ml of ddH2O as well.

Subsequently, a total amount of 25 μg protein was separated by SDS- PAGE involving 12% or 6% resolving gel (1.5M Tris-HCl buffer, pH 8.8; BIO-RAD, USA) with 5% stacking gel (0.5M Tris-HCl buffer, pH 6.8; BIO-RAD, USA) at 100 V (Bio-Rad PowerPac 200, BIO-RAD, USA) for approximately 30 minutes or until the ladder formulated and then increased to 120 V for 90 minutes. After that, I transferred the proteins in the gel to a polyvinylidene difluoride (PVDF) membrane (#IPVH00010, Millipore, Germany) for running at 75 V on ice for an hour

and thirty minutes. Membranes were then blocked in 5% bovine serum albumin (BSA) at room temperature on a rocker (Stuart SSL4 See-Saw Rocker, Scientific Laboratory Supplies, UK) for one hour. Next, incubation was done overnight on a rocker with primary antibodies rabbit anti-FLNC (1:1000; ab180941, Abcam, UK) anti-connexin 43 (1:1000; Millipore, Germany), and anti-Nav1.5 (1:200; Merck Life Science UK Limited, UK) diluted in 5% BSA and placed in a cold room at 4 °C. The following day, primary antibodies were rinsed 3 times every 10 minutes with Tris-buffered saline 0.2% Tween (TBST). Subsequently, 2 µl of targeting secondary antibodies horseradish peroxidase (HRP) goat anti-rabbit (ab6721; Abcam, UK) or rabbit anti-mouse (ab97046; Abcam, UK) were added to 10 mL TBST 5% BSA (1:5000) and incubated with membranes at room temperature for minimum 60 minutes on a rocker. The protein bands were visualised on X-ray film via GeneSystem software (G:BOX, SYNGENE, Cambridge, UK) using Immobilon Crescendo western HRP substrate (# WBLUR0100; Millipore, USA), which depends on secondary antibodies that are labelled with HRP. To determine the loading control of the blots, mouse monoclonal anti-GAPDH antibody (1:1000; Santa Cruz, USA) was used and visualised as described above.

3.6 *Multielectrode array (MEA)*

MEA systems have been widely used for the detection of sharp spike signals to analyse the propagation of APs in excitable cells. In this study, I adapted the MEA protocol published by Sala and his colleagues (166) for electrophysiological analysis of hiPSC-CMs. The MEA system consists primarily of electrodes that measure the cellular electrical activity and enables for a long-term assessment. This technology allows recording of the extracellular field potentials (FPs), which correlate with cardiac action potential. Unlike single cell patch clamp recording, the measured FP is a consequence of the spread of the cardiac AP across the monolayer cell sheets or clusters attached to the recording electrodes. As a result, the acquired electrical signals from MEA system are comparable to the clinical ECGs that basically depicts voltage variation over time (Figure 3. 8). By using MEA systems, it is possible to measure field potential duration (FPD), which is an in vitro analogue for QT interval (167), and conduct high-throughput measurements with a non-invasive procedure, making them a useful tool for understanding the basic mechanisms of arrhythmogenesis in preclinical experimental models designed to study the electrophysiology of cardiomyocyte.

A

B

FP Morphology	Physiological Parameter
Spatiotemporal Assessment	Propagation velocity, direction origin of AP spread
FP Duration	QT interval of AP
FPs Over Time	Beating frequency
Spike Amplitude	Na^+ current
Spike Plateau	Ca^{2+}/K^+ current
Beat-to-Beat Interval	AP duration
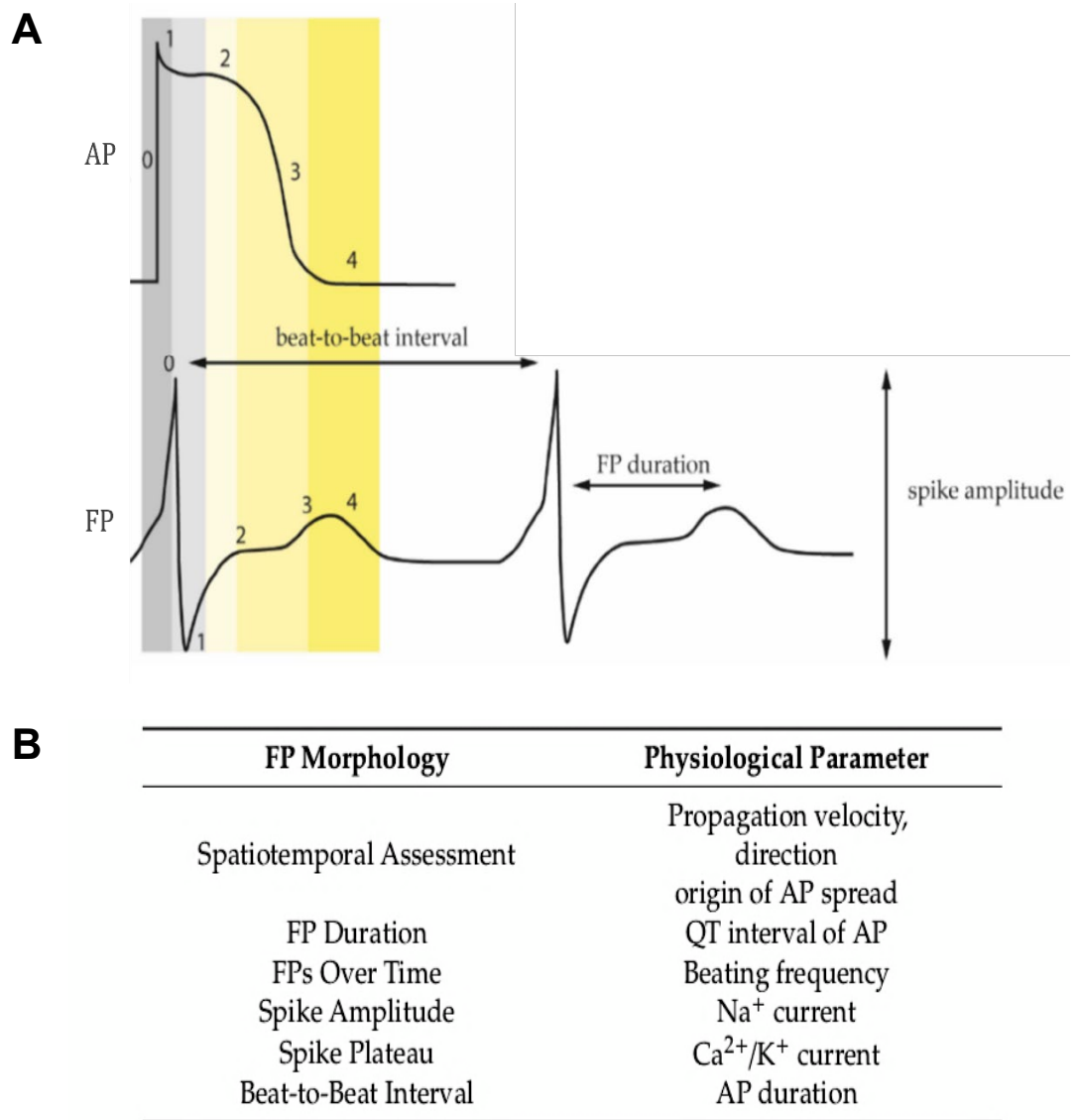
Figure 3. 8. **Functional parameters acquired by field potential measurements using MEA systems.** *Both AP and FP are describing the membrane potential of cardiomyocytes. (A) Comparison of recorded action potential and field potential at different phases of electrical signal movement in ventricular cardiomyocytes. (B) Important physiologic parameters of electrically active cells can be derived from field potentials. Action potential (AP); field potential (FP); field potential duration (FPD). Figures obtained from Kussauer et al (168).*

In this study, I used a standard microelectrode array 60MEA200/30iR-Ti-gr (Multichannel Systems, Germany) which can be autoclaved and coated for cell culture procedure and composed of 59 electrodes and one reference electrode that are organised in an 8 x 8 layout grid with electrode diameter of 30 μm and interelectrode distances of 200 μm (Multichannel Systems, Germany). The MEA signals were recorded using MultiChannel Experimenter and stored in MultiChannel Data Manager, where the data can be exported into HDF5 files for signal processing analysis. Electrode raw data acquired from the MEA chip is amplified by a filter amplifier with default settings for the hardware filter between 1 Hz to 3 kHz and digitised by the analog/digital converter that is integrated in the headstage at sampling rates at 10,000 Hz. The McsMatlabDataTools generated by a software from MultiChannel systems provide simple access to all MEA data using functions of MATLAB (MathWorks, USA). Figure 3. 10 illustrates the MEA data that were analysed using MATLAB and/or VCSF MEA Viewer, developed by Dr. Aled Rhys Jones, which relies mainly on MATLAB functions. Figure 3. 9 shows the general workflow of MEA experiment.

1 reference electrode
59 microelectrodes
8 x 8 layout grid
200 μm interelectrode distance
30 μm electrode diameter

MEA dish

Heat controller

Amplifying

Recording
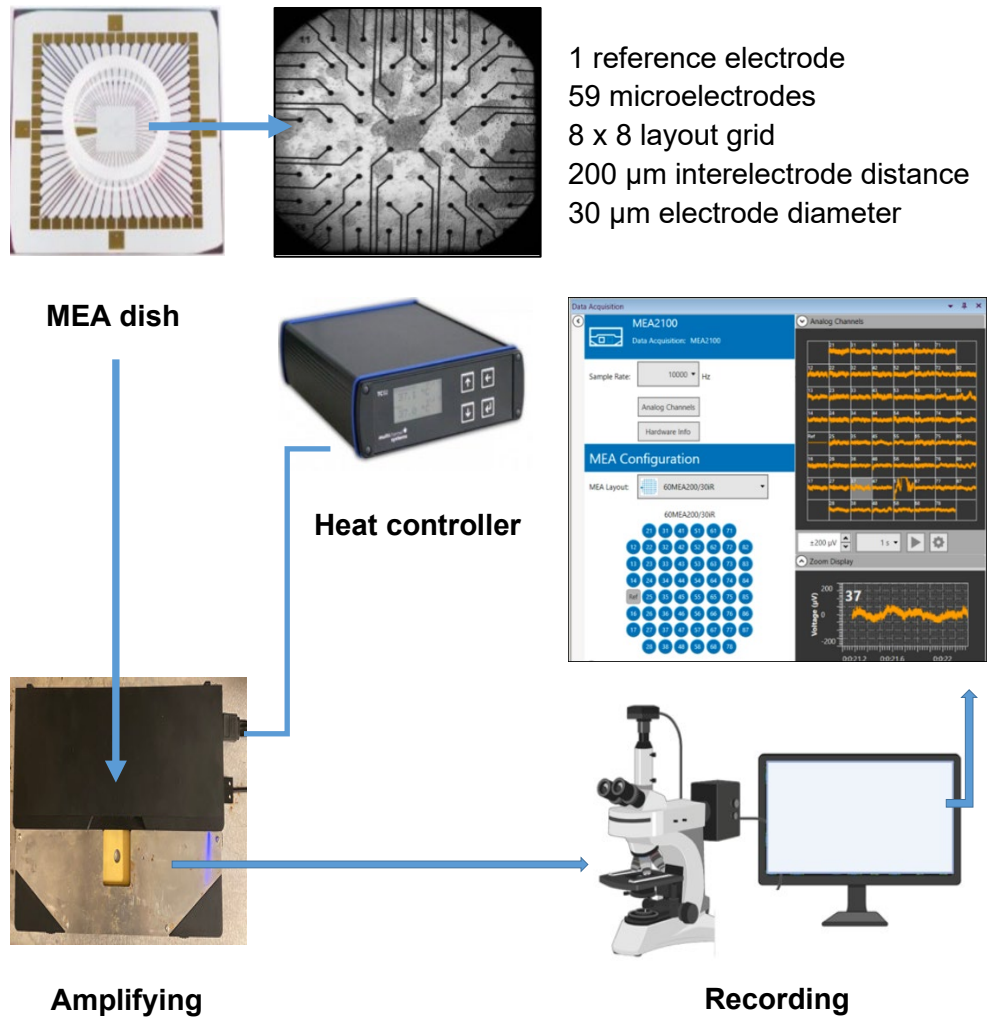
Figure 3. 9. **The general workflow of MEA experiment**. Adapted from Alayoubi (169).

A

B

116
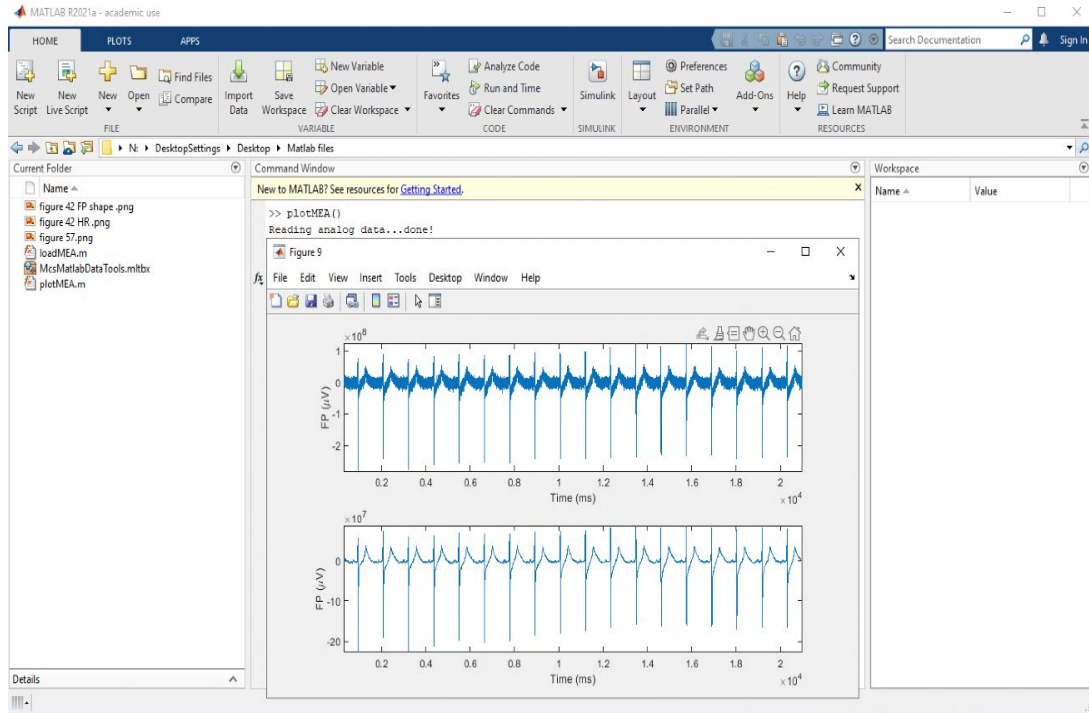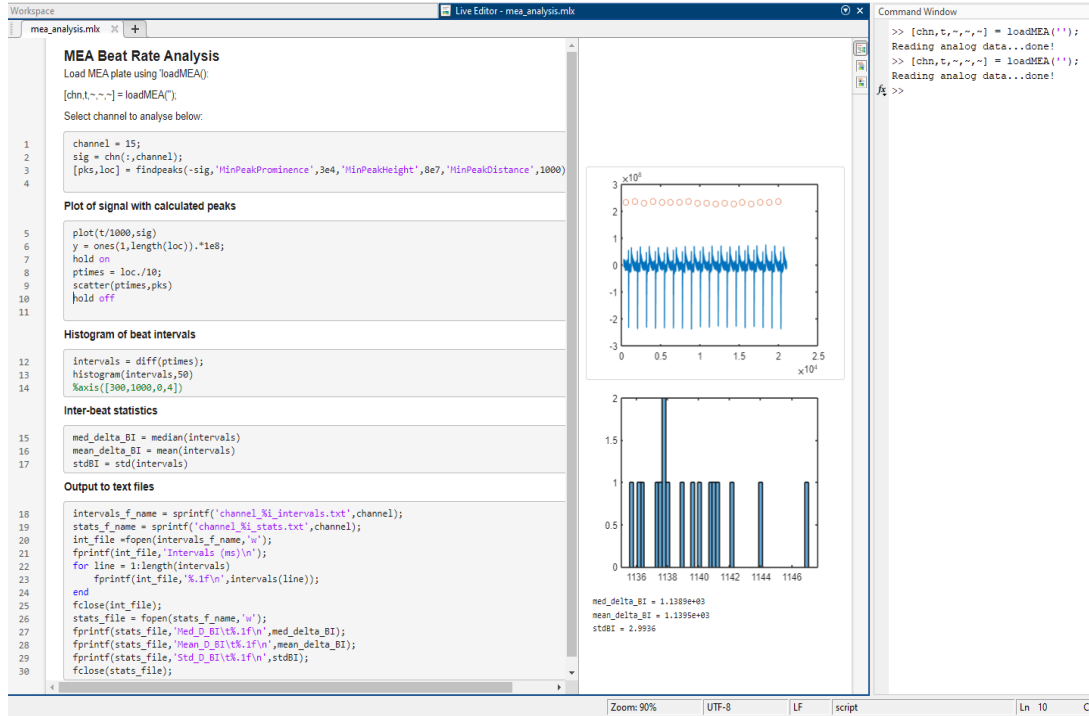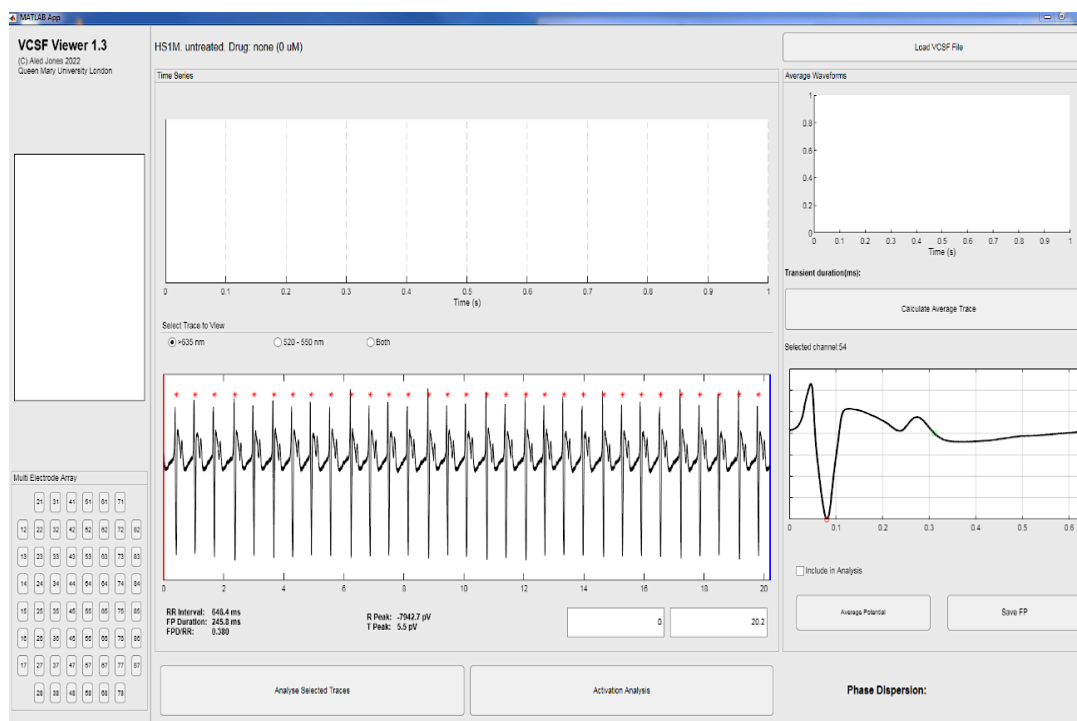
*Figure 3. 10. **(A) & (B) Screen shot of MATLAB functions used to analyse the MEA data**. These MATLAB scripts were created and developed in Tinker's laboratory at Queen Mary University of London by Dr. Aled Rhys Jones and allowed me to analyse the MEA traces and beat rate variability. (C) VCSF viewer is an alternative software, which was also developed by Dr. Aled Rhys Jones and was used to obtain MEA data, particularly RR interval and field potential duration.*

117

Initially, electrode chambers were coated with Matrigel or Geltrex and incubated for 1 hour at 37 °C. Next, the medium from the hiPSC-CMs was removed and rinsed once with 2-3 mL of PBS. After washing the cells, 3 mL of TryplE was added to the flask and moved to the incubator for 10-20 minutes at 37 °C. After that, 2 mL of Low insulin, BSA, polyvinylalcohol, essential lipids (LI-BPEL) medium (Table *4*) was added to dilute the dissociation enzyme and then 5ml pipette was used to detach the monolayer of hiPSC-CMs. The flask was rinsed with 2 mL of LI-BPEL to collect any remaining cells and a further 3 mL of LI-BPEL was added to obtain a total volume of 10 mL per flask. The cell suspension was collected in a 50 mL falcon tube and gently mixed up and down 3 times to dissociate cell clumps. Following that, cells were centrifuged at room temperature for 3 minutes at 300 x g, the supernatant aspirated, and cells resuspended in 2 mL of LI-BPEL. Approximately, 1 mL of cell suspension contain ~500,000 cells, which was sufficient to cover the area of the electrodes, was added to the MEA and transferring to a Petri dish prior to incubated overnight at 37 °C to facilitate cell attachment. Next day, cells were refreshed with 1 mL of LI-BPEL and incubated at 37 °C prior to electrophysiological assessment.

Table 4: LI-BPEL medium composition

Component	Supplier	Catalogue number	Quantity for 50 mL
Iscove's Modified Dulbecco's Medium (IMDM)	Thermo Fisher scientific	31980030	21.5 mL
F12 nutrient mixture + GlutaMax + Phenol Red	Thermo Fisher scientific	31765035	21.5 mL
Ascorbic Acid 2-phosphate (5mg/ml in distilled water)	Sigma-Aldrich	A8960	0.5 mL
Protein Free Hybridoma Medium-II (PFHMII)	Thermo Fisher scientific	12040077	2.5 mL
Bovine Serum Albumin (10% wt/vol in IMDM)	Sigma-Aldrich	A2153	1.25 mL
Chemically Defined Lipid Concentrate (CDLC)	Thermo Fisher scientific	11905031	0.5 mL
Poly Vinyl Alcohol (5% wt/vol in distilled water)	Sigma-Aldrich	341584	1.25 mL
Penicillin/ Streptomycin	Thermo Fisher scientific	15070063	0.25 mL
α-Monothioglycerol (13 μl in 1 mL IMDM)	Sigma-Aldrich	M1753	0.15 mL
Insulin-Transferrin- Selenium- Ethanolamine (ITS-X)	Thermo Fisher scientific	51500056	0.05 mL

3.7 *Parameter sensitive dyes for fluorescence imaging*

Normal and abnormal cardiomyocyte function is regulated by the EC coupling process, in which voltage waves are closely followed by calcium waves (Figure 1. 3). Pathological mutations as well as drug-triggering can disrupt and uncoupled these electro-mechanical waves of cardiomyocytes, leading to potentially lethal consequences. Through the use of hiPSC-CMs models, however, it is possible to treat and prevent cardiac arrhythmias by gaining a better understanding of the voltage-calcium dynamics at the cellular level, and possibly contribute to the development of drugs towards precision medicine ([170](#)).

In this study, hiPSC-CMs were plated on T25 flask prior to loading with fluorescent dyes. Initially, CMs were loaded with 3 µM calcium indicator Fluo-4 AM (#F14201, Invitrogen, ThermoFisher scientific, USA) and incubated for 20-30 minutes at room temperature. Cell cultures were then replaced with a fresh HBSS solution for recording calcium signals. Similarly, membrane potential signals from hiPSC-CM were assessed on T25 flask using voltage sensitive dye and loaded with 10 µM Di-4-ANEPPS (#61010 Biotium, Cambridge Biosciences, UK) for minimum 15 minutes in RPMI/B27 media supplemented with 1% penicillin/streptomycin at room temperature. Next, cell cultures were

replaced with a fresh RPMI/B27 plus antibiotic and containing 10uM Blebbistatin (#B0560; Sigma-Aldrich, USA). Blebbistatin is capable to minimise motion artefact and obtain improved electrophysiological phenotypes of hiPSC-CMs while recording cardiac AP as described previously ([171-174](#)). Cells were then placed in the incubator for approximately 30 minutes prior to voltage recording.

A Nikon Eclipse TE200 inverted microscope with image collection on C11440 complementary metal-oxide semiconductor (CMOS) camera (Hamamatsu corporation, Shizuoka, Japan) mounted on a beam splitter (MAG Biosystems, USA) were jointly used for live cell imaging (Figure 3. 12). The Fluo-4 AM and Di-4- ANEPPS fluorescence were excited using OptoLED light source by plan Fluor 20x and 10x objective lens, respectively. Peak excitation wavelength for Fluo-4 AM is at 488nm and emits a colour between green and yellow. On the other hand, Di-4-ANEPPS is excited at 496 nm and emits a red light **(**Figure 3. 11**)**. Light-emitting diodes (LEDs) are now widely used for fluorescence excitation and associated with setups that were supplied by Cairn Research Ltd (Kent, UK). It should be noted that when cells are illuminated using an OptoLED light source, the light wavelength is not a single wavelength (e.g., 488nm for Fluo-4 AM), unlike confocal microscopes with a single

laser. Rather, there is a small band of wavelengths originating from the LED that are filtered before the light reaches the cells ([158], [175]). For example, a green LED used for Fluo-4 AM fluorescence (calcium) was bandpass filtered (500 ± 10 nm) equipped with an optical filter to constrict the excitation band (ET500/20x, Chroma, USA), and blue LED used for Di-4-ANEPPS fluorescence (voltage) was acquired via a bandpass filter (448 ± 9.5 nm) with excitation filter (ET448/19x, Chroma, USA). An emission filter (ET535/30m, Chroma, USA) was positioned in the optical pathway of the fluorescence camera to block the excitation beam background, as described previously ([170]).
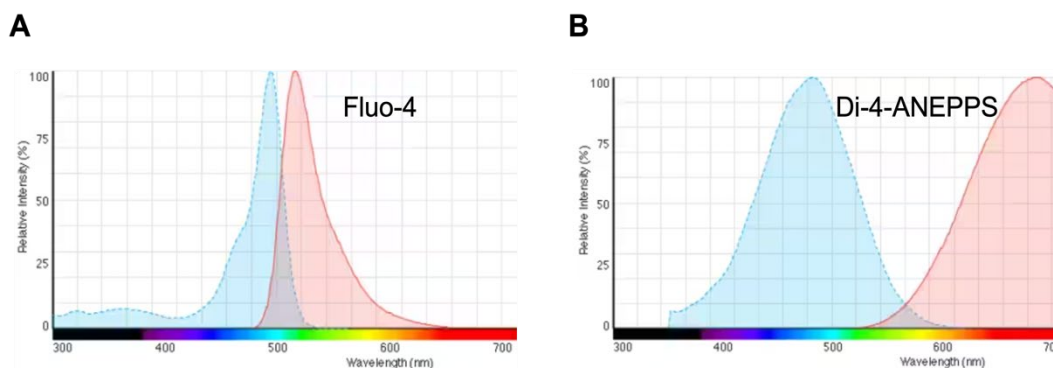
Figure 3. 11. Absorption and emission profile of Di-4-ANEPPS and Fluo-4 Ca2+ indicator dye. *(A) The Fluo-4 organic dye used as calcium indicator and has a peak absorption around 490 nm and emission at around 520 nm (ThermoFisher Scientific, USA). (B) Di-4-ANEPPS is a membrane potential dye that can responds rapidly to alterations in membrane potential with changes in fluorescence excitation intensity (in the blue-green band) at approximately 496nm and emission at around 705nm (Biotium, Cambridge Biosciences, UK; ThermoFisher Scientific, USA).*

HCImage Live application (Hamamatsu corporation, Shizuoka, Japan) was carried out for image acquisition. The hiPSC-CMs were imaged at an acquisition rate of 50 frames per second. The imaging subsets used for channel subarray were: X0: 400, Y0: 700, width: 1300, and height: 600. During the recording, the LED green light source was turned on to obtain video image while still being able to discern calcium fluctuations. Likewise, the LED blue light source was used to detect flashes of voltage signal changes. The images were saved as .TIFF files and processed by C++ programming language, by using windows command, to convert the images into VCSF files for analysing the optical signals. The recording process is illustrated in (Figure 3. 12).
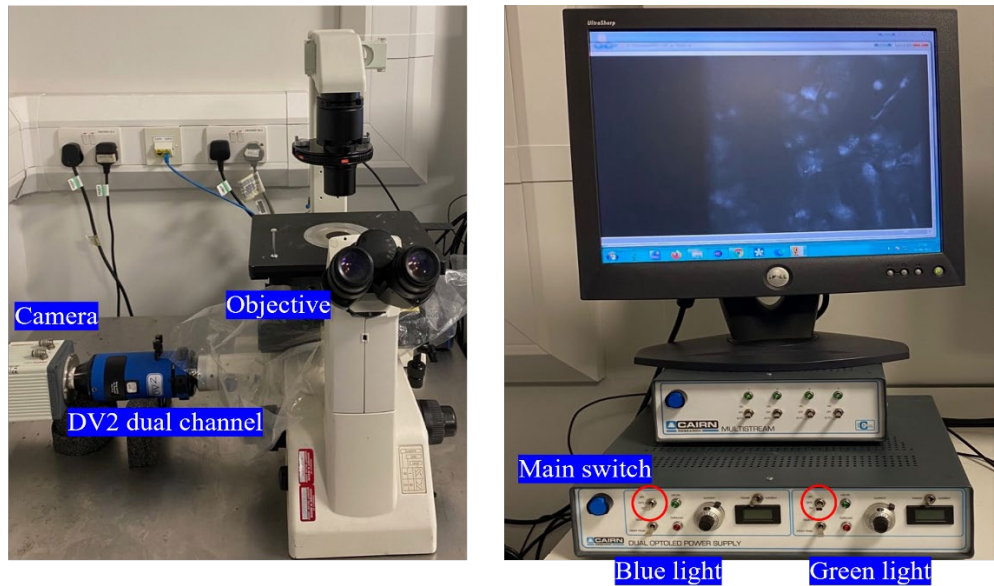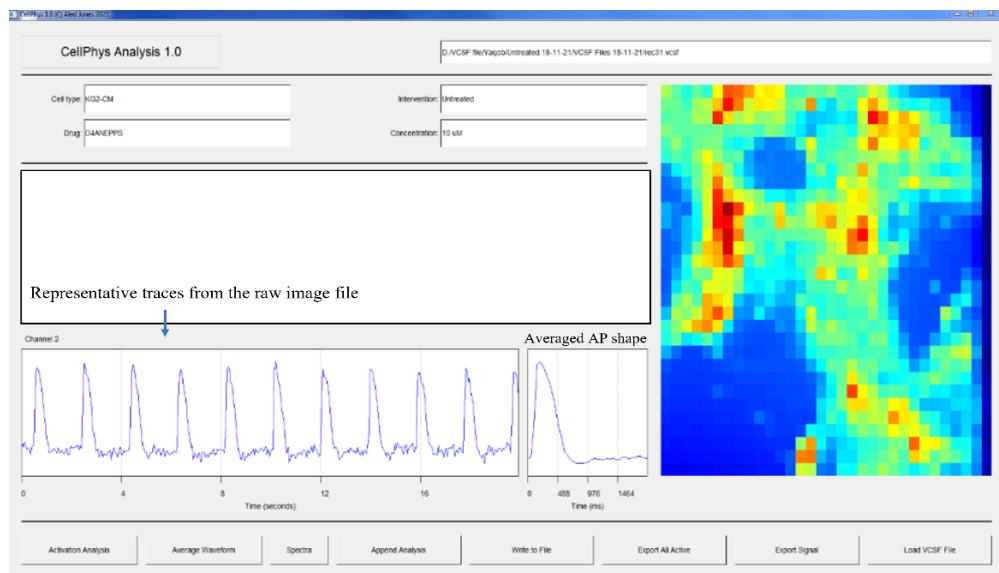
*Figure 3. 12. **Diagram of the fluorescence imaging setup**.(A) basic wide-field system comprised of inverted microscope, suitable objective lens, OptoLED light source, camera based on CMOS sensors, appropriate filters to separate excitation and emission light, and DV2 beamsplitter to separate two emission channels based on wavelength, polarisation or amplitude. HCImage Live was used for image acquisition and processing. MultiStream device was used to synchronise the LEDs with CMOS camera to allow for multi-wavelength excitation for ratiometric measurements, although was not effective in this study.(B) CellPhys 1.0 VCSF software has been developed by Dr.Aled Rhys Jones at Queen Mary University of London and used to analyse the optical signals.*

3.7.1 _**Drugs used in optical recordings**_

Drugs used on voltage recordings of hiPSC-CMs with siRNA-FLNC are isoprenaline (Sigma Aldrich, # I5637, USA) and nifedipine (Sigma Aldrich, # N7634, USA). Isoprenaline is a beta-adrenergic agonist, which stimulates adenyl cyclase and increases cAMP activating downstream signalling. Physiologically, when cAMP rises it activates protein kinase A, which phosphorylates various substrates implicated in EC coupling process, including phospholamban, L-type calcium current, RyR, and the slowly inactivating delayed rectifier (I_{ks}) altogether. The activation of L-type calcium channel triggers the increase of calcium and CICR from the SR leading to the calcium transient, and thereby eliciting contraction force. Increasing beating rate of hiPSC-CMs and shortening of APD were detected with isoprenaline (10µM) as observed previously ([176](#)). The other drug was used in this study is L-type calcium channel blocker, nifedipine. Indeed, the L-type calcium channels are known to play an important role in EC coupling in hiPSC-CMs. Since the external calcium is fundamental for triggering SR calcium release, block these channels using nifedipine can completely suppress calcium transients in hiPSC-CMs. Therefore, complete block of L-type calcium channel with nifedipine (10µM) can cause a dramatic shortening in the AP and potentially eliminates EAD-like events ([177-179](#)).

3.8 *Patch Clamp Recordings from hiPSC-CMs*

3.8.1 *The Patch Clamp Technique*

Patch clamp is a technique used to study the function of ion channels of excitable cells, such as neurones and cardiomyocytes. The passage of ionic currents through ion channels, or the changes in V_m of excitable cells such as cardiomyocytes, are governed by Ohm's law. Ohm's law describes the relationship between voltage (measured in volts, V), current (measured in amperes, I) and resistance, which is a measure of how easily the current can flows between two different solutions (measured in Ohms, Ω). Ohm's law states ([21](), [180]()):

$$V = IR$$

The inverse of resistance is conductance, Ohm's law can also be written as follows:

$$I = gV$$

The cell's membrane provides a high resistance barrier to the flow of ions across it. When ion channels open, the resistance to the ions flowing across the membrane decreases ([21]()). The increased flow of ions can be measured in real time with the patch clamp technique.

Alan Hodgkin and Andrew Huxley ([181](#)) were the early pioneers of recording cellular electrical activity when they recorded action potentials and sodium and potassium currents from the squid giant axon, thus laying the foundations for the modern electrophysiology. Building on the work of Hodgkin and Huxley and others, Bert Sakmann and Erwin Neher were able to obtain a high resistance seal on a patch of cell membrane called a giga-seal patch by using a fire-polished glass electrode and successfully measured the opening and closing of single ion channels ([182](#), [183](#)).

The plasma membrane of most living cells are electrically polarised due to the presence of membrane potential. The driving force that determines the passive transport of solutes across a permeable membrane is the electrochemical gradients between two compartments. This driving force serves as energy stored in the cell and can be used to drive a variety of transport processes across the cell membrane ([21](#)). Given the ability of the cell membrane to tightly regulate the osmolarity difference between intracellular and extracellular fluids, the concentration gradient of certain ions like Na^+, K^+, Ca^{2+} and Cl^- vary accordingly ([21](#)). Indeed, the membrane separates the unequal distribution of positive and negative ions, and hence makes a difference

in the charge between the cell's interior and exterior. Because membrane charging and discharging requires time, the cell membrane acts as a capacitor by separating and storing electrical charge, and hence slows down changes in the Vm (184).

3.8.2 *Model Electrical circuit for whole-cell patch clamp*

The patch clamp technique allows the measurement of current and voltage in response to changes in both membrane parameters. A patch clamp amplifier carriers out these measurements with the aid of an electrical circuit (Figure 3. 13). When the pipette filled with intracellular solution enters the bath (extracellular solution), a circuit is formed between the amplifier, electrode and bath electrode allowing measurement of the resistance of the pipette (Rp). The pipette also acts as a capacitor (Cp) as it forms barrier between two conducing solutions- this pipette capacitance can be compensated for by the amplifier. After formation of a high resistance seal and subsequent rupture of the cell membrane, the bath-electrode circuit is reformed with the addition of two resistor, access (Ra) and membrane (Rm) (Figure 3. 13). Here, a low access resistance is desirable to allow for increased flow of current; ideally the membrane resistance would remain high to keep 'leak' minimal (185).

The membrane also acts as a capacitor (Cm), the build-up of charge in response to voltage steps and subsequent decay can be measured and is indicative of the cell surface area. This estimate of cell

size can be used to normalise whole-cell currents to cell size. As with Cp, Cm can also be compensated by the amplifier circuitry.

The sum of all the resistances between Rp, Ra and Rm is known as 'series resistance'. This is predominantly the sum of Rp and Ra. Series resistance can be problematic because it can cause errors in the actual voltage the membrane is clamped at as well as a delay in voltage step changes. This can be especially problematic when the membrane current is large. Series resistance can be compensated for the most part (80%-90%) by the patch clamp amplifier (184).

3.8.3   *Whole-Cell Recordings*

In this thesis all patch clamp recordings were made in the whole-cell configuration. The intracellular solution used for whole-cell recordings consisted of:

Compound	Concentration (mM)	Supplier	Catalogue number
K-gluconate	110	Sigma Aldrich, USA	G4500
KCl	20	Sigma Aldrich, USA	P9333
NaCl	10	Sigma Aldrich, USA	S7653
$MgCl_2$	1	Sigma Aldrich, USA	M1028
MgATP	2	Sigma Aldrich, USA	A9187
EGTA	2	Sigma Aldrich, USA	E3889
Na_2GTP	0.3	Sigma Aldrich, USA	G8877
HEPES	10	Sigma Aldrich, USA	H3375

The pH was adjusted to 7.3 with 5M KOH. The extracellular (bath) solution consisted of:

Compound	Concentration (mM)	Supplier	Catalogue number
NaCl	130	Sigma Aldrich, USA	S7653
KCl	4	Sigma Aldrich, USA	P9333
CaCl (1M)	1.8	Sigma Aldrich, USA	21115
MgCl (1M)	1	Sigma Aldrich, USA	M1028
Glucose	10	Sigma Aldrich, USA	G5767
HEPES	10	Sigma Aldrich, USA	H3375

The pH was adjusted to 7.4 with 5M NaOH.
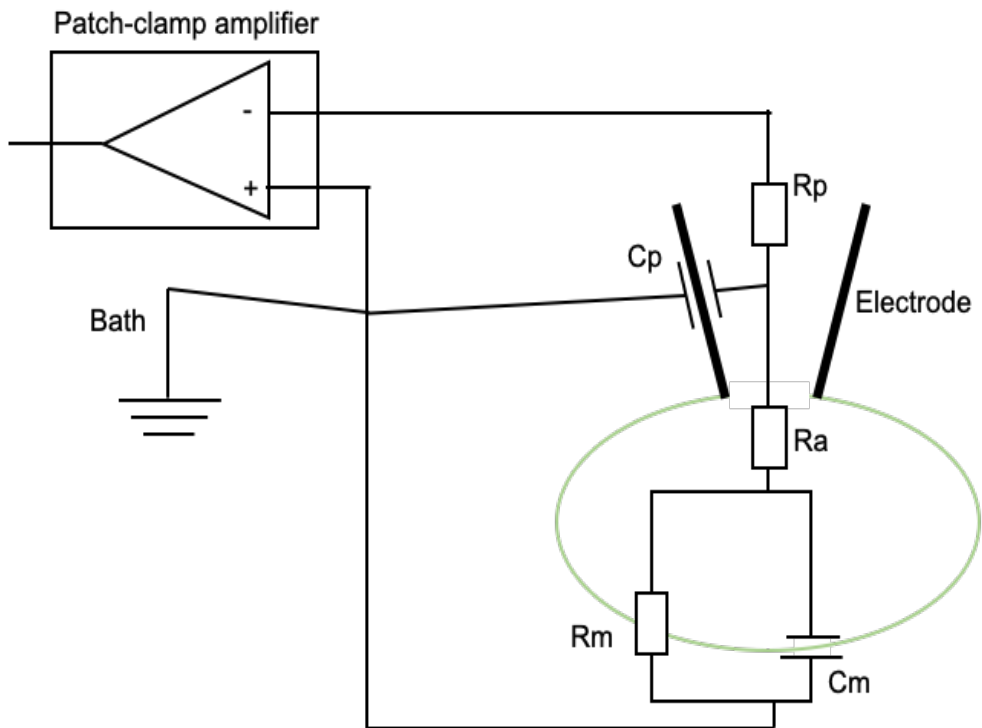
Figure 3. 13: **The equivalent electrical circuit depicted for the whole-cell patch clamp configuration**. *The schematic shows the electrical circuit established after rupture of the cell membrane to allow access to the inside of the cell. Pipette (Cp) and whole-cell membrane capacitance (Cm) are compensated for by the amplifier. Access resistance (Ra) needs to be sufficiently low (<12 MΩ for voltage-clamp recordings and <30 MΩ for current-clamp recordings) for adequate resolution of ion flow.*

Typically, cells were plated on the 10 mm glass coverslips (thickness No.1, VWR International Ltd, UK) at a density of ~300,000 cells per well and coated with 0.1% gelatin-in individual wells of a 24-well plate.

A two-stage puller was used to make micropipettes from thin wall filament borosilicate capillary glass (1.5 mm outer diameter x 1.17 mm internal diameter x 100 mm length; #GC150TF-10, Harvard Apparatus, USA) at resistance of 2-4 MΩ. The gravity-driven perfusion system was primed with experimental solutions prior to commencing experiments. On the motorised stage of an inverted microscope (Olympus IX71, Tokyo, Japan), the prepared coverslips were placed in the bath (Figure 3. 14). The micropipette was mounted onto a pipette holder attached to the headstage and was lowered into the bath using a piezo-electric micromanipulator (Scientifica Ltd, UK). Subsequently, the micropipette was manoeuvred on to the cell, causing the resistance to slightly increase (Figure 3. 15). A gentle suction was applied, using a 1 mL syringe attached to suction tubing and a pipette holder, in order to form a seal between the membrane and glass. The suction is released once membrane resistance reaches >1 GΩ. The micropipette acts as a capacitor due to the fact that it separates the two conducing solutions (185). Capacitance compensation for the pipette was applied at this stage. Following this, a further light suction was applied to break the

membrane to facilitate electrical access to the whole cell "whole-cell patch mode" via the internal pipette electrode. Whole cell capacitance and series resistance were compensated at this stage.

Using amplifier circuitry (MultiClamp 700B), capacitance transients and series resistance were compensated electronically. Data were filtered at 2 kHz (four-pole Bessel) and sampled at 10 kHz using a Digidata 1550B (Axon Instruments). I used pClamp10.6 (Axon Instruments) to record and analyse the ionic currents. A current-voltage protocol (adapted from Luca Sala ([186])) to record hERG currents from hiPSC-CMs was as follows: the cells were held at -40 mV and stepped from -40 mV to +30 mV in 10 mV increments for 2 seconds and then back to -40 mV to measure the tail current (Figure 3. 16). For data analysis, only cells with membrane resistance >800 MΩ and access resistance <12 MΩ were used. All recordings were carried out at room temperature. For data analysis, Clampfit 11.1 software (Molecular Devices, USA), MATLAB (Mathworks, USA) and GraphPad Prism 9 were used.

Whole-cell spontaneous APs were recorded using the current-clamp configuration. Data were analysed with Clampfit 11.1 (Molecular Devices, USA). After 3 minutes dialysis spontaneous APs were recorded for 2 minutes. The last 10 APs of each recording period were averaged. Measurement of AP parameters were taken as shown in the schematic example in (Figure 3. 17).
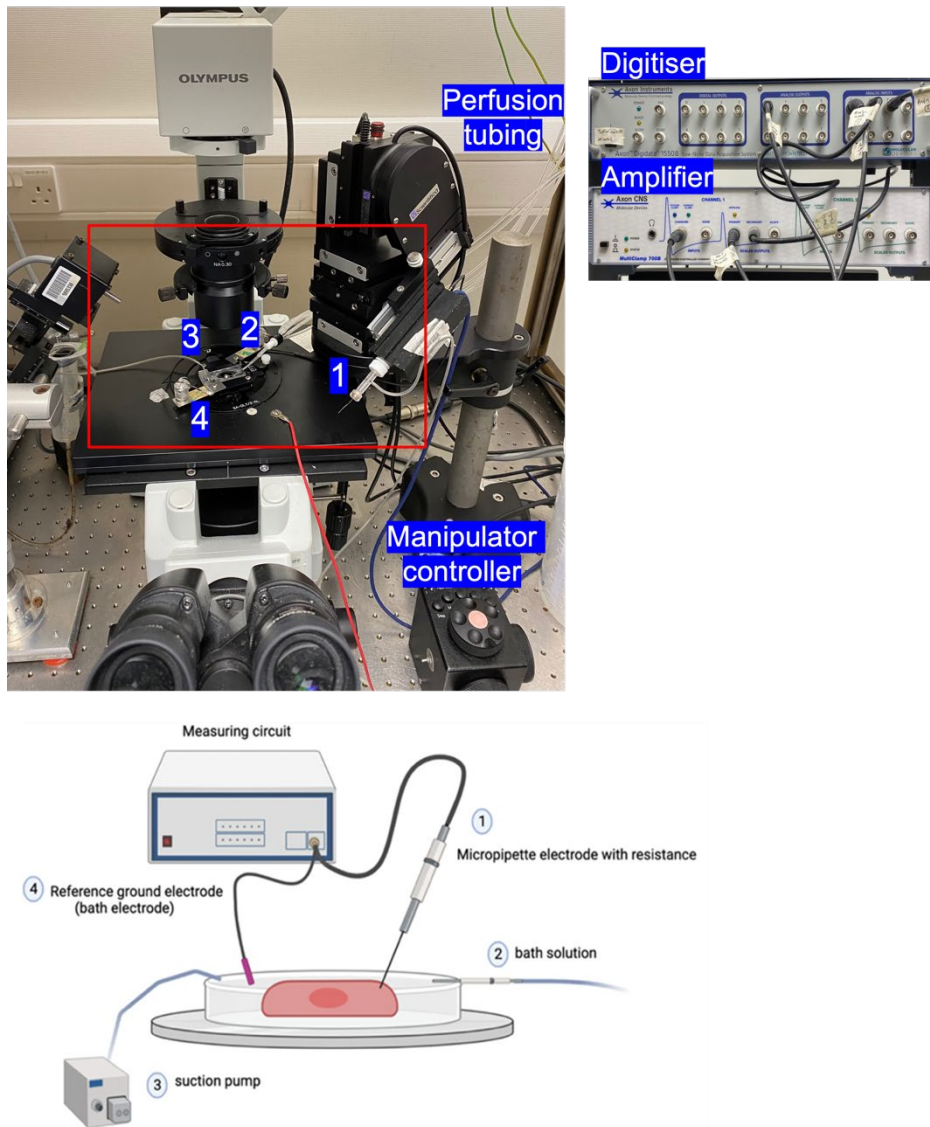
*Figure 3. 14. **Experimental setup for patch clamp recordings (Actual and schematic).** A photograph of the patch clamp setup sued for whole-cell recordings showing the microscope with recording platform (4), pipette headstage (1), perfusion inflow (2) and outflow (3). A Multiclamp 700B amplifier and 1550B digitiser were used. Created with Biorender.com.*
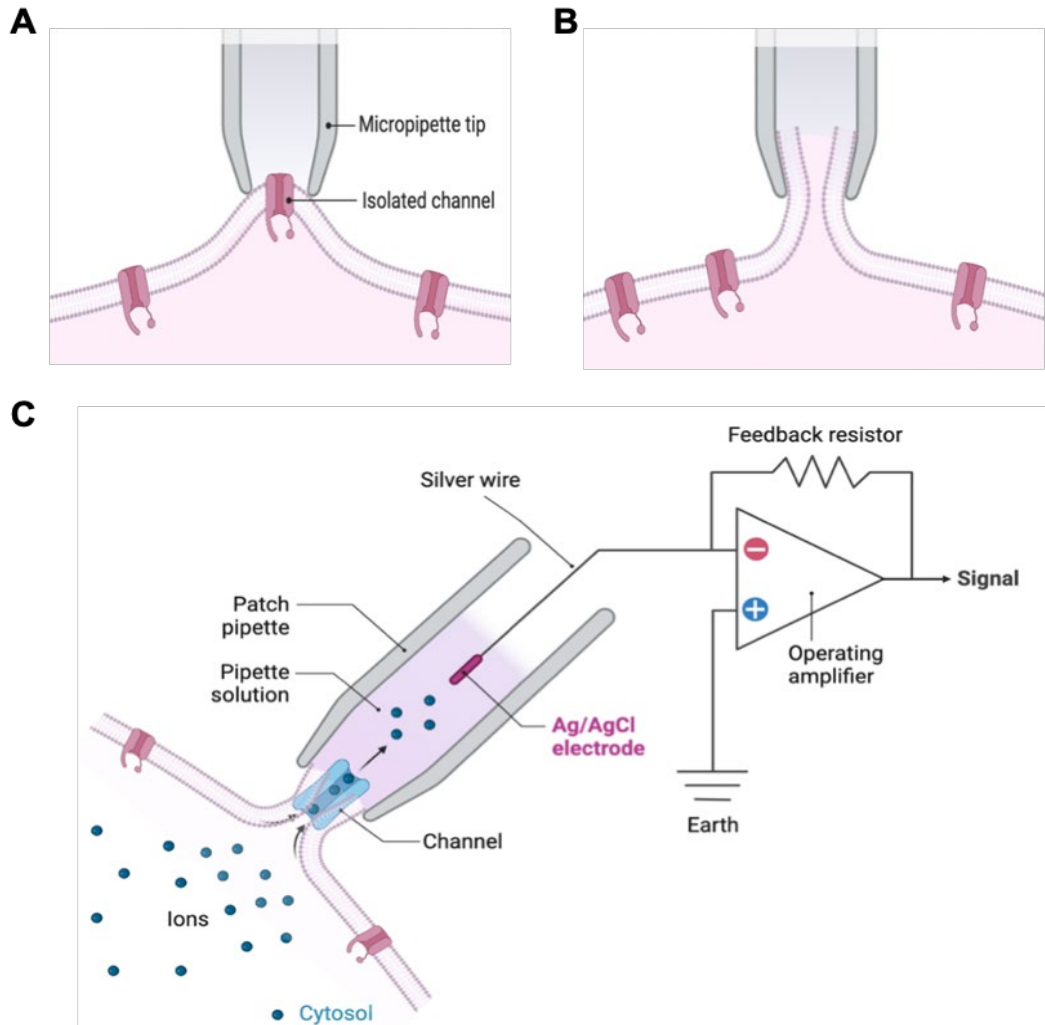
Figure 3. 15. **Schematic of the patch clamp technique.** *Patch clamp involves the use of a glass micropipette that is placed on to single cell (ideally pipette resistance inside the bath should be between 2-4 MΩ). Gentle suction after touching the cell with the micropipette facilitates the formation of a tight electrical seal- this is the cell -attached patch configuration which allows the measurement of current flow from single ion channels (A). The whole-cell configuration is achieved by additional negative pressure until the membrane ruptures allowing access to the inside of the cell and measurement of whole-cell currents (B). Following membrane rupture, the pipette-bath (Ag/AgCl) electrode circuit is reformed – but now moves through two different resistors (C). The cytoplasmic 'access' acts as a resistor, whilst the membrane should ideally function as a high ohmic resistor. Low access resistance is necessary for optimal whole-cell conditions, while maintaining high seal and membrane resistance. The amplifier can now measure the membrane's current flow in response to voltage alterations. Created with Biorender.com.*
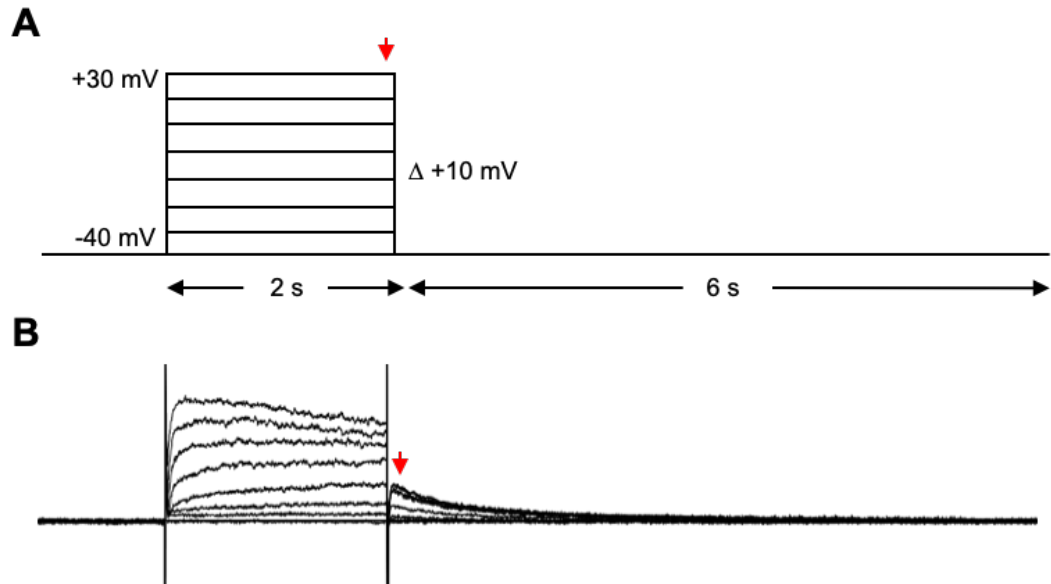
Figure 3. 16. **Representative voltage-gated ionic current traces of the hERG channel from hiPSC-CMs.** *(A). Voltage protocol used to measure hERG currents. Cells were voltage-clamped at a holding potential of -40 mV stepped sequentially to +30 mV for 2 seconds in 10 mV increments before returning to -40 mV. (B). Typical recording of Ikr current, showing a 2 seconds of slow channel activation followed by a slowly inactivating tail current at -40 mV. The red arrows denote the measurement of tail current following each test potential.*
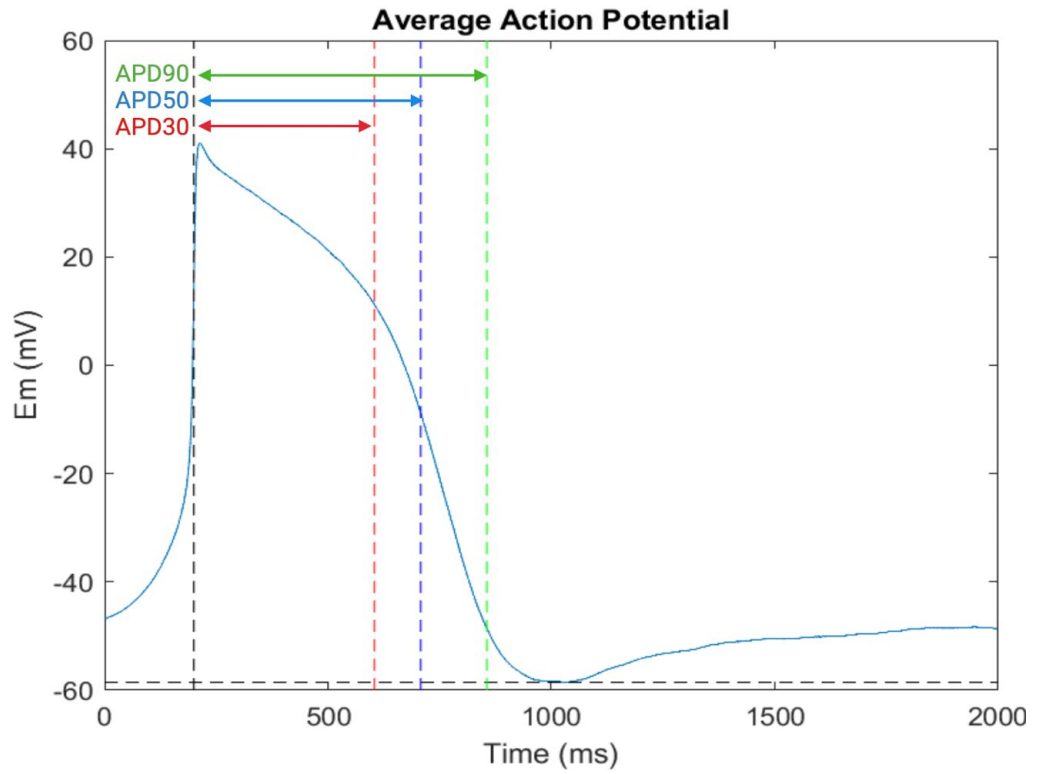
*Figure 3. 17. **An averaged action potential from hiPSC-CMs** illustrating the measurement of AP ;parameters using a custom MATLAB script (Dr. Aled Rhys Jones at Queen Mary University of London). Shown are the averaged waveform, AP amplitude, and AP durations (APD) at 30%/50%/90% maximum of delta voltage.*

3.9 *Statistical analyses*

GraphPad Prism 9 software was used for the statistical analysis. All data were reported as mean±SEM. All differences amongst untreated, scrambled, and siRNA-FLNC were compared with one-way ANOVA test. An unpaired t-test was used to compare action potential parameters of hiPSC-CMs between scrambled and siRNA-FLNC in patch-clamp recordings. The Pearson correlation coefficient was conducted for FPD-RR relationship. Paired t-test (two-tailed) was used to analyse statistical differences of data before and after application of isoprenaline. Histogram and scatter dot analysis were performed to plot the interbeat intervals for the assessment of the beat rate variability. A two-way ANOVA was used to analyse the tail currents between scrambled and siRNA-FLNC groups. On graphs the n number denotes the replication of the experiment, and *** indicates P<0.001; **P<0.01; and *P<0.05.

Chapter 4 : Results - Characterisation and expression of FLNC knockdown in hiPSC-derived cardiomyocytes

4.1 *Introduction*

siRNA-transfection was introduced into hiPSC-CMs in vitro to investigate the effect of knockdown of FLNC expression on the function and distribution of various proteins that are involved in AC disease. FLNC is located at IDs in the fascia adherens where ends of myofiber can reach to the sarcolemma, close to the site of desmosomal junctions (11). Therefore, immunofluorescence staining and western blotting of differentiated cardiomyocyte monolayers were performed for characterisation of the protein expression and subcellular localisation in the hiPSC-CMs for FLNC, Cx43, Nav1.5, and desmosomal proteins (DSP, plakoglobin, and plakophilin-2).

In the present study, hiPSC-CMs were plated as monolayers in T25 flask or 24- well plates and showed spontaneous beating upon visual inspection. Figure 4. 1 illustrates the schematic of chemically defined cardiac differentiation including the purification method using lactate enrichment and optional expansion of hiPSC-CMs between day 12 and day 20. Burridge and others have generally divided the cardiac differentiation into three phases for systemic optimisation: phase 1, uniform undifferentiation hPSC growth; phase 2, mesoderm formation and induction; and phase 3, cardiac specification and maturation (149).
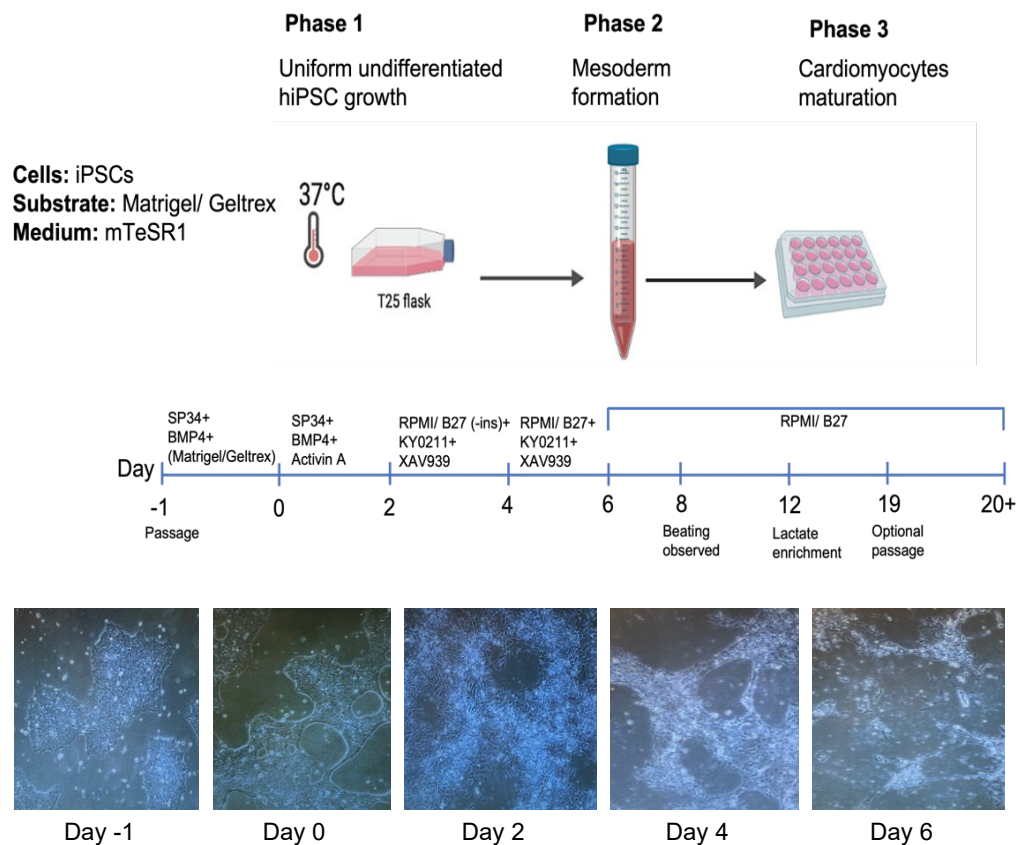
Figure 4. 1. **Timeline of the protocol for differentiation of CMs from hiPSCs**. *Phase 1, uniform growth of hiPSC as monolayer ([149]). Phase 2 (day 0 – day 2), Wnt/β-catenin signalling is initially stimulated in differentiation process and then inhibited after mesoderm formation ([142]).Phase 3 (day 2 – day 4), combined use of Wnt inhibitors (KY0211 and XAV939) are essential for cardiac specification and maturation. Supplementing B27 minus Insulin in day 2 is necessary to avoid suppression of cardiac differentiation during the first five days ([146]).*

143

4.2 *Immunofluorescence staining of differentiated hiPSC-CMs for the cardiac-specific markers*

Initially, the cardiac differentiation of hiPSC-CMs was confirmed by the staining of sarcomeric cardiac troponin T and cell adhesion molecules (N-cadherin) using appropriate secondary antibodies.
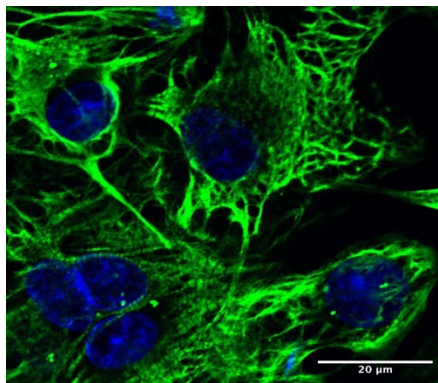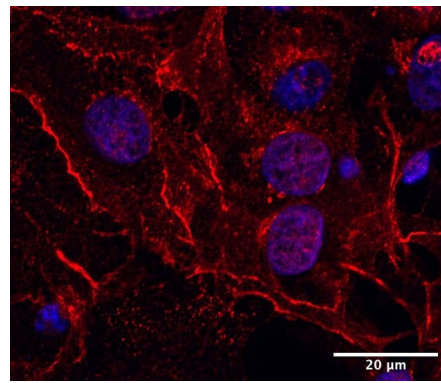
Troponin T: DAPI   **N-cadherin: DAPI**

4.3 *Effects of siRNA-silencing on proteins of interest*

Before siRNA treatment   **After siRNA treatment**

DSP: DAPI   DSP: siGLO: DAPI

Plakoglobin: DAPI   Plakoglobin: siGLO: DAPI

Cx43: DAPI   Cx43: siGLO: DAPI

Nav1.5: DAPI   Nav1.5: siGLO: DAPI
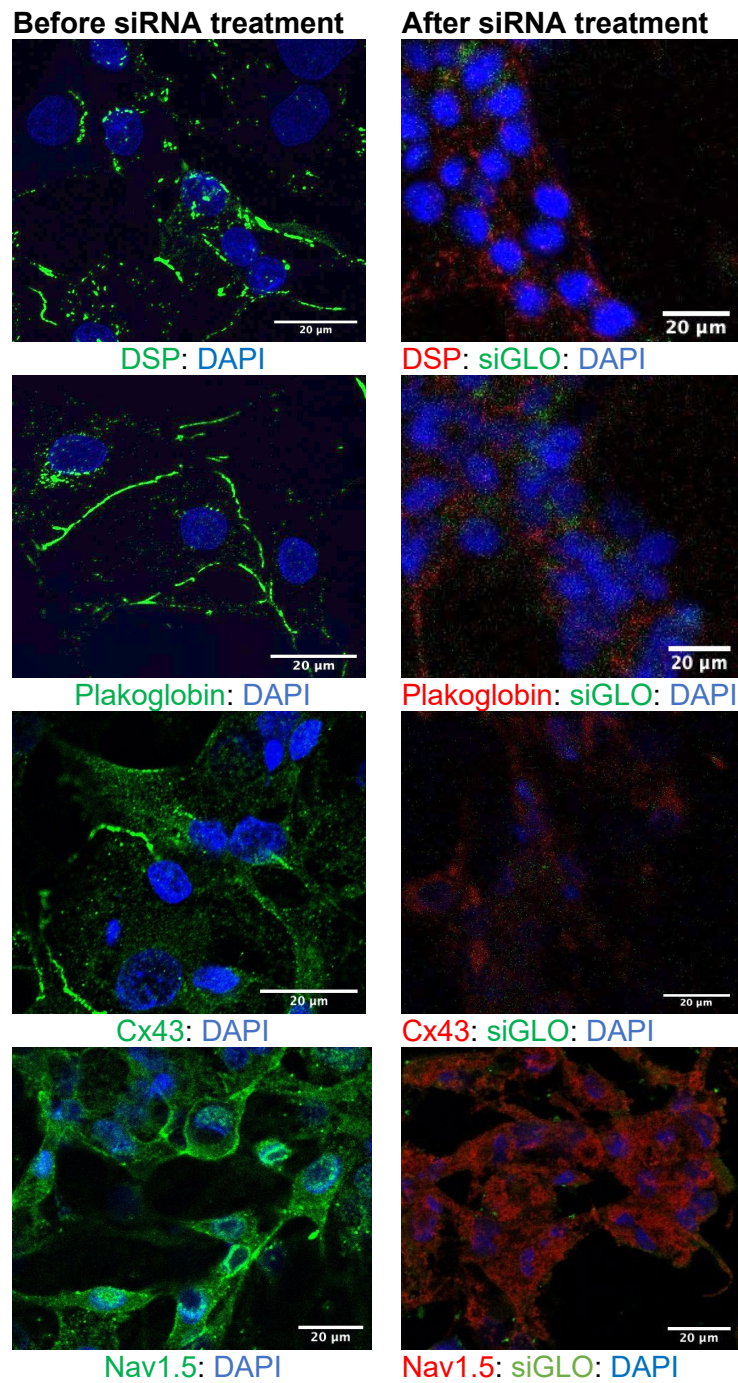
4.4 *Immunofluorescence staining for FLNC and Cx43/Nav1.5 proteins after treatment with siRNA to FLNC*

hiPSC-CMs were imaged using a Zeiss CLSM710 microscope under three different conditions and showed positive staining for siGLO. Initially, a transfection concentration of 10nM siRNA for 48 hours was used for mRNA analysis, but no significant changes ($P > 0.05$) were observed (Figure 4. 2). As a result, the transfected cells were tested again at higher concentrations either 20nM or 40nM and incubated longer for 72 hours for protein analysis. There was a pronounced decrease ($P < 0.01$) in immunofluorescence signals for FLNC (Figure 4. 3) and in addition Cx43 ($P < 0.05$) signals (Figure 4. 4) when the siRNA concentration was increased to 40nM. However, the levels of staining for Nav1.5 were not significantly changed ($P > 0.05$) following siRNA-knockdown of FLNC when compared with scrambled and untreated cells (Figure 4. 5). The immunofluorescence signals of desmosomal proteins (plakoglobin and DSP) in hiPSC-CMs (Figure 4. 6) were also significantly reduced ($P < 0.05$) compared with untreated and scrambled control when transfected with siRNA to FLNC. The staining intensity of Plakophilin-2 (Figure 4. 6) displays comparable levels ($P > 0.05$) among the three different conditions (untreated, scrambled, siRNA-FLNC).

146

Western blot analysis was conducted to measure the effect of siRNA-FLNC treatment on the expression of FLNC, Cx43, and Nav1.5 proteins in hiPSC-CMs. Similar to what was shown by immunofluorescence imaging, expression levels of FLNC and Cx43 were reduced following siRNA-FLNC, but the expression level of Nav1.5 was not obviously changed when compared with untreated and scrambled treatments.

A

FLNC siRNA – 10nM (48 hours)

B

FLNC siRNA – 20nM (72 hours)

FLNC   Cx43   Nav1.5

C
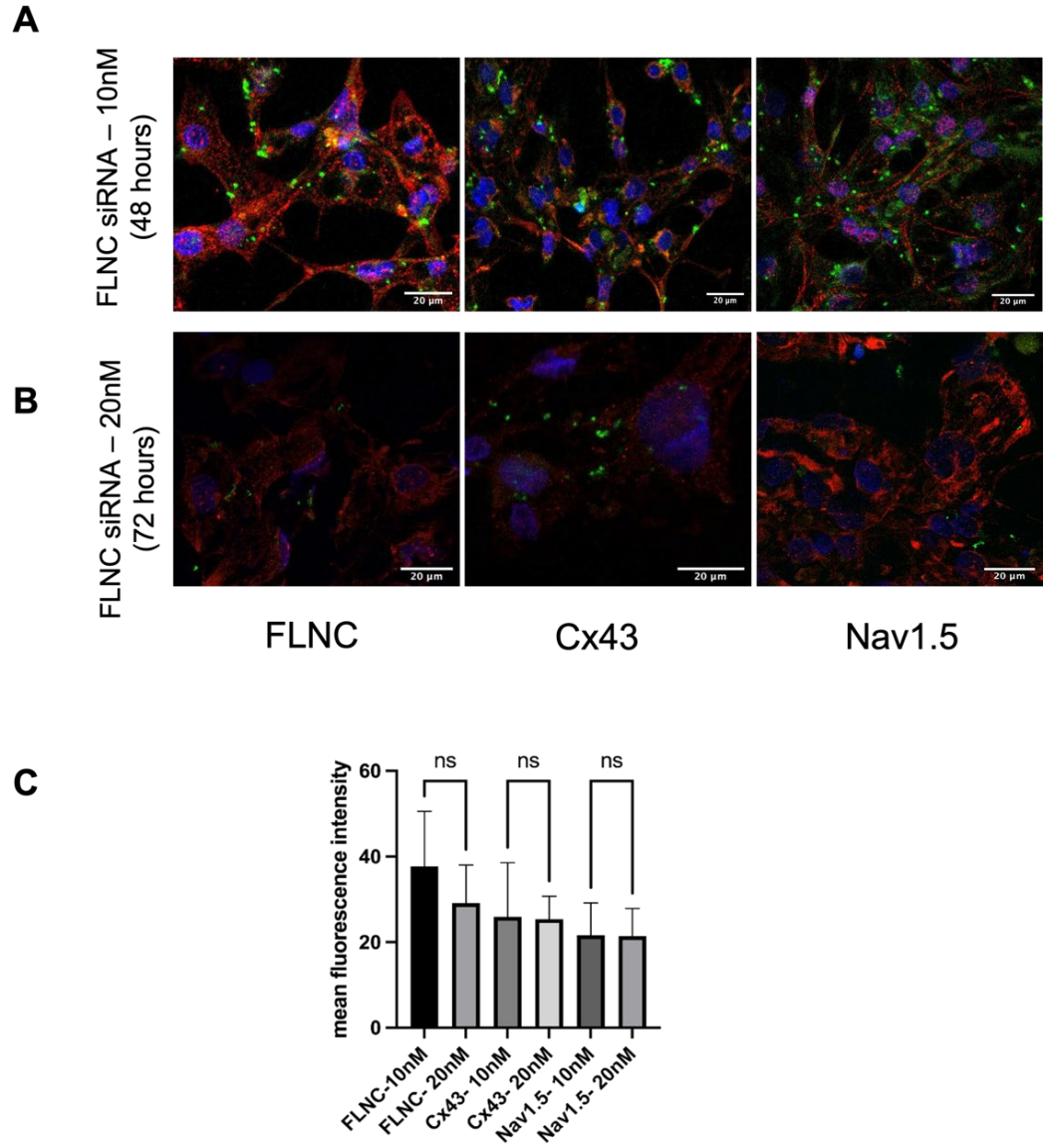
*Figure 4. 2. **Effect of FLNC siRNA on FLNC, Cx43, and Nav1.5**. (A) & (B) Representative immunofluoresence images of hiPSC-CMs cultures treated for 48 or 72 h with 10nM or 20nM siRNA-FLNC, respectively. (C) The Image J software was used to perform quantitative analysis of the mean staining intensity of FLNC, Cx43, Nav1.5 following treatement with siRNA-FLNC. Quantitative evaluation of the staining intenstiy at 10nM concentration of siRNA transfection for FLNC (n=3), Cx43 (n=2), and Nav1.5 (n=3) have shown similar levels of staining (P>0.05). A slight decrease in FLNC(n=9) and Cx43 (n=3) signals was only observed in comparison with untreated and scrambled when cells treated for 72 h at 20 nM, although not statistically significant (P>0.05). siRNA-FLNC causes signifcant Cx43 mis-localisation whereas Nav1.5 and FLNC were retained intracellulary. Similar levels of staining for Nav1.5 (n=3) were detected for hiPSC-CMs following siRNA-FLNC when compared with control samples. FLNC, Cx43, and Nav1.5 stained red, siGLO stained green, and cell nuclei stained blue with DAPI. Overall, P>0.05 by one-way ANOVA among the 6 groups.*

4.4.1 _Representative immunofluorescence images of FLNC_

A

| FLNC | siGLO | DAPI | Merge |
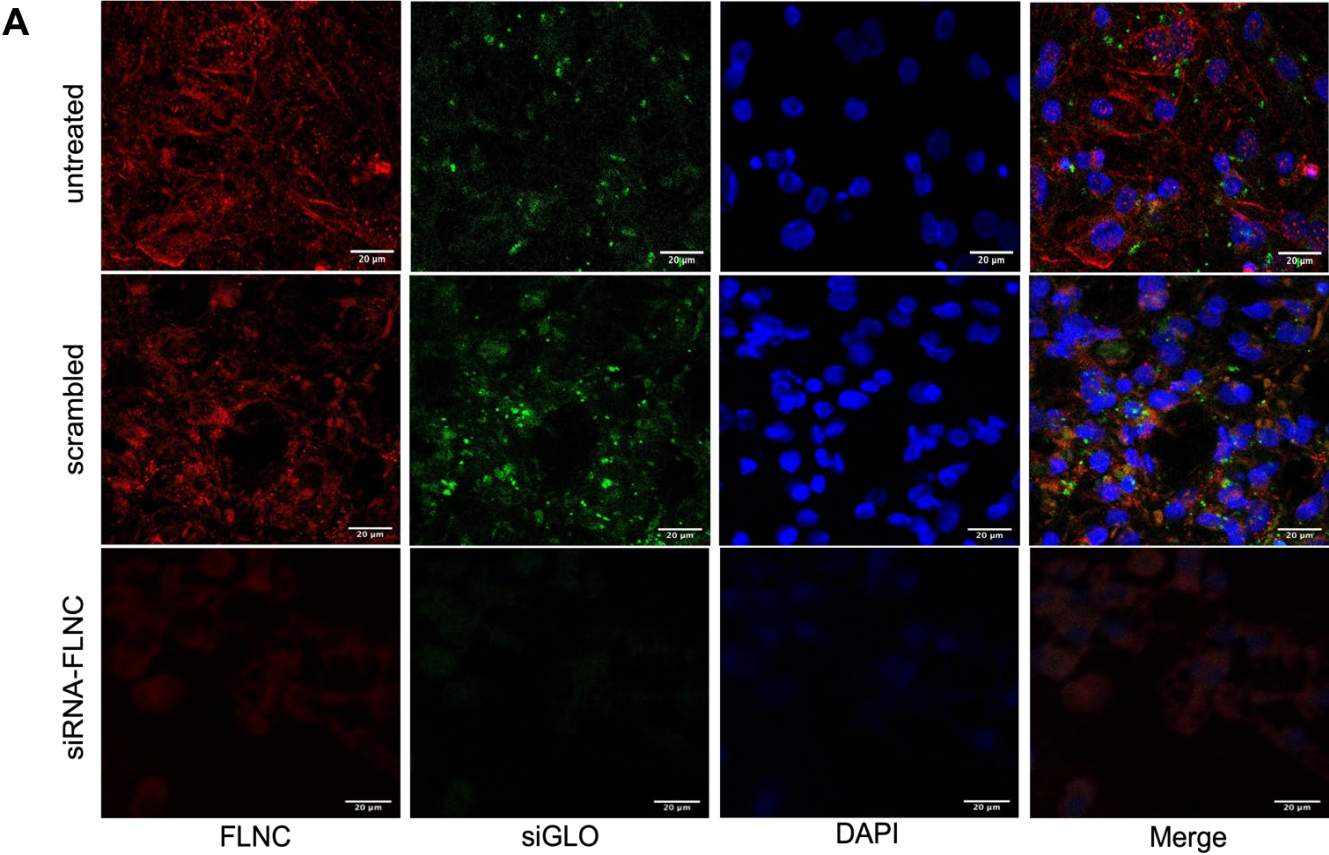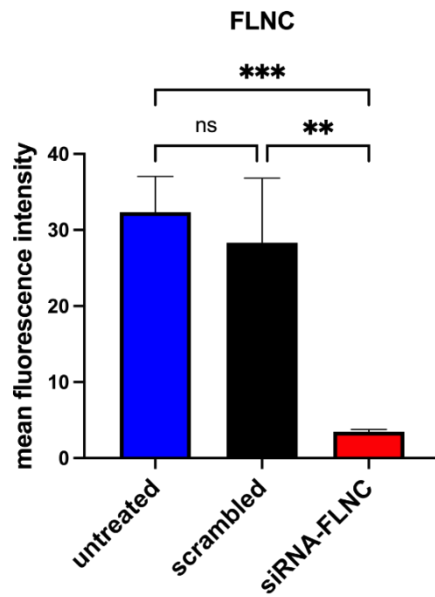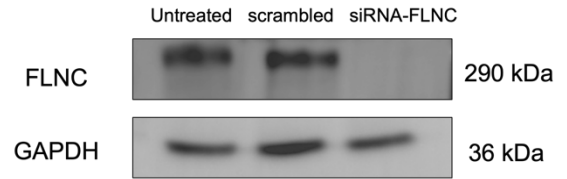
*Figure 4. 3. **Effect of FLNC-siRNA on expression and distribution of FLNC in hiPSC-CMs**. (A) Immunofluorescence staining of hiPSC-CMs treated for 72 hrs with FLNC-siRNA (n=12), scrambled control siRNA (n=8) or without any treatment (n=8). The FLNC is stained red, siGLO stained green, and cell nuclei stained blue with DAPI. The immunofluorescence staining signals of FLNC was significantly reduced in hiPSC-CMs (P<0.01) following siRNA-FLNC. The hiPSC-CMs treated with siRNA-FLNC had significant alterations in FLNC expression and localisation. (B) Image J software was used to quantify the mean staining intensity of FLNC following siRNA treatment. (C) Western blot analysis of FLNC protein (n=2) showed a reduction in expression following FLNC siRNA in hiPSC-CMs.*

4.5 *Effect of FLNC knockdown on the expression of Cx43/Nav1.5 and desmosomal proteins*

A

| Cx43 | siGLO | DAPI | Merge |
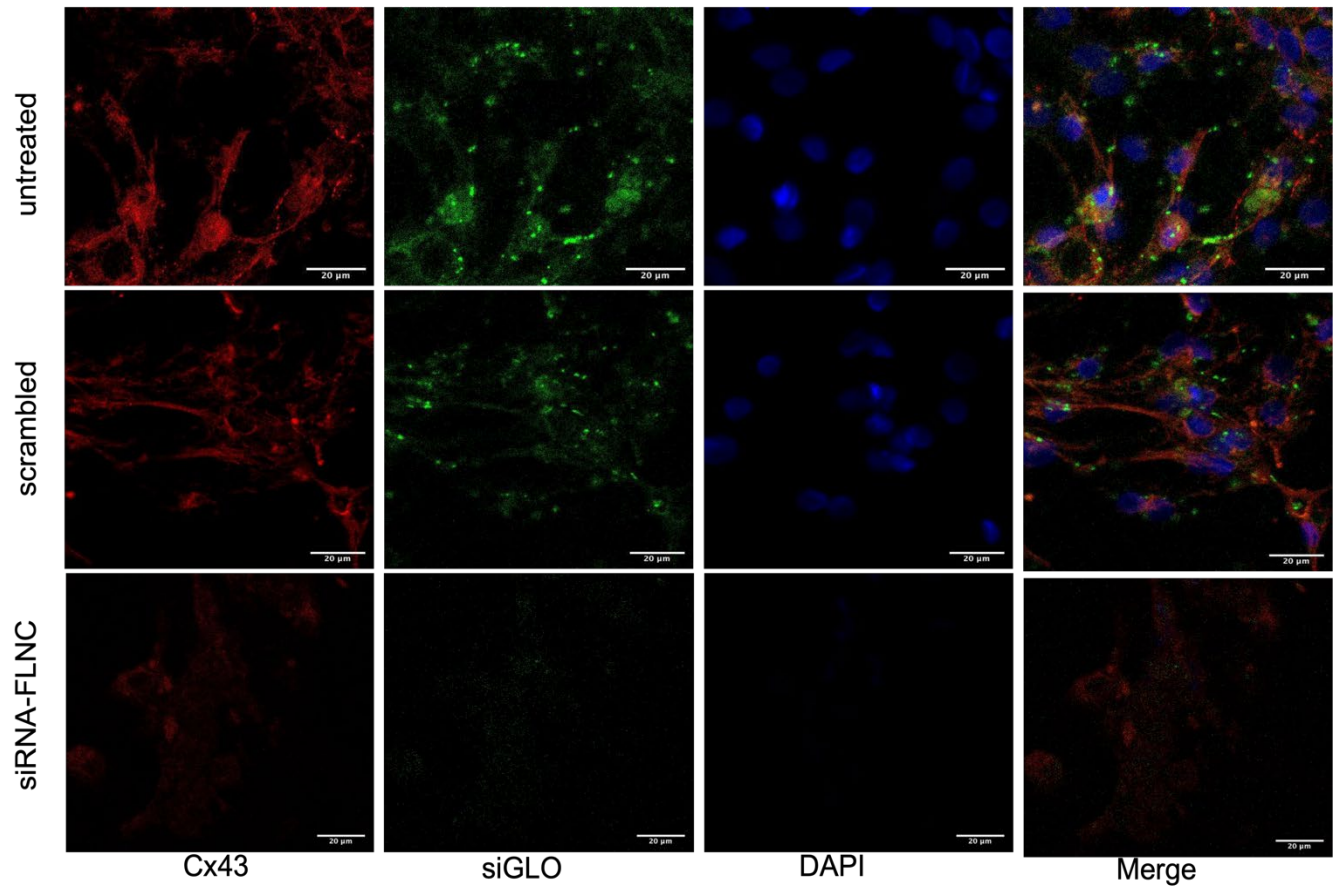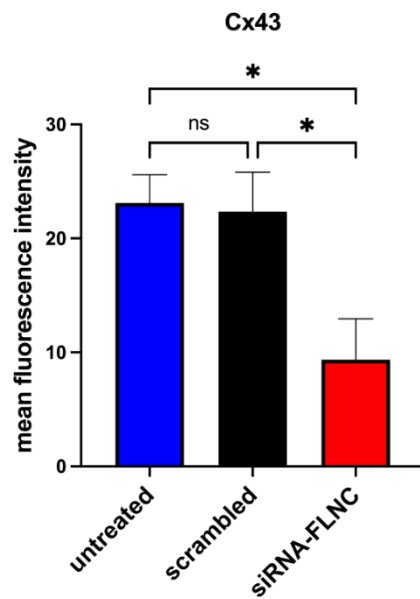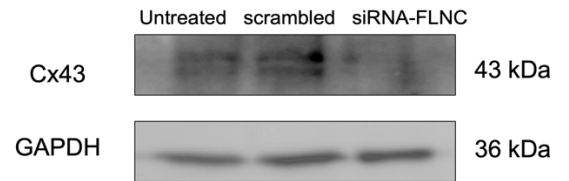
*Figure 4. 4. **Effect of FLNC-siRNA on expression and distribution of Cx43 in hiPSC-CMs.** (A) Immunofluorescence microscopy of hiPSC-CMs treated for 72 h with FLNC-siRNA, scrambled control siRNA or without any siRNA. Cx43 stained red, cell nuclei stained blue with DAPI, and siGLO stained green. (B) The immunofluorescence staining signals of Cx43 was significantly reduced in hiPSC-CMs (P<0.05) treated with siRNA-FLNC and Cx43 mis-localisation was observed when compared with untreated and scrambled hiPSC-CMs. The Image J software was utilised to quantify the mean staining intensity of Cx43 (n=5 for all conditions). (C) Western blot analysis of Cx43 protein (n=2) showed a reduction in expression following FLNC siRNA in hiPSC-CMs.*

A

Nav1.5   siGLO   DAPI   Merge
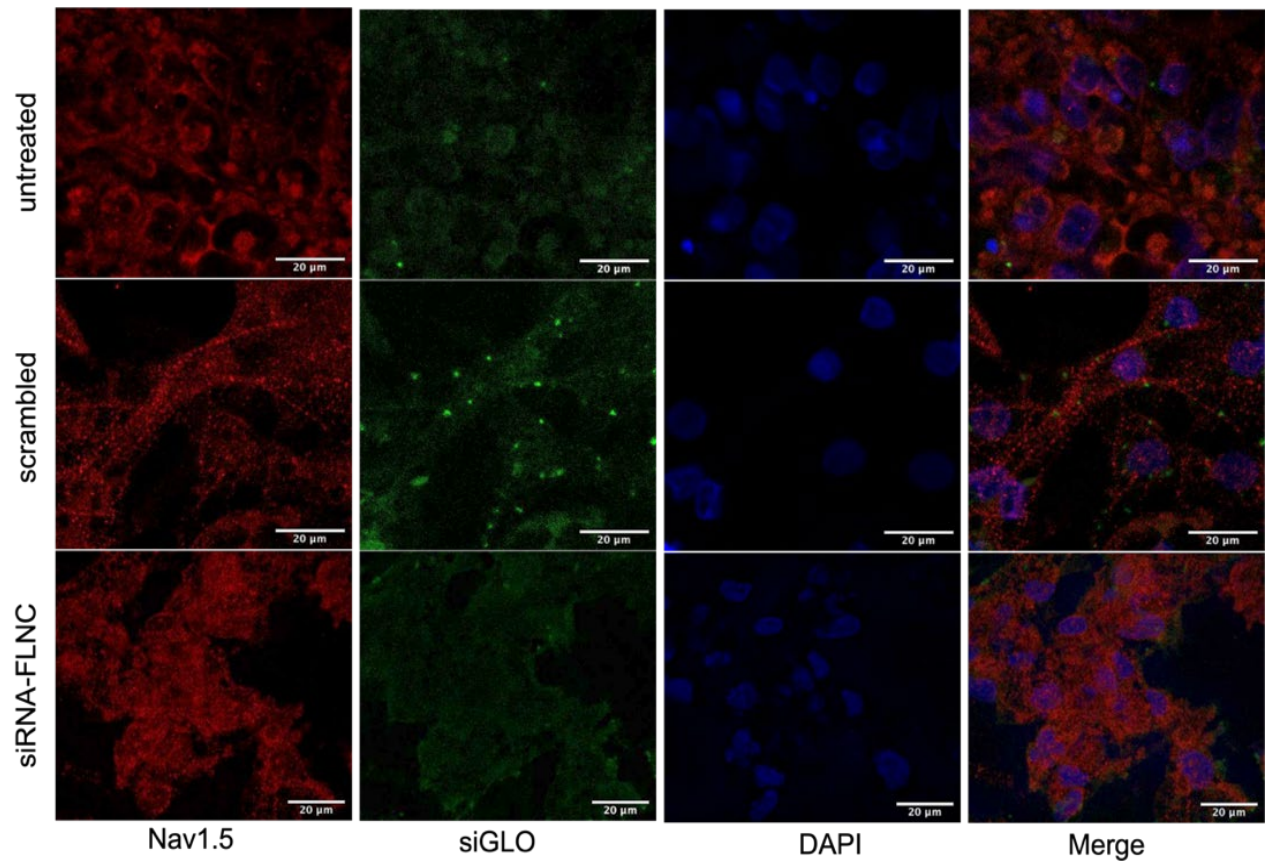
B
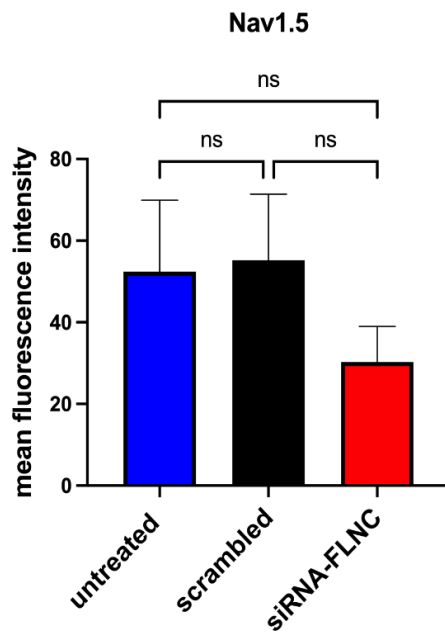
C
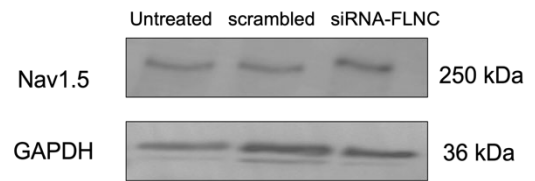
*Figure 4. 5. **Effect of FLNC-siRNA on expression and distribution of Nav1.5 in hiPSC-CMs.** (A) Immunofluorescence microscopy of hiPSC-CMs treated for 72 h with FLNC-siRNA, scrambled control siRNA or without any siRNA. Nav1.5 stained red, cell nuclei stained blue with DAPI, and siGLO stained green. (B) The immunofluorescence staining signals of Nav1.5 was not markedly different (P>0.05) between silenced and control cells although mis-localisation of Nav1.5 was observed after treatment with siRNA to FLNC. The Image J software was utilised to quantify the mean staining intensity of Nav1.5 (untreated; n=5, scrambled; n=7, siRNA-FLNC; n= 8) following treatement with siRNA. (C) Western blot analysis of Nav1.5 was not severely influenced when compared with untreated and scrambled lysates.*

4.5.1 *Immunofluorescence images of desmosomal proteins in hiPSC-CMs after transfection with siRNA-FLNC*
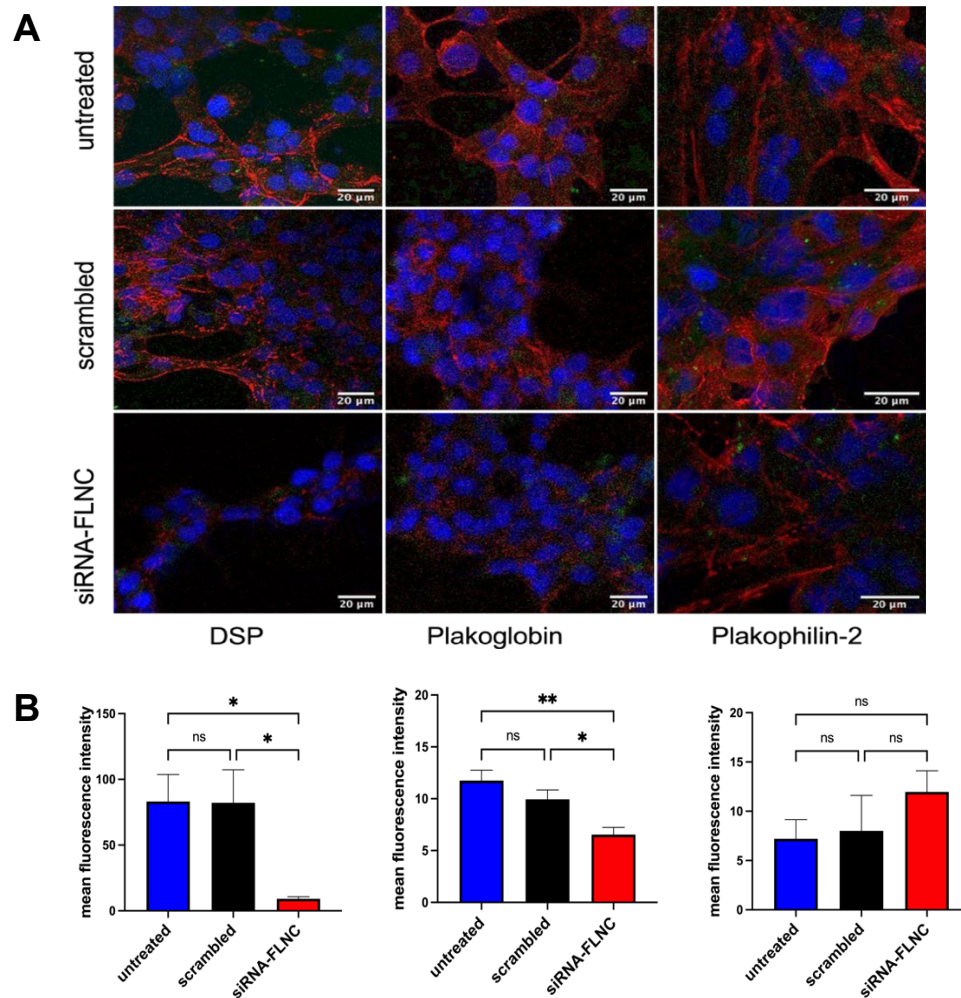
Figure 4. 6. **Effect of FLNC-siRNA on the structure and distribution of desmosomal proteins in hiPSC-CMs.** *(A) Immunofluorescence microscopy of hiPSC-CMs cultures treated for 72 h with FLNC-siRNA (n=6 plakophilin2; n=9 DSP; n=7 plakoglobin), scrambled non-targeting control siRNA (n=6 plakophilin2; n=7 DSP; n=7 plakoglobin) or without any siRNA (n=6 plakophilin2; n=10 DSP; n=7 plakoglobin). The proteins of interest (DSP, plakoglobin, plakophilin2) are stained red, cell nuclei stained blue with DAPI, and siGLO stained green. The immunofluorescence staining signals of DSP and plakoglobin were significantly decreased in hiPSC-CMs (P<0.05) whereas the staining intensity of plakophilin-2 was showing (P>0.05) comparable levels between silenced FLNC and control cells. (B) The Image J software was utilised to quantify the mean staining intensity of desmosomal proteins following treatement with siRNA-FLNC.*

4.6 *Summary*

By studying cardiomyocytes differentiated from hiPSCs and comparing three different conditions (untreated, scrambled siRNA treatment, and FLNC siRNA treatment), I was able to identify cellular abnormalities in hiPSC-CMs transfected with siRNA-FLNC in both immunofluorescence microscopy studies and western blot analysis. An intriguing finding in my hiPSC-CMs model was that the protein expression levels for Cx43 were significantly reduced with FLNC knockdown, whereas the expression of Nav1.5 following siRNA-FLNC did not differ significantly between untreated and treated cells. Previous studies have shown that loss of FLNC led to changes in distribution and expression levels of DSP, plakoglobin, Cx43 ([105], [115], [122]). My results support previous findings and suggest that Nav1.5 and plakophilin-2 may not be directly influenced by FLNC downregulation. However, it should be noted the cons of signal quantification in immunofluorescence microscopy and the need to further optimise staining approaches, such as producing a binary result (presence versus loss of signal) and increasing the reproducibility across different groups. Nonetheless, a supportive contribution in the understanding of FLNC-related AC came with the realisation that reduction in expression of FLNC can affect a number of intercalated disc proteins, including desmosomal proteins.

The reduction in Cx43 may promote a slower conduction velocity which may be proarrhythmic. The lower expression and mis-localisation of desmosomal proteins such as DSP may disrupt the integrity of the desmosomes. These factors may all contribute to the AC phenotype.

Chapter 5　　　Results - Electrophysiological phenotypes associated with silencing of FLNC in hiPSC-derived cardiomyocytes

5.1 *Introduction*

Clinical ECGs in patients harbouring truncating pathogenic variants in FLNC exhibited minor repolarisation changes and low QRS voltages (87, 115). In contrast to ARVC caused by desmosomal mutations, ECG abnormalities do not appear to be an early marker of disease in FLNC-related AC and may present a distinctive electrophysiological phenotype, according to a 2019 expert consensus statement from the Heart Rhythm Society (11). As discussed previously (Figure 1. 8), FLNC is known to interact with components of the IDs (87) and may interconnect with Cx43. Gap junction Cx43 is the predominant connexin expressed in the ventricular myocardium, which is essential for conduction of the cardiac impulse and is also localised to the IDs (3). Given the decreased Cx43 levels detected by western blot and mis-localisation in immunofluorescent microscopy after using siRNA-FLNC and the association between abnormal desmosomal proteins and a reduction in Cx43 expression at the gap junctions (49), this phenomenon may impair the electrical coupling between cardiomyocytes in the hiPSC model. Therefore, MEA systems were used to characterise the electrophysiological effects and proarrhythmic potential.

hiPSC-CMs were seeded at ~40,000/cm^2 and used ~30 days after the differentiation process. The electrophysiological assessment was conducted on hiPSC-CMs to identify the normal electrical signals in control conditions and compared to the signals following the addition of siRNA to FLNC. The traces recorded with the MEA (Figure 5. 1) show spontaneous electrical activity with good signals in untreated and those hiPSC-CMs treated with scrambled siRNA. Specifically, beat rate and field potential morphology were measured to identify the baseline signals of untreated hiPSC-CMs for comparison with scrambled and silenced FLNC. Both EADs and DADs-like events were observed in the recordings after treatment with siRNA-FLNC compared to the control conditions. This indicated the potential severe impact of reduced FLNC protein level on the electrophysiology of hiPSC-derived cardiomyocytes. All traces were recorded using Multichannel Experimenter setup (Multichannel systems, Germany) and data were saved as .h5 files. MATLAB and VCSF 1.2. software (Dr Aled Rhys Jones, Queen Mary University of London, UK) were used to analyse the recorded data.

5.2 *MEA traces for untreated and scrambled hiPSC-CMs*

A

B
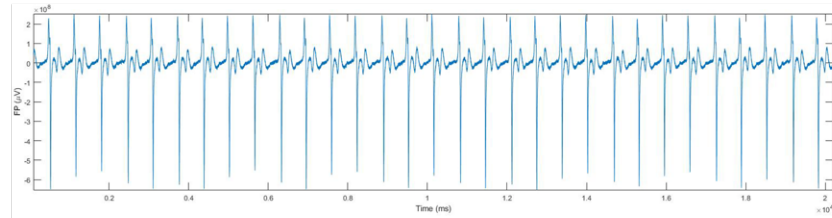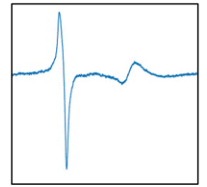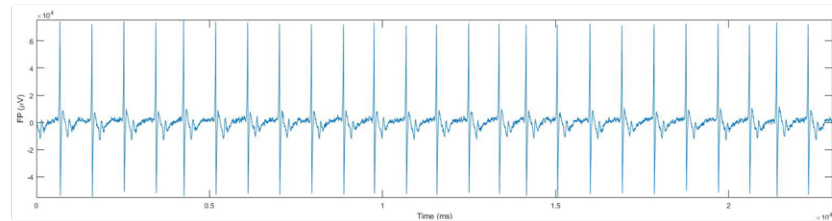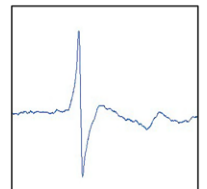
*Figure 5. 1. **MEA recording of hiPSC-CMs**. (A) & (B) Recorded traces showing a good signals with regular beating rate of untreated (n=4 MEAs) and scrambled hiPSC-derived ventricular cardiomyocytes (n=4 MEAs). FP morphology demonstrates normal shape of R/Q and T peaks for untreated and scrambled hiPSC-CMs.*

5.3 *MEA traces for hiPSC-CMs with siRNA-FLNC*

Extracellular MEA recordings for the hiPSC-CMs transfected with siRNA to FLNC revealed marked electrophysiological abnormalities. Variability in beat-to-beat interval, cellular arrhythmias, and electrical alternans were all occasionally observed (Figure 5. 2). The results of the correlation analysis between FPD and RR interval is not significant (P>0.05) for hiPSC-CMS following siRNA-FLNC when compared with scrambled and untreated cells (Figure 5. 3 A). The number of cells exhibiting arrhythmic-like events (EADs and DADs) was significantly higher (P<0.01) in hiPSC-CMs following siRNA-FLNC (Figure 5. 3 C) compared to untreated and scrambled hiPSC-CMs. The range of the histogram is one indicator of the beat-beat variability for interbeat intervals over a period of time (Figure 5. 4). The coefficient of variance values for interbeat intervals were larger (62.14%) in the hiPSC-CMs treated with siRNA-FLNC than in scrambled (31%) and untreated hiPSC-CMs (28.67%).

hiPSC-CMs following siRNA-FLNC — **FP shape**
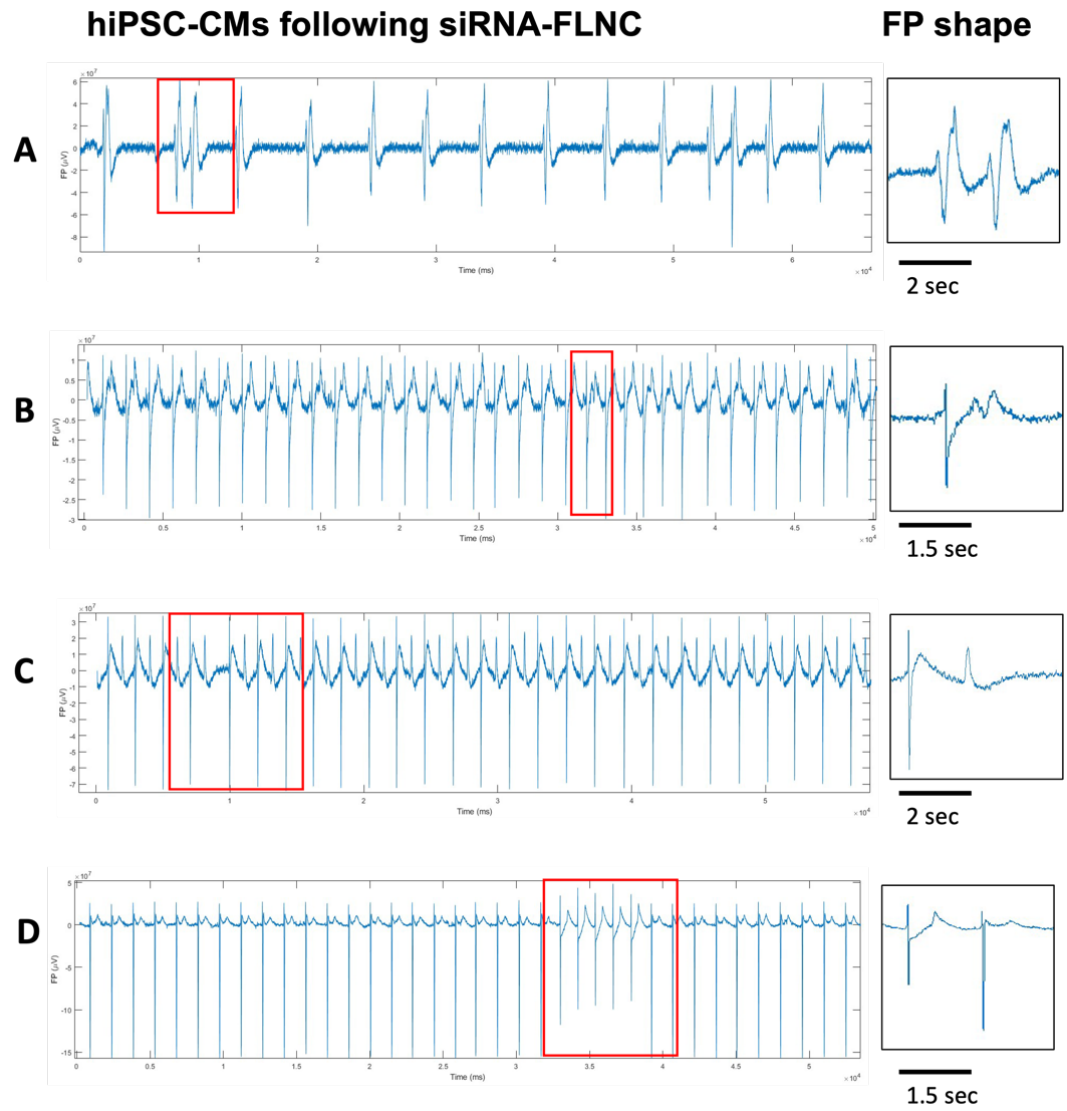
*Figure 5. 2. **The effect of siRNA-FLNC on hiPSC-CMs** was demonstrated by abnormal traces captured with MEA (n=6 MEAs). (A) DAD-like events and (B) EAD-like events were exhibited in MEA recordings of hiPSC-CMs following siRNA-FLNC treatment. (C) Knockdown of FLNC may cause variation between beats in hiPSC-CMs. (D) Electrical alternans were also observed in hiPSC-CMs following siRNA-FLNC, albeit less frequently.*

5.4 *Relationship between RR intervals and field potential duration for untreated, scrambled, and siRNA-FLNC of hiPSC-CMs*

A

FPD-RR relationship
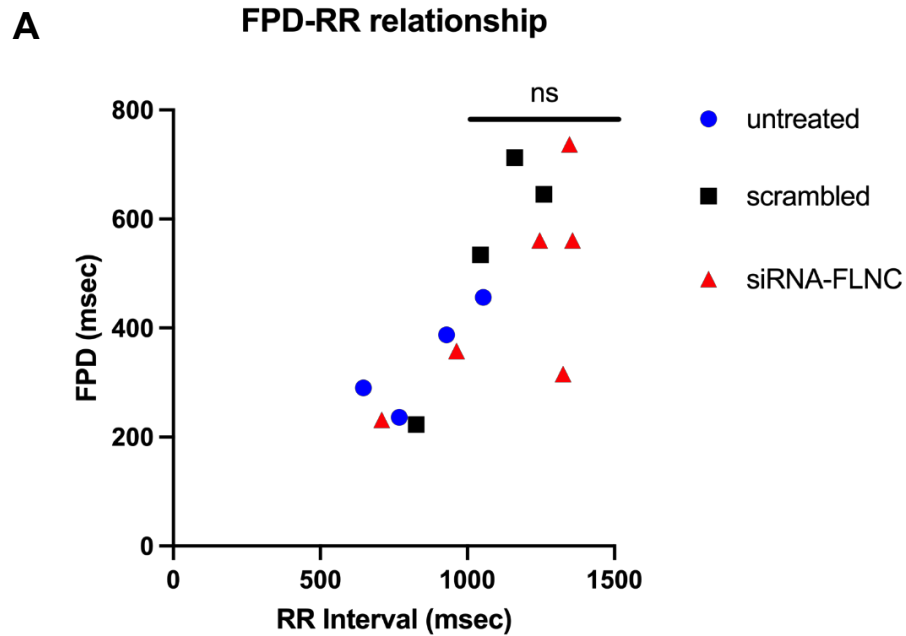
Untreated	P =0.1276	r =0.8724	95% CI= -0.5490 to 0.9973
Scrambled	P =0.0665	r =0.9335	95% CI= -0.2686 to 0.9986
siRNA-FLNC	P =0.1111	r =0.7138	95% CI= -0.2324 to 0.9659
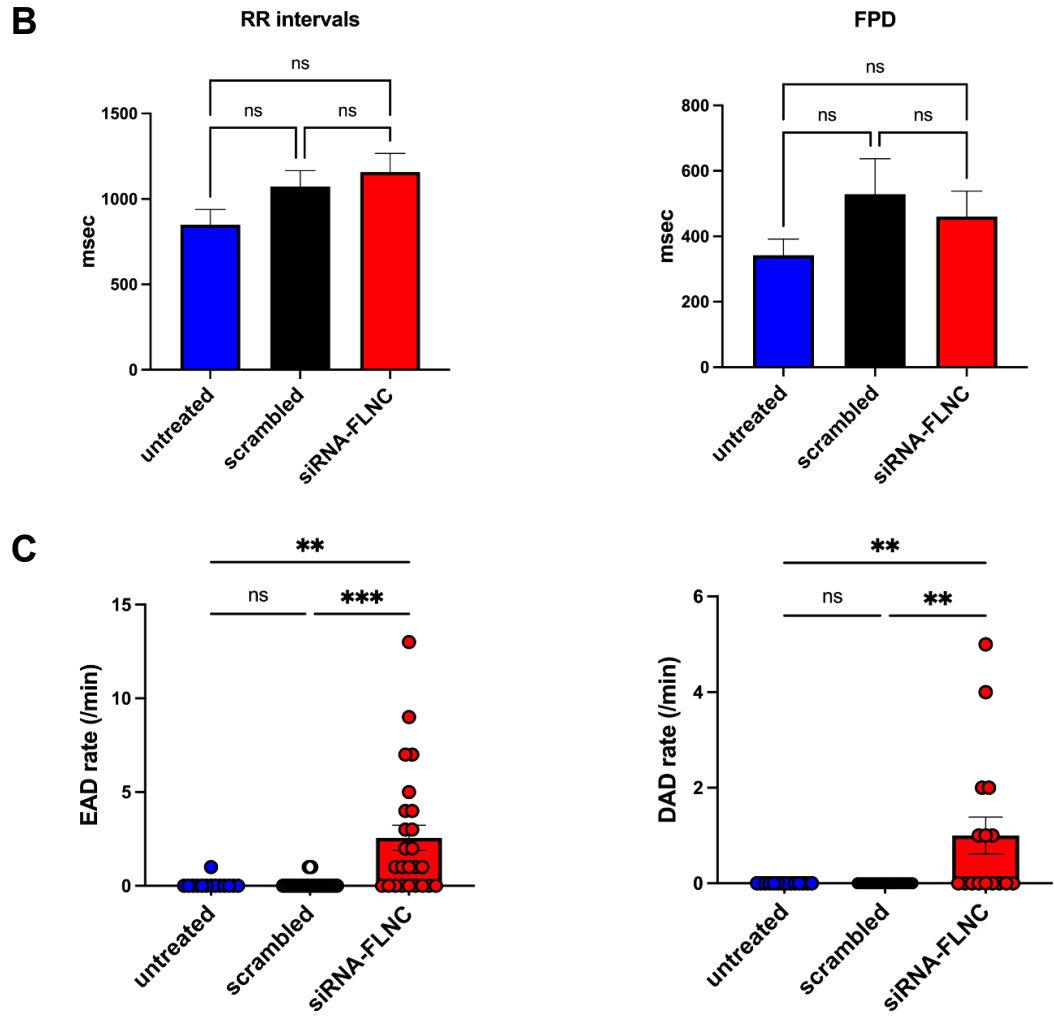
*Figure 5. 3. (A) **The relationship between field potential duration (FPD) and RR interval for hiPSC-CMs before and after siRNA treatment**. There were no significant (P>0.05) changes of FPD-RR relationship of hiPSC-CMs following siRNA-FLNC compared with scrambled and untreated cells. Pearson's r correlation was used for FPD-RR plot. (B) Summary of mean (±SEM) FPD and RR intervals were not significantly different among untreated, scrambled, and siRNA-FLNC. One-way ANOVA was used to analyse the mean (±SEM) FPD and RR intervals among the three conditions. (C) The incidence of DADs and EADs per minute of all investigated MEAs (untreated hiPSC-CMs: n=4; scrambled hiPSC-CMs: n=4; siRNA-FLNC hiPSC-CMs: n=6). The number of cells exhibiting cellular arrhythmias was significantly higher in hiPSC-CMs treated with siRNA-FLNC. CI, confidence interval.*

5.5 *Beat-Beat variability analysis*

Untreated hiPSC-CMs

Scrambled hiPSC-CMs

hiPSC-CMs with siRNA-FLNC
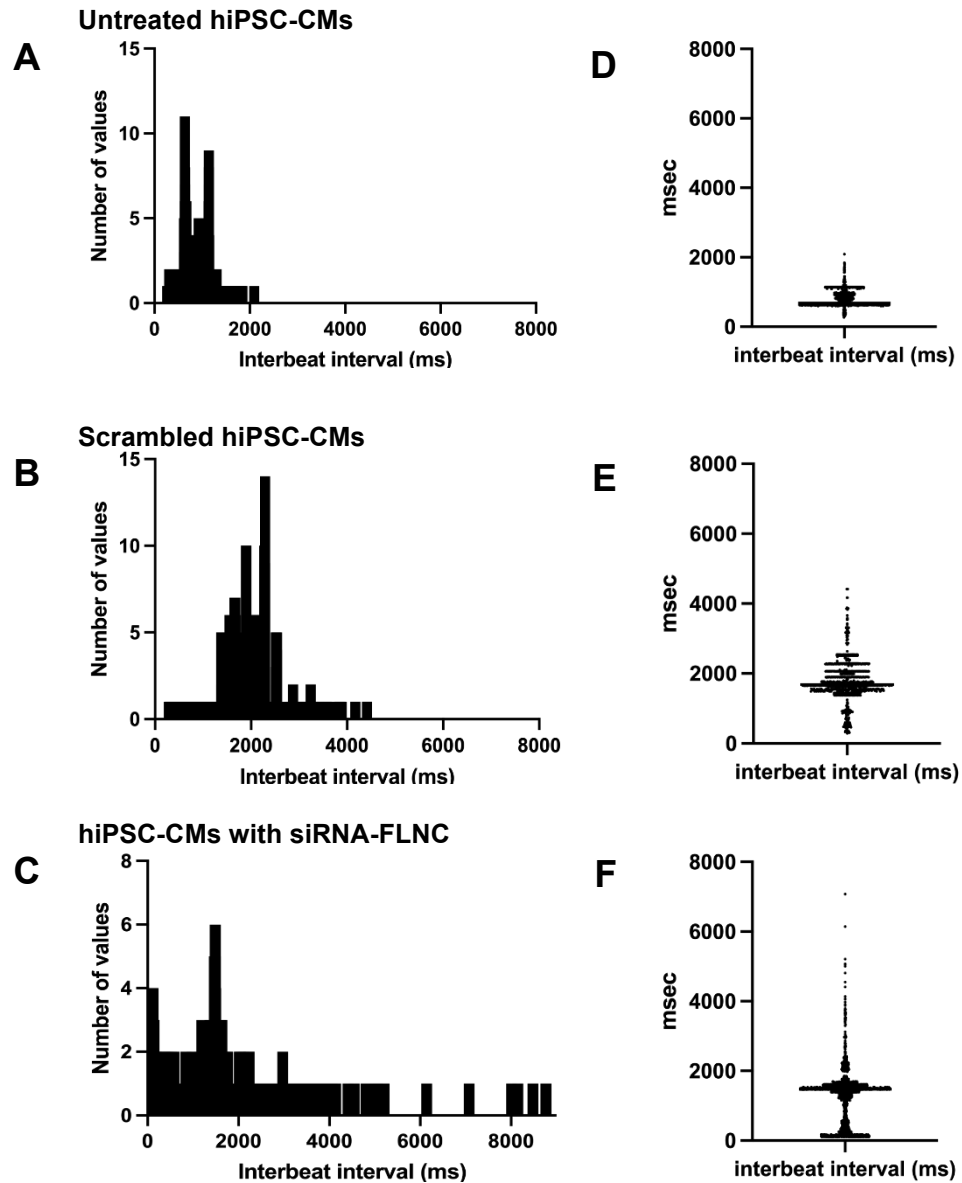
Figure 5. 4. (A)-(C) **Histogram distribution of Interbeat intervals for hiPSC-CMs pre and post siRNA treatment**. *(D)-(F) Scatter dot plot of the median interbeat intervals among untreated, scrambled, and siRNA-FLNC. The range of the histogram can be used as an indicator for the variation of the beating rate (41, 187). As shown above, the range of interbeat intervals was larger in siRNA-FLNC than in scrambled and untreated hiPSC-CMs. Relative variability or coefficient of variation (population standard deviation divided by the mean) for untreated was 28.67% and for scrambled was 31% and for siRNA-FLNC was 62.14%.*

5.6 *Summary*

In this chapter, I examined the long-term effects of FLNC knockdown on cell electrophysiology and viability of hiPSC-CMs model. This study demonstrates that the electrophysiological phenotype resulting from knockdown of FLNC by siRNA transfection is characterised by a more irregular spontaneous beat rate and directly increases cellular proarrhythmia mediated by DADs-like events and EADs-like events when compared to scrambled and untreated cells. The beat rate is the major driver of FPD variability because of their inverse relationship; the faster the beating rate, the shorter the FPD (188). Because of this, the RR-FPD relationship was analysed and showed that there was no significant variability of RR and FPD in treated and untreated cells. However, some variable values emerged from the FPD and beat-beat variability data of scrambled hiPSC-CMs during MEA recordings and are discussed in detail below in chapter 7 (section 7.2). Despite this, MEA systems and hiPSC-CMs are frequently used for studying the effect of drugs on cellular electrophysiological parameters such as beat rate and FPD. Therefore, further investigations are needed to establish antiarrhythmic drugs that could eliminate these pro-arrhythmic events and aid for the development of personalised therapies.

Chapter 6   Results - Silencing of FLNC causes abnormality in action potential morphology and calcium handling of hiPSC-CMs

6.1 *Introduction*

Optical cardiac electrophysiology studies were conducted alongside MEA recordings for better understanding of the cellular electrophysiological abnormalities in hiPSC-CMs following siRNA-FLNC. However, due to the limitation of MEA parameters to provide suitable capture of repolarisation dynamics, such as APD and AP shape, which are considered to be some of the most predictive signs of pro-arrhythmic responses ([189](#)), I used alternative methods. Using voltage and calcium-sensitive dyes (Figure 6. 1) can offer mechanistic insights into heart rhythm disorders and provides a more detailed assessment of signal instability during the repolarisation phase of hiPSC-derived ventricular cardiomyocytes. Calcium imaging is the most widely used technique due to the fact that calcium-sensitive fluorescent probes can produce significant changes in emission upon binding calcium, although these changes are not necessarily a direct correlate of electrical activity, especially AP morphology ([190](#)). Thus, examining the differences of both electrophysiological characteristics (AP shape and APD) and calcium transients between ventricular-like CMs is essential to the phenotypic analysis, specifically before and after gene knockdown in hiPSC-CMs ([10](#)).

A

Di-4-ANEPPS

Fluo-4 AM

Untreated   Scrambled   siRNA-FLNC

B

Rise Time

Early Rep.
APD10-30

Medium Rep.
APD40-60

Late Rep.
APD70-90

C

10%
25%
50%
80%
90%

Figure 6. 1. (A) **Microscopy images of hiPSC-CMs** *loaded with 10µM Di-4-ANEPPS (magnification 10x) for optical voltage measurements and 3µM Flou-4 AM (magnification 20x) for calcium transients. (B) Parameters of action potential duration (modified from Maria Pura Hortigon Vinagre et al (176)). (C) calcium transient duration (obtained from A. Ahola et al (191)) are defined as percentages from the peak maximum of the amplitude.*

Initially, ratiometric imaging was employed for recording of membrane voltage with Di-4-ANEPPS because it was thought to reduce or eliminate movement artefacts according to the previous studies ([192-194](#)). However, I found non-ratiometric imaging provided less noisy voltage signals for this study due to the lower frame rate involved (Figure 6. 2). When using excitation ratiometry, the exposure time is halved to maintain temporal resolution, leading to more noisy signals. Ratiometric imaging can be defined as the ratio of the fluorescence emission at two different excitation wavelengths ([194](#), [195](#)). Fluo-4 is a non-ratiometric intracellular calcium indicator that fluoresces upon calcium binding and thus ratiometric approach was excluded for calcium imaging ([196](#), [197](#)).
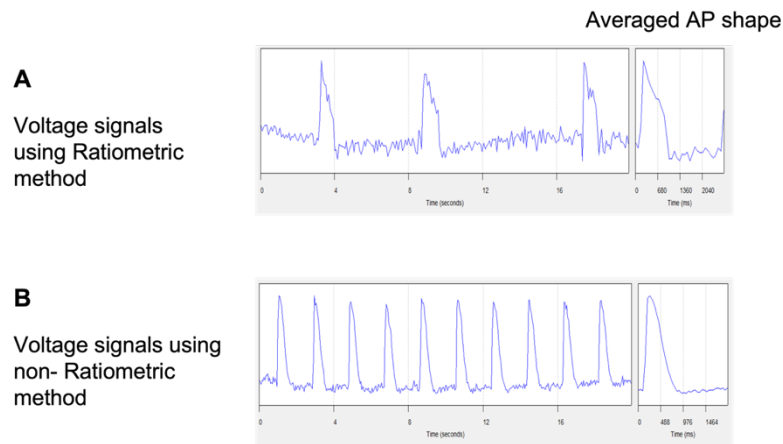
Figure 6. 2. ***Ratiometric and nonratiometric imaging.*** *(A). An example of a ratiometric recording. (B). Non-ratiometric imaging provides better quality traces of membrane action potential. VCSF software was used to analyse the optical signals.*

Optical action potentials and calcium transients were analysed using VCSF programme to measure the amplitude, rise time, APD at 50% (APD50) and 90% (APD90) repolarisation, and also calcium transient duration at 50% (CaTD50). The normalised calcium amplitudes were slightly lower than usual due to high background fluorescence obtained from low magnification imaging. Representative action potential (Figure 6. 3) and calcium signal (Figure 6. 4) recordings in cellular monolayer among three different conditions are shown below. Silencing of FLNC in hiPSC-CMs showed predominantly EAD-like arrhythmic events, which were not observed with untreated cells and scrambled siRNA. DAD-like events were not observed. Transfected hiPSC-CMs with siRNA-FLNC were associated with prolongation of CaTD50 ($P < 0.05$), APD50 ($P < 0.05$), and APD90 ($P < 0.05$) when compared with untreated hiPSC-CMs. The rise time of the AP was showed similar values among the three different conditions (Figure 6. 3). Calcium amplitude did not show any statistically differences in hiPSC-CMs treated with siRNA-FLNC compared to untreated and scrambled cells (Figure 6. 4). Cycle lengths were excessively prolonged ($P < 0.01$) in voltage and calcium signals of hiPSC-CMs after knockdown of FLNC.

6.2 *Voltage signals*
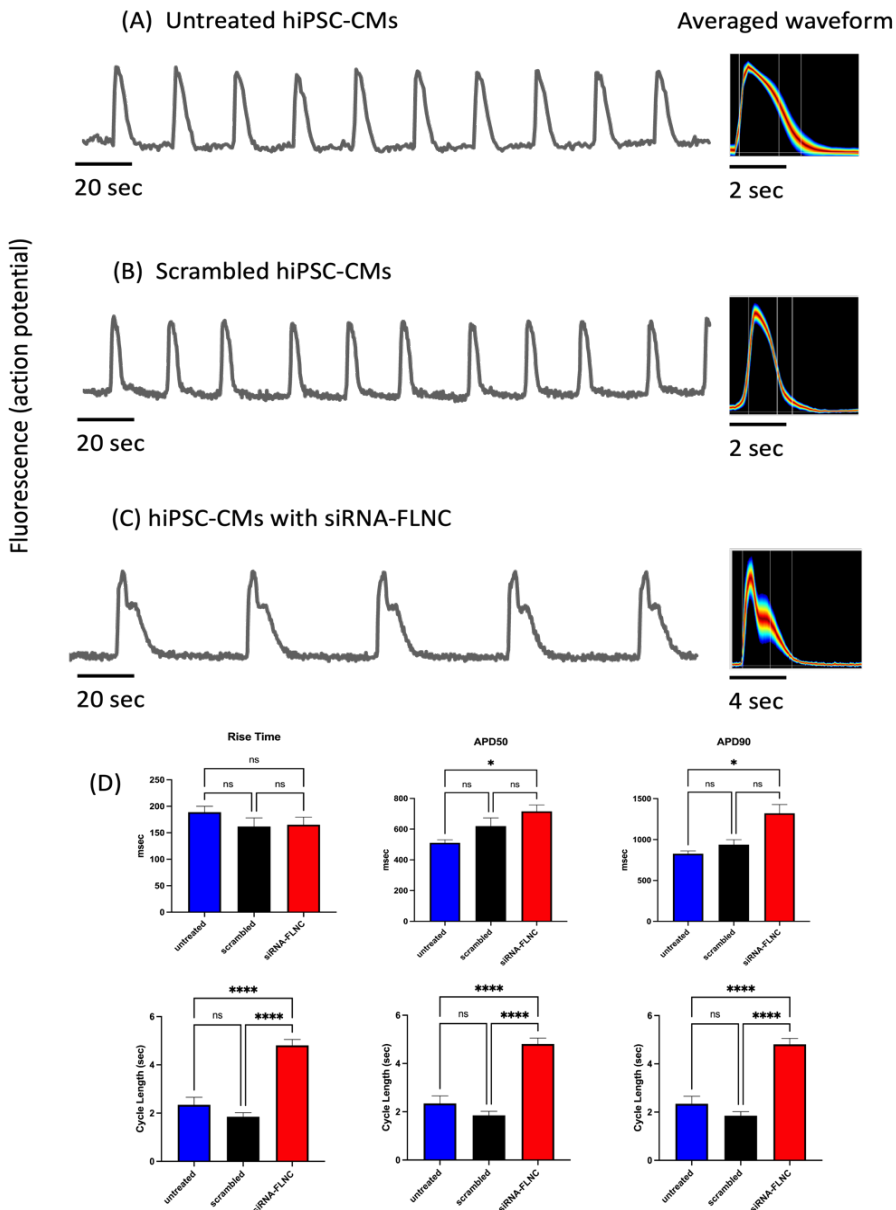
Figure 6. 3. **Action potential recorded via fluorescence imaging of a representative ventricular hiPSC-CMs** *showing the APD. Twenty seconds of recordings is shown in A, B, and C. Note the similarity between the traces of (A) untreated (n=9) and (B) scrambled hiPSC-CMs (n=11). (C) siRNA-FLNC (n=35) causes a prolonged action potential duration which ultimately precedes EAD formation. Note that the averaged waveform has a different timescale than the traces. (D) APD50 and APD90 were significantly increased in siRNA-FLNC compared to untreated cells. No significant changes in Rise time among the three different conditions. For all three parameters, siRNA-FLNC had significantly longer cycle lengths.*

6.3 *Calcium signals*
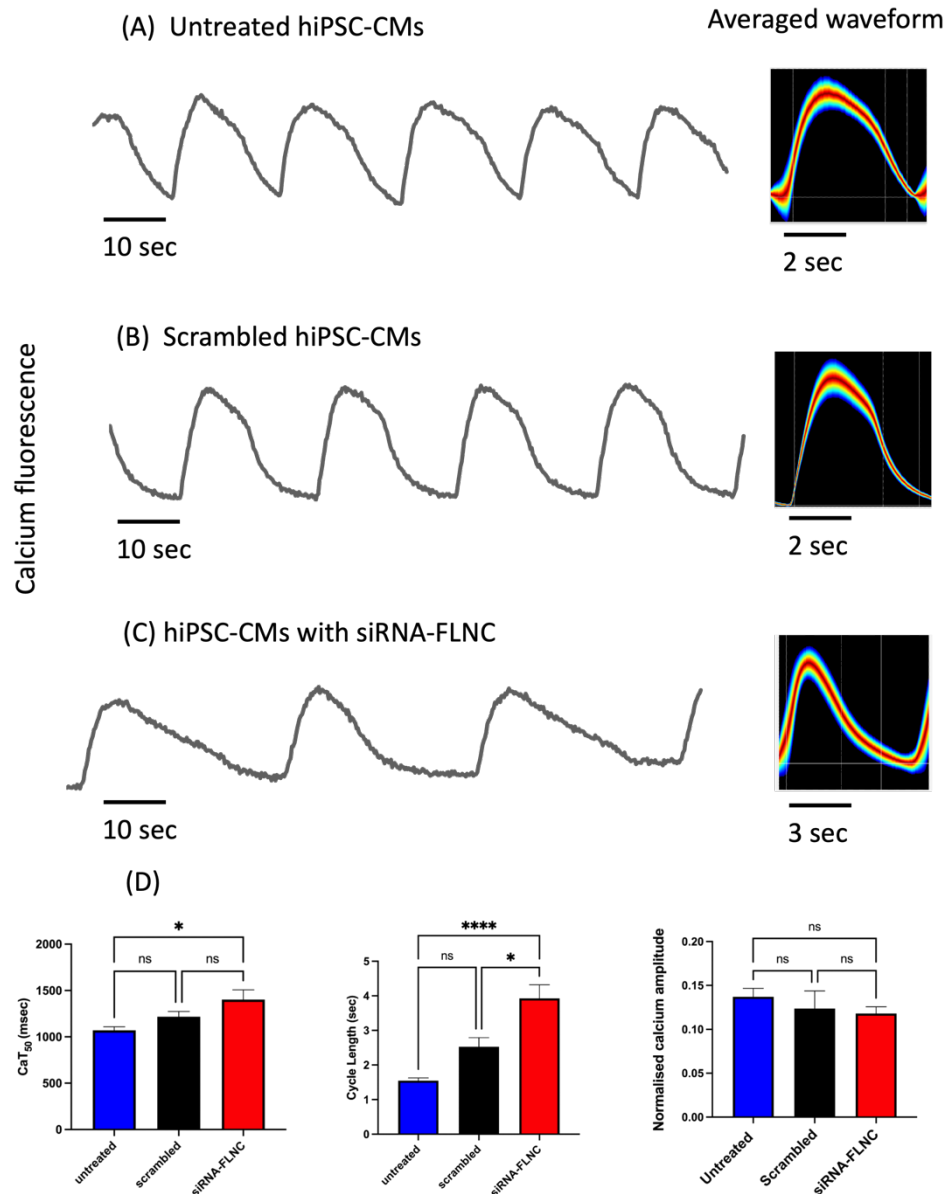
*Figure 6. 4. **Calcium transients recorded via fluorescence imaging of a representative ventricular hiPSC-CMs** showing the calcium transient duration. Ten seconds of recording is shown in A, B, and C. Note the similarity between the traces of (A) untreated (n=10) and (B) scrambled (n=6) hiPSC-CMs. (C) siRNA-FLNC (n=12) causes a prolonged calcium transient duration when compared with untreated hiPSC-CMs. (D) CaT50 and cycle length are significantly increased in cells transfected with siRNA-FLNC. No significant changes on normalised values of calcium amplitude among the three conditions. Note that the averaged waveform has a different timescales across the traces.*

6.4 *AP recordings of drug-induced effects in transfected hiPSC-CMs with siRNA-FLNC*

I tested two drugs in this study: isoprenaline, a beta adrenergic agonist that can increase the beating rate and contractility, and nifedipine, calcium channel blocker that can inhibit L-type calcium channels. Isoprenaline will increase the beating rate and contractility of the myocytes but is also known to provoke arrhythmia under some conditions. Nifedipine may antagonist any abnormal arrhythmic events dependent on calcium by reducing calcium entry across the sarcolemma. Initially isoprenaline was added to the transfected hiPSC-CMs with siRNA-FLNC to evaluate the effect of the drug on action potential in several recordings. Figure 6. 5 shows representative action potential traces recorded before and following the addition of 10μM isoprenaline to hiPSC-CMs. The 4 parameters plotted are the cycle length, APD at 50% and 90% repolarisation as well as the AP rise time. Isoprenaline caused a significant shorten APD50, APD90, and cycle length in hiPSC-CMs ($P<0.05$) following silencing of FLNC. The rise time displayed no

significant differences (P>0.05) in pre and post isoprenaline treatment.

A

Baseline recording of hiPSC-CMs with siRNA-FLNC
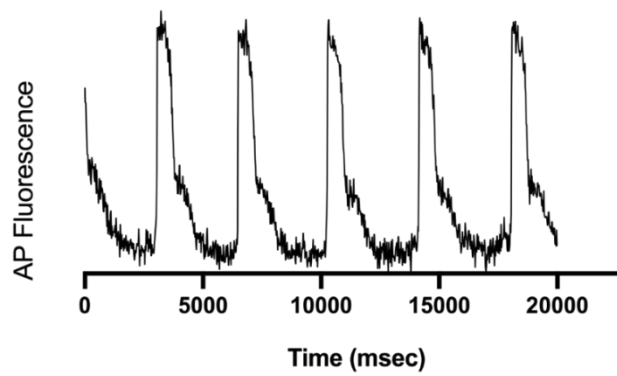
B

Drug recording of hiPSC-CMs with siRNA-FLNC following Isoprenaline (10μM)
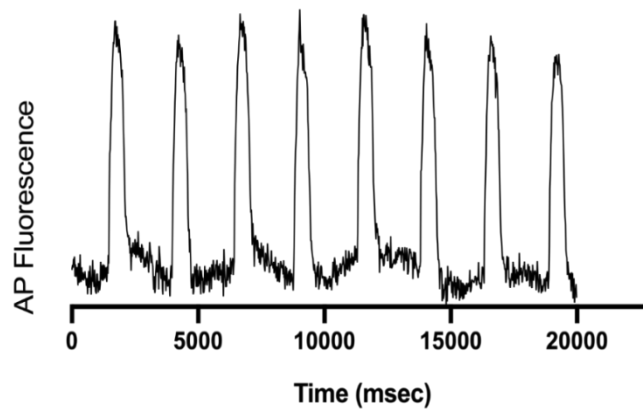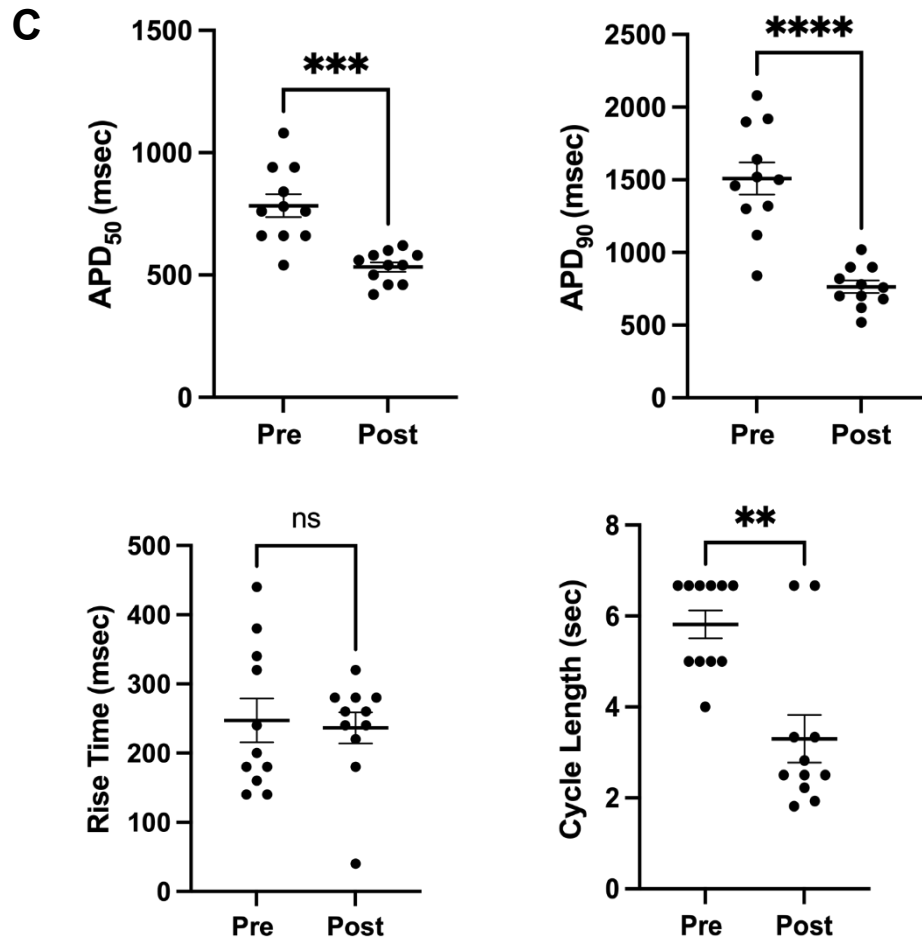
Figure 6. 5. **Effect of isoprenaline on APD50, APD90, rise time, amplitude, and cycle length of the action potential in hiPSC-CMs with FLNC knockdown**. *The application of 10µM isoprenaline was for testing its effects on action potential parameters. (A) Relevant traces of hiPSC-CMs with siRNA-FLNC before adding isoprenaline. (B) Relevant traces of hiPSC-CMs with siRNA-FLNC following isoprenaline treatment. (C) Isoprenaline caused a significant shorten APD50, APD90, and cycle length (mean±SEM, n=11) in hiPSC-CMs (P<0.05) following silencing of FLNC. The rise time (mean±SEM) displayed no significant differences (P>0.05) in pre and post isoprenaline treatment. Paired t-test was used to compare pre and post effect of isoprenaline on hiPSC-CMs with siRNA-FLNC .*

Only one recording was completed for testing the combination of two drugs isoprenaline and nifedipine on hiPSC-CMs following siRNA-FLNC. Three more recordings were obtained to examine the effect of using nifedipine solely on hiPSC-CMs following siRNA-FLNC. The following traces show the AP activity before and after drug intervention with the averaged waveform on the top right side.

Recording 1

Before any drug

APD50: 860 ms
APD90: 1660 ms
Rise Time: 80 ms
Cycle length: 5 sec

Isoprenaline (10μM)

APD50: 740 ms
APD90: 1440 ms
Rise Time: 80 ms
Cycle length: 4 sec

Nifedipine (10μM)
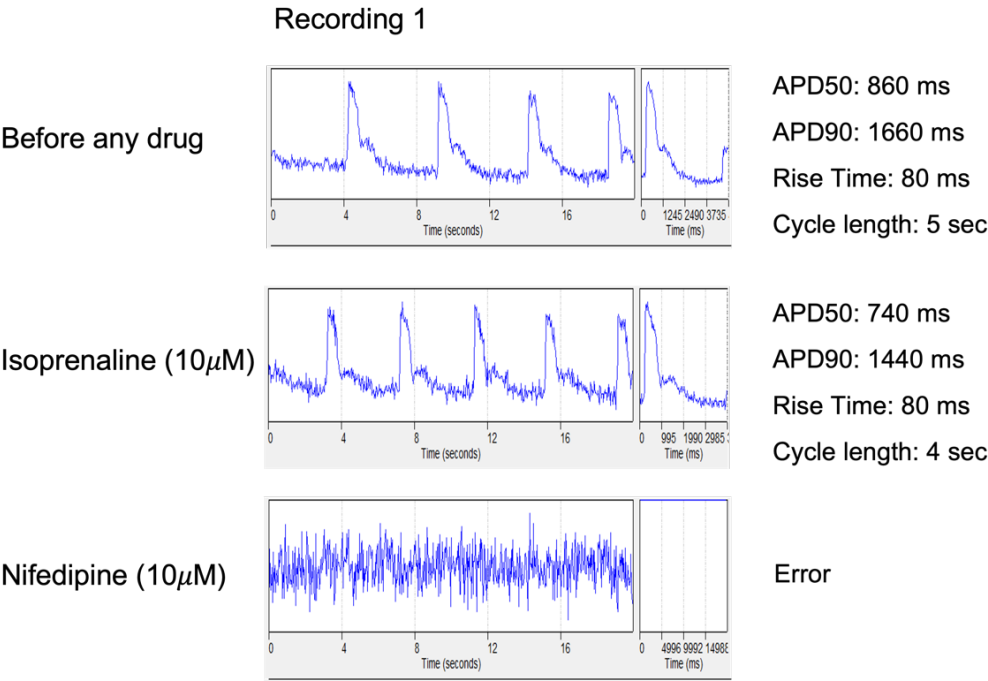
Error

Recording 2

Before nifedipine
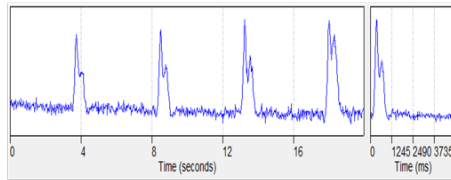
APD50: 840 ms
APD90: 4021 ms
Rise Time: 200 ms
Cycle length: 5 sec

After nifedipine
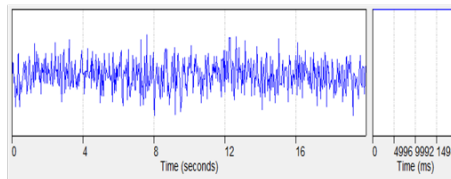
Error

Recording 3

Before nifedipine
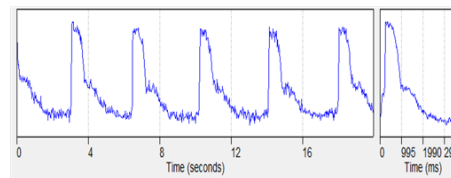
APD50: 840 ms
APD90: 1380 ms
Rise Time: 180 ms
Cycle length: 4 sec

After nifedipine
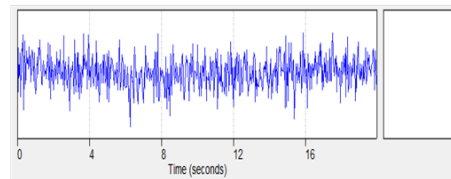
Error

The potential interpretation for the above recordings is related to the severe impact of using 10μM nifedipine on hiPSC-CMs. It is clear that both in the presence and absence of isoprenaline, nifedipine abolishes the electrical activity of the hiPSC-CMs transfected with siRNA-FLNC.

In the figure below, I examined if spontaneous activity resumed in the presence of nifedipine when recording one and five minutes after adding the drug. In both cases, there was no spontaneous electrical activity. More optical recordings and applying lower drug concentrations are needed to validate these observations in the future. Therefore, I decided to pursue more detailed single cell studies with patch clamping to dissect mechanistic effects of FLNC knockdown.

Recording 4

Before addition nifedipine

APD50: 880 ms
APD90: 1500 ms
Rise Time: 100 ms
Cycle length: 5 sec

1 minute later

Error

5 minute later

Error
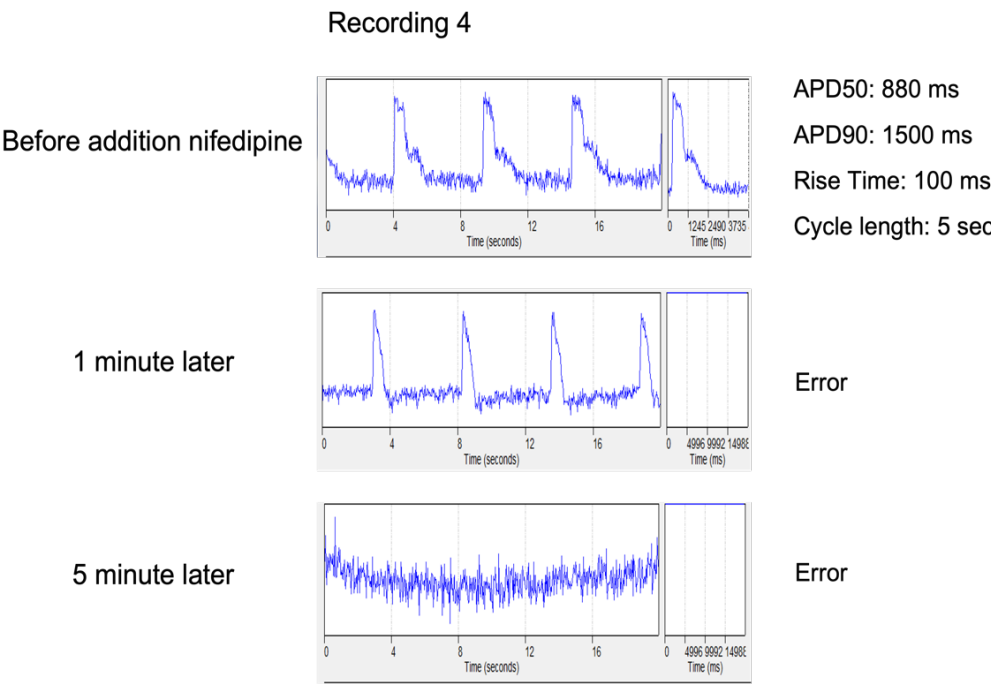
6.5 *Electrophysiological studies using patch clamp technique*

Intracellular recording of APs using patch clamp is an important method for studying the excitability of single cells. In order to study mechanistic basis of the potential prolongation of APD and arrhythmic-like events, spontaneous action potentials were recorded in the whole-cell configuration at room temperature. For cells treated with siRNA-scrambled, action potential parameters were derived from runs of recording where there were no EADs. The cells treated with siRNA-FLNC showed a tendency to longer APD30 and APD50 compared with scrambled cells, although this was not statistically different (Figure 6. 6). However, the APD90 in transfected cells with siRNA-FLNC was significantly longer than that in scrambled cells. The resting membrane potential and the amplitude of action potential were not significantly changed between the two groups (Figure 6. 6). EADs and DADs were observed in hiPSC-CMs with siRNA-FLNC in patch clamp recordings (Figure 6. 6). However, the number of DAD events in these cells was not statistically different (P>0.05) when compared with hiPSC-CMs with scrambled siRNA (Figure 6. 6). This may be due to the limited number of actual recordings obtained. There was excessive prolongation of the APD resulted in EADs and arrhythmia as shown in (Figure 6. 6). EADs

were previously detected from hiPSC-CMs with siRNA-FLNC in MEA recordings and fluorescence imaging, and the number of EAD events in patch clamp recordings was also statistically significant ($P < 0.01$) when compared to the scrambled control (Figure 6. 6). Cells treated with non-targeting scrambled siRNA were used as the control.

A Scrambled hiPSC-CMs   Average Action potential

B hiPSC-CMs with siRNA-FLNC

C hiPSC-CMs with siRNA-FLNC
   exhibited DADs and EADs
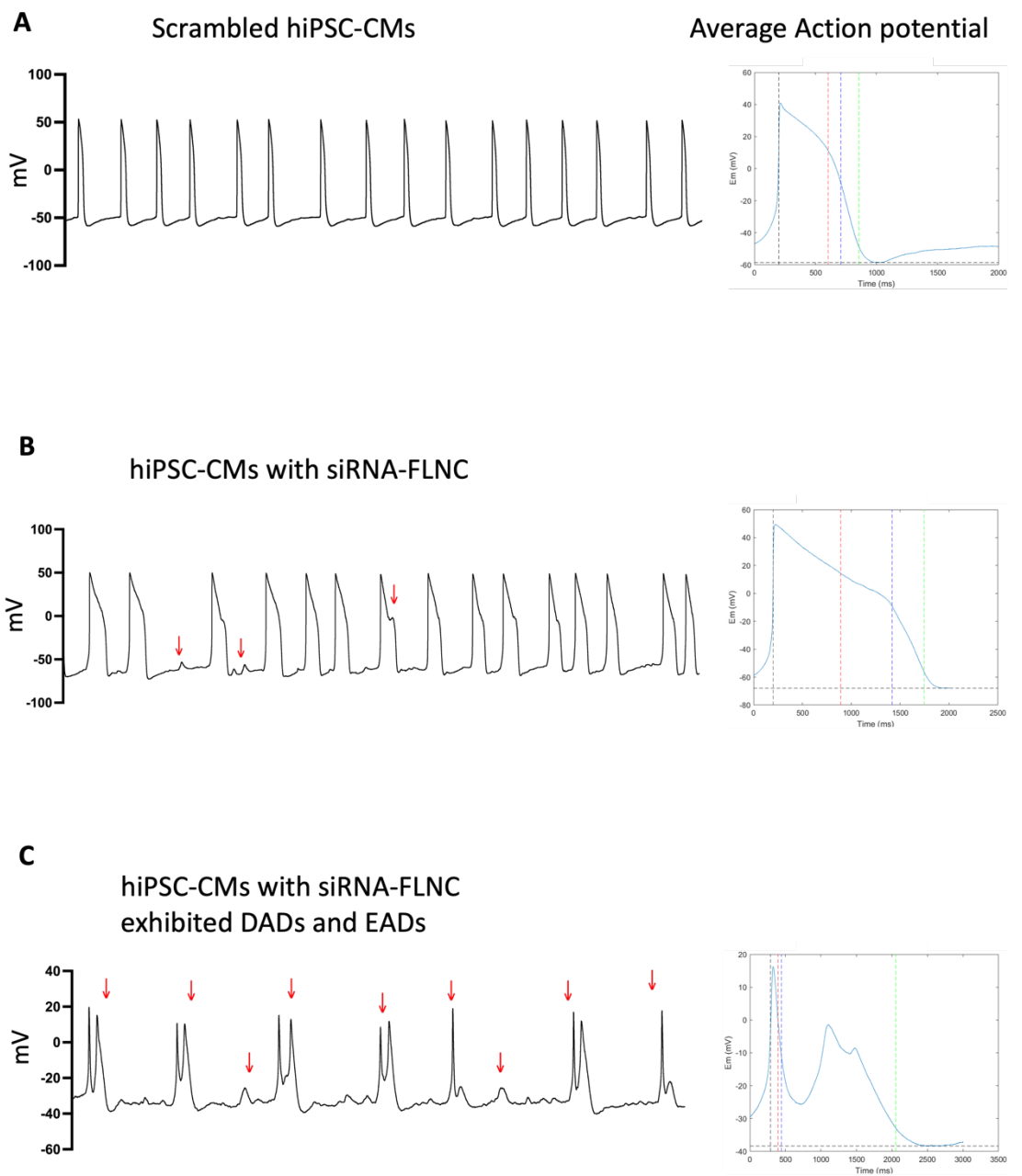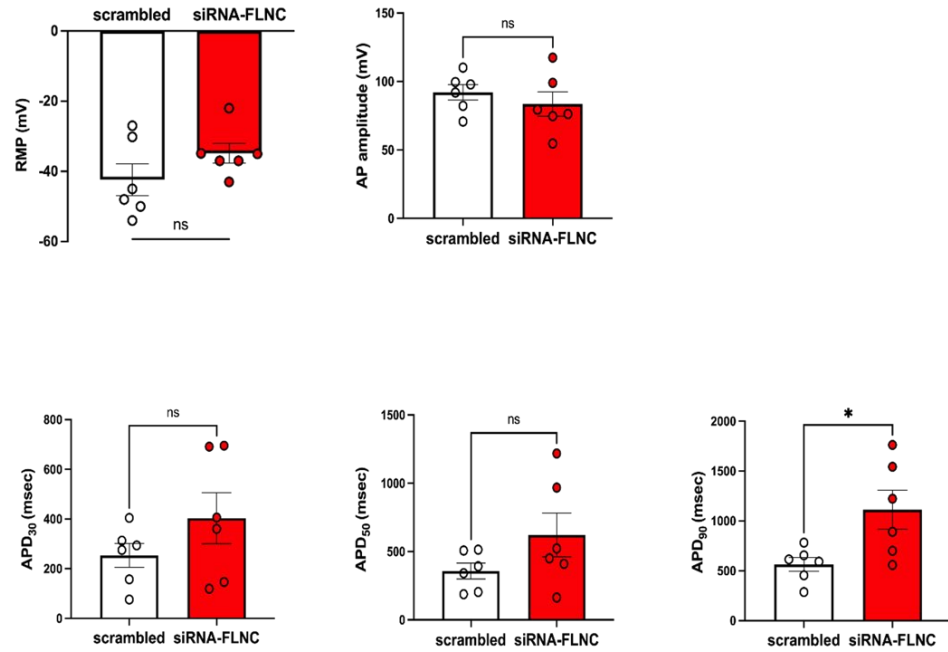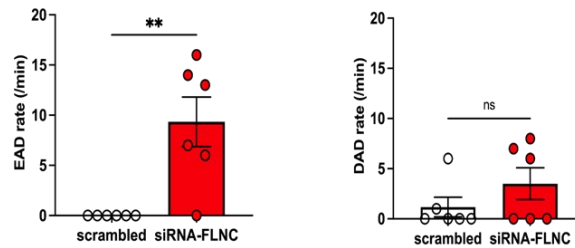
*Figure 6. 6. **Action potential recordings in the current clamp from the spontaneously beating hiPSC-CMs.** One minute of recording is shown in A, B, and C. (A) Representative traces of action potential from scrambled hiPSC-CMs. (B) The basal APD was prolonged in hiPSC-CMs when treated with siRNA-FLNC. (C) The red arrows indicate the occurrence of both DADs and EADs in action potentials of hiPSC-CMs following siRNA-FLNC. (D) Action potential parameters, including AP amplitudes, resting membrane potential (RMP), and APD30 and APD50 were measured and there was little difference, although not statistically significant (P>0.05), in APD30 and APD50 of hiPSC-CMs with siRNA-FLNC compared to those with scrambled siRNA. APD90 was significantly prolonged (P<0.05) in hiPSC-CMs with siRNA-FLNC. (E) Action potentials during arrhythmia in hiPSC-CMs following siRNA-FLNC exhibited DADs and EADs. There was no significant difference in the number of cells exhibiting DADs (P>0.05), whereas the number of EADs was significantly higher in siRNA-FLNC vs scrambled control (P<0.01).*

One explanation for the prolonged APD in hiPSC-CMs following siRNA-FLNC is that hERG function or expression is reduced. The I_{Kr} (rapid repolarising potassium current) is arising from channels composed of hERG subunits and also KCNE2 as an auxiliary subunit ([21](), [198]()). According to a previous study ([132]()), the interaction between FLNC and KCNE2 was found under hypoxic conditions and the authors suggested that it may contribute to the pathogenesis of long QT syndrome. Indeed loss of functional I_{Kr} current in long QT syndrome causes delayed repolarisation and prolongation of APD, resulting in the formation of EADs ([199]()).

Voltage clamp analysis was conducted by Dr Qadeer Aziz (Queen Mary University of London) to assess hERG channel current activity that thought to be responsible for the AP changes in hiPSC-CMs following siRNA-FLNC. I prepared the cells and Dr Aziz performed the patch clamping. The hERG current measured in hiPSC-CMs treated with siRNA-FLNC was compared to that measured in hiPSC-CMs treated with scrambled control siRNA. I_{Kr} is activated during repolarisation, and E-4031 (#1808, biotechne TOCRIS, USA) was used to inhibit I_{Kr} in hiPSC-CMs in order to assess the response of cells treated with either scrambled control or siRNA-FLNC. The current density of I_{Kr} was not

significantly reduced (P>0.05) in cells transfected with siRNA-FLNC, but there was a trend indicating a possible effect if the number of recordings was increased (Figure 6. 7). The normalised tail currents of hiPSC-CMs with siRNA-FLNC were comparable to those obtained from the scrambled control. Activation curves, determined from peak tail currents normalised to the maximal value and plotted against the voltage were fitted with Boltzmann equation (I/Imax= [1+exp {(V-V$_{1/2}$) /k}], where V$_{1/2}$ is the half maximal voltage of activation, and k is the slope factor. The voltage dependence of activation parameters (V$_{1/2}$ and k) were relatively similar between scrambled control and hiPSC-CMs treated with siRNA-FLNC (Figure 6. 7).
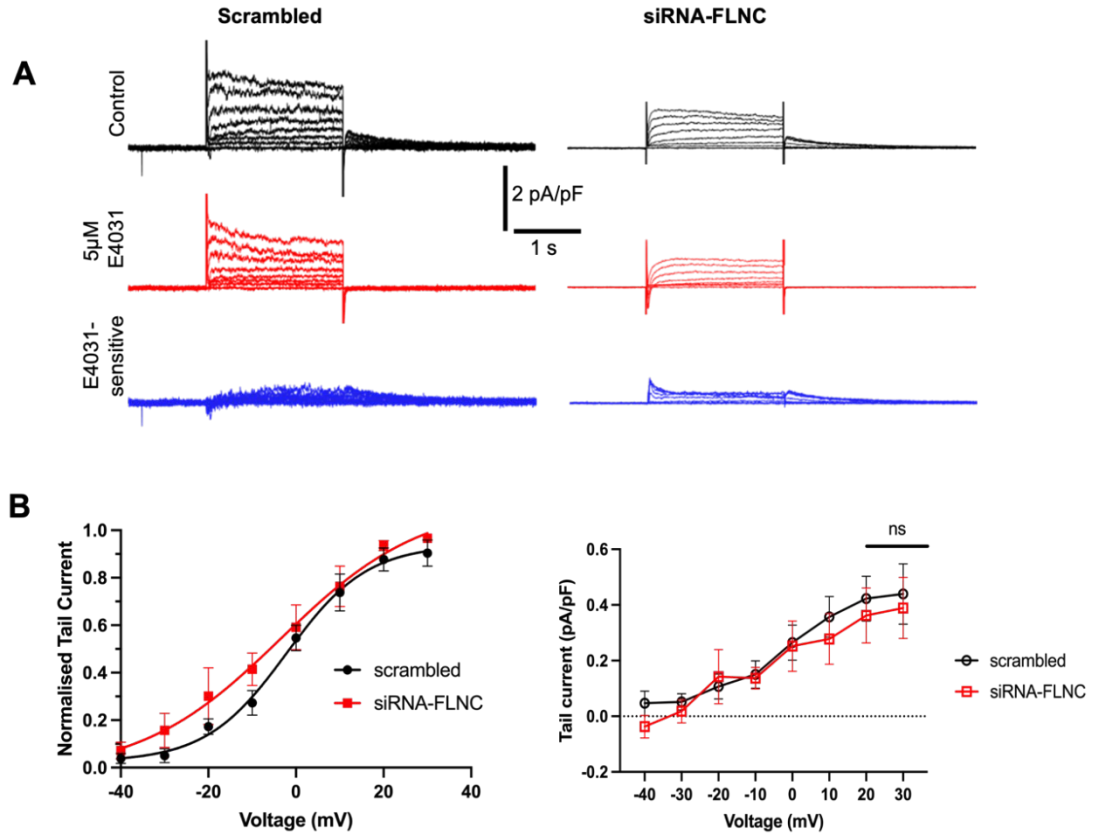
*Figure 6. 7. **Patch clamp recordings of hiPSC-CMs in voltage clamp mode**. (A) Representative voltage clamp recordings of K^+ current pre and post E4031 treatment in scrambled (n=6) and siRNA-FLNC cells (n=6). Notably, these currents were subtracted to obtain E4031-senstive I_{Kr}. (B) I-V graph and normalised tail current were assessed. It can be clearly seen that scrambled hiPSC-CMs had slightly higher currents at 10 mV and 20 mV in I-V graph compared to hiPSC-CMs with siRNA-FLNC. Averaged I_{Kr} tail current normalised to maximal current and fitted with Boltzmann function $(I/I_{max}) = 1/(1+exp(V_{1/2} - V_m)/k)$ following repolarisation to -40 mV in both scrambled and siRNA-FLNC of hiPSC-CMs.*

6.6 *Summary*

I have for the first time conducted two functional studies of FLNC knockdown in a cellular model and this has revealed electrophysiological abnormalities in hiPSC-CMs. I examined the AP profile and measured the APD and CaTD values among untreated cells and compared with scrambled siRNA and siRNA-FLNC. In optical recordings, I found abnormal APs with prolonged APD50 and APD90 in cells with siRNA-FLNC transfection. Rise time was not significantly changed in cells following siRNA-FLNC. The changes in calcium transients in hiPSC-CMs were also assessed and found that knockdown of FLNC caused a prolongation in CaT50 with no effect on calcium amplitudes. Additional recordings and transfection of minimum two to three independent batch of cells are needed to validate these findings. Moreover, both EAD-like events and DAD-like events were detected in patch clamp recordings, whereas only EAD-like events were observed in optical recordings. In patch clamp recordings, hiPSC-CMs with siRNA-FLNC showed a tendency to longer APD30 and APD50 when compared with scrambled cells, although these parameters were not statistically different, whereas the APD90 was significantly different between the two groups. There is ongoing work to increase the number of recordings and examine the effect of siRNA-FLNC on the hERG

current density in hiPSC-CMs model. Perhaps other currents (for example, the L-type calcium current) could be examined and may be impacted by FLNC knockdown.

The interpretation of the results is complicated by the different cycle length after treatment with siRNA-FLNC. Repolarisation is highly rate dependent and the increases in cycle length was linked to QT interval prolongation at slow heart rate. Therefore, the APD is likely influenced by the heart rate because differences in APD are reflected in differences in ion channel properties, and these properties determine the rate dependence of APD. Prolongation of APD is potentially arrhythmogenic, especially due to ion channel mutations or by abrupt alterations in cycle length (200).

Chapter 7   General discussion

7.1 *Summary of major findings*

This thesis aimed to examine the electrophysiological effects caused by loss of FLNC in a cellular model. There are various cellular models that can be used for studying the electrophysiological effects of FLNC downregulation, but the use of hiPSC-CMs has gained prominence for drug screening and elucidating the functions of inherited arrhythmias such as AC.

In the present study, I aimed to evaluate the ability to model FLNC mutations using hiPSC-CMs and recapitulate the disease phenotype of AC. Recent clinical studies have revealed that FLNC mutations have been associated with different cardiomyopathies and cause electrophysiological abnormalities. This concept was the precursor to demonstrate that downregulation of FLNC can reduce the expression of Cx43 and potentially lead to myocardial electrical dysfunction in hiPSC-CMs model. Previous studies have revealed an association between Cx43 and Nav1.5 in arrhythmogenesis of AC ([56], [201]). Nav1.5 was hypothesised to be impacted in hiPSC-CMs, but the current observations indicate that loss of FLNC may not have a significant impact on Nav1.5 expression. Conduction velocity, which is dependent on both Nav1.5 and Cx43, will need to be examined in the future.

Immunostaining signal for DSP was found to be reduced at cell-cell junction in patients with FLNC mutations ([87](#), [105](#), [115](#)) and in this study DSP demonstrated a significant reduction in mean fluorescence intensity by knocking down FLNC in hiPSC-CMs. Junctional plakoglobin was not found to be reduced in heart samples of patients bearing FLNC variants, but does appear to be reduced in this cellular model. This needs to be more investigated and it could be due to the binding sites implicated in the interaction with DSP at desmosome. Also, it should be noted that the heart is a multicellular system while hiPSC-CMs are only representing the cardiomyocytes and this could exhibit some variability when comparing between two models. The signals of junctional plakoglobin were reduced by immunofluorescence staining in hiPSC-CMs treated with siRNA-FLNC. These findings are consistent with the notion that FLNC-deficient hiPSC-CMs affect the distribution and expression levels ([122](#)) of intercalated disc proteins, including desmosomal proteins (desmoplakin and plakoglobin). However, two separate studies suggest that FLNC may have a distinct phenotype in terms of imaging scar patterns and arrhythmia risk compared to classic forms of ARVC ([115](#), [117](#)). On the other hand, FLNC has been found to be more frequently associated with ALVC. In this study, knockdown of

FLNC in hiPSC-CMs yields a likely phenotype of ALVC based on the proteins affected.

ECG abnormalities are common in FLNC variant carriers and present with low QRS voltages and repolarisation defects (87, 108). Therefore, different functional approaches were employed to examine the electrophysiological abnormalities at the cellular level. In chapter 5 using MEA recordings, I was able to show EADs and DADs-like events following knockdown of FLNC in hiPSC-CMs. In this set of experiments the beat rate\ R-R intervals was highly variable and there was a trend to a slower rate but this was not significant. In chapter 6 using optical techniques, changes in AP shape, prolonged calcium transient duration at 50% of repolarisation, and increased incidence of arrhythmic-like events were all observed in hiPSC-CMs with siRNA-FLNC. The explanation for the variation in the results with respect to beat rate\ R-R intervals between the different experiments is not clear. In these optical recordings, APD50 and APD90 were prolonged and EAD-like events became more prevalent. In addition, the prolongation of repolarisation is difficult to interpret as there is a significant dependence on heart rate. This is illustrated in the MEA recordings in (Figure 5. 3) and when adjusted for rate there was no difference in FPD between the conditions. DAD-like events were also observed in some cells, indicating that the

arrhythmogenicity of FLNC downregulation is complex and may be classified under cellular arrhythmic depolarisations (CAD) ([202](#)), whereby both EADs and DADs are implicated as the mechanisms of arrhythmogenesis ([203](#)). Indeed, the incidence of both of these events were identified previously in atrial fibrillation ([203](#)). Thus, further studies are needed to understand the mechanism of ionic currents and efforts should be increased to characterise the electrophysiological effects of drugs on hiPSC-CMs with FLNC knockdown. L-type calcium channel blockers (for example, nifedipine) could be used in this model to shorten the APD and potentially eliminate EADs ([179](#), [204](#), [205](#)).

One other study has reported the development of an iPSC model of FLNC cardiomyopathy ([122](#)). Suet Nee Chen and co-authors found the activation of platelet-derived growth factor receptor alpha (PDGFRA) signalling is likely responsible for the contractile dysfunction and electrical abnormality observed in FLNC mutants hiPSC-CMs. They suggested that loss of FLNC perturbed the cytoplasmic β-catenin and also increased nuclear localisation of β-catenin, which in turn activates transcription of PDGRFA signalling, leading to continuous upregulation at the cell-cell membrane. This upregulation of PDGFRA signalling can then activate extracellular regulated kinase (ERK) signalling, which leads to internalisation of Cx43, resulting in arrhythmias in the heart of

patient with arrhythmogenic dilated cardiomyopathy caused by FLNC mutations. Also, they found that the arrhythmic phenotype was characterised by increased variability in beating rate and abnormal AP morphology. DADs were detected in this model and were also observed in my study. DADs are typically observed during calcium overload and I_{NCX} is widely considered to be responsible for DAD formation ([25]). Given that DADs were also displayed in MEA and patch clamp recordings, it would be of value to investigate the role of I_{NCX} in hiPSC-CMs following siRNA-FLNC. This could provide more information for understanding the pathogenic mechanisms and aid to establish personalised drug treatments in patients with arrhythmias resulting from FLNC mutations.

In summary, I have demonstrated a broad cellular arrhythmogenic phenotype characterised by EADs, and DADs. Changes in the expression or function of HERG may not be responsible and the exact electrophysiological mechanism remains to be determined. The complex results emphasis why the patients have such a clear arrhythmic phenotype.

7.2 *Strengths and Limitations*

Typically, adult cardiomyocytes isolated from animal models or human heart tissues are more appropriate for studying cardiac cellular electrophysiology, particularly action potential characteristics and ion channel activity. However, these models do have some challenges like the limited availability of human samples and possible remodelling of cell's function and structure during culturing process ([206](#)). Furthermore, animal models cannot express all the human ion channels and therefore cannot adequately mimic human physiology ([207](#), [208](#)). On the other hand, iPSCs are a promising alternative since they have the benefit of their human origin and easy accessibility for use in scientific investigations. However, despite the ability of hiPSC-CMs to overcome the limitation of species differences, the foetal identity in derived tissues and the variability in genetic background of iPSC lines, still represent challenges for disease modelling ([209](#)). These limitations led to efforts to improve methods for the maturation of hiPSC-CMs. Hormonal approaches, electrical and/or mechanical stimulation, long-term culture, and other methods have been found to mature hiPSC-CMs. In this study, hiPSC-CMs were treated with T3 and dexamethasone ([210](#)). Despite the fact that these methods can improve the structural, metabolic, and electrophysiological properties of hiPSC-CMs, they still

cannot fully recapitulate adult cardiomyocytes ([76]). Future research may require the combination of these methods with other more complex techniques such as engineered heart tissue or co-culturing with other cell types in order to produce a more mature phenotype for these cells.

Currently, there are several invasive and non-invasive methods used for hiPSC-CM analyses, including patch clamp, fluorescence imaging, multielectrode array, and cellular impedance assays. Although these techniques are feasible in many laboratories, some difficulties arise when implemented in the functional study on hiPSC-CMs. Patch clamp, for example, requires advanced skills and equipment though it can provide precise data on cardiac action potentials and ionic currents. Other obstacles such as low throughput and time-consuming, are still existing in manual patch clamp investigations ([211]). However, all the previous mentioned methods suffer from some serious limitations, such as difficulties to obtain detailed data on ionic currents in multielectrode array, and misinterpretation of impedance assay data as the beating pattern of cells depends primarily on changes in resistance and not on direct electrical activity ([212], [213]). Also, optical measurements using fluorescent dyes have several disadvantages, including challenges of loading conditions (duration and temperature). Other challenges that could be expected to affect the optical data are spatiotemporal

variations associated with probe bleaching, motion artefacts, and phototoxicity ([25](#), [157](#)) ([189](#), [214](#)). Despite the above-mentioned shortcomings, the capability to integrate each of these techniques into a single study would facilitate obtaining broad functional data.

By using transfection reagents to deliver siRNA into cultured cardiomyocytes in question with possible interacting proteins of interest, their modulatory effect can be investigated. This enables study of the functional and morphological consequences identified in patients with cardiac arrhythmias caused by these genetic mutations. However, due to the use of different iPSC cell lines and the need to optimise the transfection conditions for each particular cell line, the transfection efficiency and cell viability could be affected by differences in cell growth characteristics and cell densities. Thus, it would be necessary to use iPSC line generated from a patient carrying a mutation in FLNC to minimise the risk of cytotoxicity caused by transfection reagents.

Time and high costs are also limiting factors in the hiPSC-CMs differentiation process. Due to the genetic and phenotypic heterogeneity of iPSC cell lines, the output of this study may be affected by the use of different iPSC cell lines, hence it is recommended to study two different cell lines ([215](#)). Moreover, the use of different culture substrates, such as Matrigel or Geltrex, may result in variable electrophysiological

characteristics ([139-141](#)). Despite this, hiPSC-CMs can provide valuable information to study the basic mechanisms of cardiac arrhythmias resulted from cardiomyopathies.

It is nevertheless noteworthy to observe that some variable values emerged from the scrambled hiPSC-CMs during MEA recordings, which I attributed to the potential cytotoxicity caused by transfection reagents, as well as the use of different iPSC cell lines and/or the application of different coating substrates ([140](#), [215](#), [216](#)). Furthermore, the manufacturer (Horizon Discovery) has issued a statement outlining experimental considerations for the scrambled control pool #1 that I used in this study. The supplier stated on its website that "siGENOME Non-targeting siRNA #1 reduces EGFR in an assay and cell specific manner by ~50%" and it was suggested to use an alternative formulation siRNA non-targeting Pool #2. This statement was issued after some of the experiments were completed and made me aware of that this phenomenon might have some consequences in my studies.

7.3 *Future directions*

The work presented in this thesis has opened several avenues for further investigations. A better understanding of the electrophysiological phenotype could be carried out by using CRISPR-I system in hiPSC-CMs to examine whether the functional changes observed during FLNC knockdown would be comparable to those demonstrated by siRNA. Also, this could be further supported with different multicellular models, such as mouse heart. Given that hiPSCs are heterogenous and represent an individual's unique genotype as they derived from somatic cells and also using different adhesion matrix coating protocol may contribute to discrepancies and hinder the quality of the results. Ideally, comparing the results from different cell lines would provide a comprehensive understanding of the electrophysiological phenotype with knockdown of FLNC. Alternatively, using gene editing system would aid to create the isogenic iPSC lines from well-characterised pre-existing iPSC lines obtained from healthy donors and can solve this problem with cell line variations (217). In addition, using CRISPR activation would be beneficial to evaluate the improvement in phenotype by upregulating the gene expression.

While it was observed that FLNC expression was decreased in hiPSC-CMs treated with siRNA-FLNC compared to control conditions,

the changes in subcellular localisation was only observed but not confirmed its protein interactions. Therefore, additional experiments such as co-localisation and co-immunoprecipitation would be necessary to elucidate this hypothesis. In addition, western blots need to be performed to examine the expression levels for desmoplakin, plakoglobin, and plakophilin-2.

As mentioned previously, several studies showed the co-regulation between Cx43 and Nav1.5 ([52], [57], [201]) and it is of value to examine the sodium current in hiPSC-CMs following the siRNA-FLNC by the whole-cell patch clamp technique. In this work, Nav1.5 showed no or modest decrease in the protein expression levels in cells transfected with siRNA-FLNC. It would be interesting to examine sodium currents in hiPSC-CMs to explore Nav1.5-related electrophysiology changes.

The most promising direction for the future experiments is drug testing. Many papers have shown that calcium channel blockers can be used to shorten APD. In this study, nifedipine completely suppressed the transient and perhaps a lower dose (1µM) would be needed to investigate the effect of this drug on the prolonged APD that was displayed with FLNC knockdown in hiPSC-CMs. Also, pacing the monolayers at different cycle lengths would need to be performed to assess the APD and conduction velocity in these cells.

In addition to the previously published work describing the interaction between FLNC and KCNE2 ([132](#)) and since EADs caused by prolonged APD were detected in the present study, it would be useful to characterise the expression and subcellular localisation of hERG channel with FLNC knockdown and assess the modulation of hERG current density in hiPSC-CMs. Some efforts have been made in this thesis but need to include a high number of recordings to validate these findings. However, we have not studied other relevant currents, such as the L-type calcium current and whether the density and regulation of this current is abnormal needs to be determined.

Recently, Suet Nee Chen and co-authors ([122](#)) have provided valuable information to understand the pathogenesis of FLNC-related AC. They used hiPSC-CMs model and revealed that loss of FLNC disturbed the cytoplasmic β-catenin and activated both PDGFRA and extracellular regulated kinase (ERK) signalling, leading to internalisation of gap junction protein and arrhythmia. Interestingly, they were able to rescue the phenotype of hiPSC-CMs using a PDGFRA inhibitor. Therefore, future work will consider a panel of arrhythmia-inhibiting drugs to test in the hiPSC model following FLNC downregulation.

Finally, desmin is an important protein that needs to be studied in order to understand how it interacts with FLNC. Given that these two

proteins cause the left dominant form of AC, which appears to be linked in the cytoskeleton of cardiomyocytes. Desmin is a structural intermediate filament that is connected to the desmosome via DSP. Thus, mutations that affect the cellular function of FLNC or desmin may impair DSP distribution at junctional sites, resulting in the AC phenotype, as suggested in previous studies (109, 110). Moreover, other proteins associated with AC disease, whose distribution/expression could potentially be impacted, need to be analysed in the future studies such as SAP97, GSK3β and RelA.

Taken together, hiPSC-CMs is promising for cardiovascular research. The availability and feasibility are encouraging for scientific investigations and therapeutic use in inherited heart diseases. This thesis demonstrates that ability to measure the physiologically important proteins and functional parameters in hiPSC-CMs as well as examining the electrophysiological phenotypes before and after gene silencing. Therefore, hiPSC-CMs are powerful tool for future research in cardiovascular medicine.

Chapter 8　　Reference

1.　　Pai SG, Carneiro BA, Mota JM, Costa R, Leite CA, Barroso-Sousa R, et al. Wnt/beta-catenin pathway: modulating anticancer immune response. Journal of hematology & oncology. 2017;10(1):1-12.

2.　　Bennett RG, Haqqani HM, Berruezo A, Della Bella P, Marchlinski FE, Hsu C-J, et al. Arrhythmogenic cardiomyopathy in 2018–2019: ARVC/ALVC or both? 2019;28(1):164-77.

3.　　Austin KM, Trembley MA, Chandler SF, Sanders SP, Saffitz JE, Abrams DJ, et al. Molecular mechanisms of arrhythmogenic cardiomyopathy. Nature reviews Cardiology. 2019.

4.　　Mangum KD, Ferns SJJEjomg. A novel familial truncating mutation in the filamin C gene associated with cardiac arrhythmias. 2019;62(4):282-5.

5.　　Bosman LP, Te Riele AS. Arrhythmogenic right ventricular cardiomyopathy: a focused update on diagnosis and risk stratification. Heart. 2022;108(2):90-7.

6.　　Lin Y-N, Ibrahim A, Marbán E, Cingolani E. Pathogenesis of arrhythmogenic cardiomyopathy: role of inflammation. Basic Research in Cardiology. 2021;116(1):39.

7.　　Guo G-r, Chen L, Rao M, Chen K, Song J-p, Hu S-s. A modified method for isolation of human cardiomyocytes to model cardiac diseases. Journal of translational medicine. 2018;16(1):1-9.

8.　　Coppini R, Ferrantini C, Aiazzi A, Mazzoni L, Sartiani L, Mugelli A, et al. Isolation and functional characterization of human ventricular cardiomyocytes from fresh surgical samples. JoVE (Journal of Visualized Experiments). 2014(86):e51116.

9.　　Hwang HS, Kryshtal DO, Feaster TK, Sánchez-Freire V, Zhang J, Kamp TJ, et al. Comparable calcium handling of human iPSC-derived cardiomyocytes generated by multiple laboratories. Journal of molecular and cellular cardiology. 2015;85:79-88.

10.　　Pourrier M, Fedida D. The emergence of human induced pluripotent stem cell-derived cardiomyocytes (hiPSC-CMs) as a platform to model arrhythmogenic diseases. International journal of molecular sciences. 2020;21(2):657.

11.　　Towbin JA, McKenna WJ, Abrams DJ, Ackerman MJ, Calkins H, Darrieux FC, et al. 2019 HRS expert consensus statement on evaluation, risk stratification, and management of arrhythmogenic cardiomyopathy: Executive summary. Heart rhythm. 2019;16(11):e373-e407.

12.   Bang M-L, Bogomolovas J, Chen J. Understanding the Molecular Basis of Cardiomyopathy. American Journal of Physiology-Heart and Circulatory Physiology. 2021.

13.   McKenna WJ, Maron BJ, Thiene GJCr. Classification, epidemiology, and global burden of cardiomyopathies. 2017;121(7):722-30.

14.   James CA, Calkins HJArom. Arrhythmogenic right ventricular cardiomyopathy: progress toward personalized management. 2019;70:1-18.

15.   Corrado D, Link MS, Calkins HJNEjom. Arrhythmogenic right ventricular cardiomyopathy. 2017;376(1):61-72.

16.   SEN-CHOWDHRY S, Syrris P, McKENNA WJJJoce. Genetics of right ventricular cardiomyopathy. 2005;16(8):927-35.

17.   Meraviglia V, Alcalde M, Campuzano O, Bellin M. Inflammation in the pathogenesis of arrhythmogenic cardiomyopathy: secondary event or active driver? Frontiers in cardiovascular medicine. 2021;8:784715.

18.   Corrado D, Marra MP, Zorzi A, Beffagna G, Cipriani A, De Lazzari M, et al. Diagnosis of arrhythmogenic cardiomyopathy: the Padua criteria. International journal of cardiology. 2020;319:106-14.

19.   Corrado D, Link MS, Schwartz PJ. Implantable defibrillators in primary prevention of genetic arrhythmias. A shocking choice? European Heart Journal. 2022.

20.   Corrado D, Wichter T, Link MS, Hauer RN, Marchlinski FE, Anastasakis A, et al. Treatment of arrhythmogenic right ventricular cardiomyopathy/dysplasia: an international task force consensus statement. Circulation. 2015;132(5):441-53.

21.   Boron WF, Boulpaep EL. Medical physiology. Third edition. ed. Philadelphia, PA: Elsevier; 2017. xii, 1297 pages p.

22.   Leonard SL. Pathophysiology of heart disease: A collaborative project of medical students and faculty, 6e. Wolters Kluwer; 2015.

23.   Mulroney SE, Myers AK. Netter's essential physiology: Saunders/Elsevier; 2009.

24.   Song W, Shou W. Cardiac sodium channel Nav1. 5 mutations and cardiac arrhythmia. Pediatric cardiology. 2012;33(6):943-9.

25.   Varró A, Tomek J, Nagy N, Virag L, Passini E, Rodriguez B, et al. Cardiac transmembrane ion channels and action potentials: cellular physiology and arrhythmogenic behavior. Physiological Reviews. 2021;101(3):1083-176.

26.   Liu M, Yang K-C, Dudley SC. Cardiac sodium channel mutations: why so many phenotypes? Nature Reviews Cardiology. 2014;11(10):607-15.

27.   Jiang D, Shi H, Tonggu L, El-Din TMG, Lenaeus MJ, Zhao Y, et al. Structure of the cardiac sodium channel. Cell. 2020;180(1):122-34. e10.

28.   Bartos DC, Grandi E, Ripplinger CM. Ion channels in the heart. Comprehensive Physiology. 2015;5(3):1423.

29.   Catterall WA. Voltage-gated calcium channels. Cold Spring Harbor perspectives in biology. 2011;3(8):a003947.

30.   Huang H, Pugsley MK, Fermini B, Curtis MJ, Koerner J, Accardi M, et al. Cardiac voltage-gated ion channels in safety pharmacology: Review of the landscape leading to the CiPA initiative. Journal of Pharmacological and Toxicological Methods. 2017;87:11-23.

31.   Grant AO. Cardiac ion channels. Circulation: Arrhythmia and Electrophysiology. 2009;2(2):185-94.

32.   Specterman MJ, Behr ER. Cardiogenetics: the role of genetic testing for inherited arrhythmia syndromes and sudden death. Heart. 2022.

33.   Chen H, Chatelain FC, Lesage F. Altered and dynamic ion selectivity of K+ channels in cell development and excitability. Trends in pharmacological sciences. 2014;35(9):461-9.

34.   Lilly LS, School HM. Pathophysiology of Heart Disease: A Collaborative Project of Medical Students and Faculty: Wolters Kluwer; 2016.

35.   Shattock MJ, Ottolia M, Bers DM, Blaustein MP, Boguslavskyi A, Bossuyt J, et al. Na+/Ca2+ exchange and Na+/K+-ATPase in the heart. The Journal of physiology. 2015;593(6):1361-82.

36.   Fearnley CJ, Roderick HL, Bootman MD. Calcium signaling in cardiac myocytes. Cold Spring Harbor perspectives in biology. 2011;3(11):a004242.

37.   Moccia F, Lodola F, Stadiotti I, Pilato CA, Bellin M, Carugo S, et al. Calcium as a Key Player in Arrhythmogenic Cardiomyopathy: Adhesion Disorder or Intracellular Alteration? International journal of molecular sciences. 2019;20(16):3986.

38.   Landstrom AP, Dobrev D, Wehrens XH. Calcium signaling and cardiac arrhythmias. Circulation research. 2017;120(12):1969-93.

39.   Torres NS. Activation of reverse Na+-Ca2+ exchanger by skeletal Na+ channel isoform increases excitation-contraction coupling efficiency in rabbit cardiomyocytes. American Journal of Physiology-Heart and Circulatory Physiology. 2021;320(2):H593-H603.

40.   Sutanto H, Lyon A, Lumens J, Schotten U, Dobrev D, Heijman J. Cardiomyocyte calcium handling in health and disease: Insights from in vitro and in silico studies. Progress in Biophysics and Molecular Biology. 2020;157:54-75.

41.   Yang B, Lowenthal J, Tomaselli GF, Tung L. Human iPSC models of cardiac electrophysiology and arrhythmia. iPSCs-State of the Science: Elsevier; 2022. p. 29-93.

42.   Antzelevitch C, Burashnikov A. Overview of basic mechanisms of cardiac arrhythmia. Cardiac electrophysiology clinics. 2011;3(1):23-45.

43.   Kulkarni K, Merchant FM, Kassab MB, Sana F, Moazzami K, Sayadi O, et al. Cardiac alternans: mechanisms and clinical utility in arrhythmia prevention. Journal of the American Heart Association. 2019;8(21):e013750.

44.   Del Álamo JC, Lemons D, Serrano R, Savchenko A, Cerignoli F, Bodmer R, et al. High throughput physiological screening of iPSC-derived cardiomyocytes for drug development. Biochimica et Biophysica Acta (BBA)-Molecular Cell Research. 2016;1863(7):1717-27.

45.   Kanaporis G, Blatter LA. The mechanisms of calcium cycling and action potential dynamics in cardiac alternans. Circulation research. 2015;116(5):846-56.

46.   Zhao G, Qiu Y, Zhang HM, Yang D. Intercalated discs: cellular adhesion and signaling in heart health and diseases. Heart failure reviews. 2019;24(1):115-32.

47.   Rampazzo A, Calore M, van Hengel J, van Roy F. Intercalated discs and arrhythmogenic cardiomyopathy. Circulation Cardiovascular genetics. 2014;7(6):930-40.

48.   Calore M, Lorenzon A, De Bortoli M, Poloni G, Rampazzo A. Arrhythmogenic cardiomyopathy: a disease of intercalated discs. Cell and tissue research. 2015;360(3):491-500.

49.   Gomes J, Finlay M, Ahmed AK, Ciaccio EJ, Asimaki A, Saffitz JE, et al. Electrophysiological abnormalities precede overt structural changes in arrhythmogenic right ventricular cardiomyopathy due to mutations in desmoplakin-A combined murine and human study. European heart journal. 2012;33(15):1942-53.

50.   Noorman M, Hakim S, Kessler E, Groeneweg JA, Cox MG, Asimaki A, et al. Remodeling of the cardiac sodium channel, connexin43, and plakoglobin at the intercalated disk in patients with arrhythmogenic cardiomyopathy. 2013;10(3):412-9.

51.   Gerull B, Brodehl A. Insights into genetics and pathophysiology of arrhythmogenic cardiomyopathy. Current Heart Failure Reports. 2021;18(6):378-90.

52.   Sottas V, Wahl C-M, Trache MC, Bartolf-Kopp M, Cambridge S, Hecker M, et al. Improving electrical properties of iPSC-cardiomyocytes by enhancing Cx43 expression. 2018;120:31-41.

53.   Weber PA, Chang H-C, Spaeth KE, Nitsche JM, Nicholson BJ. The permeability of gap junction channels to probes of different size is dependent on connexin composition and permeant-pore affinities. Biophysical journal. 2004;87(2):958-73.

54.   Nielsen MS, Nygaard Axelsen L, Sorgen PL, Verma V, Delmar M, Holstein-Rathlou NH. Gap junctions. Comprehensive Physiology. 2012;2(3):1981-2035.

55.   Rhett JM, Ongstad EL, Jourdan J, Gourdie RG. Cx43 associates with Na(v)1.5 in the cardiomyocyte perinexus. J Membr Biol. 2012;245(7):411-22.

56.   Agullo-Pascual E, Cerrone M, Delmar MJFl. Arrhythmogenic cardiomyopathy and Brugada syndrome: diseases of the connexome. 2014;588(8):1322-30.

57.   Jansen JA, Noorman M, Musa H, Stein M, de Jong S, van der Nagel R, et al. Reduced heterogeneous expression of Cx43 results in decreased Nav1. 5 expression and reduced sodium current that accounts for arrhythmia vulnerability in conditional Cx43 knockout mice. 2012;9(4):600-7.

58.   Zhang Q, Deng C, Rao F, Modi RM, Zhu J, Liu X, et al. Silencing of desmoplakin decreases connexin43/Nav1. 5 expression and sodium current in HL-1 cardiomyocytes. Molecular medicine reports. 2013;8(3):780-6.

59.   Rhett JM, Veeraraghavan R, Poelzing S, Gourdie RG. The perinexus: sign-post on the path to a new model of cardiac conduction? Trends in cardiovascular medicine. 2013;23(6):222-8.

60.   Costa S, Cerrone M, Saguner AM, Brunckhorst C, Delmar M, Duru F. Arrhythmogenic cardiomyopathy: An in-depth look at molecular mechanisms and clinical correlates. Trends in Cardiovascular Medicine. 2021;31(7):395-402.

61.   Stroud MJ, Fang X, Zhang J, Guimarães-Camboa N, Veevers J, Dalton ND, et al. Luma is not essential for murine cardiac development and function. Cardiovascular research. 2017;114(3):378-88.

62.   Brodehl A, Ebbinghaus H, Deutsch M-A, Gummert J, Gärtner A, Ratnavadivel S, et al. Human Induced Pluripotent Stem-Cell-Derived Cardiomyocytes as Models for Genetic Cardiomyopathies. International journal of molecular sciences. 2019;20(18):4381.

63.   Odening KE, Gomez A-M, Dobrev D, Fabritz L, Heinzel FR, Mangoni ME, et al. ESC working group on cardiac cellular electrophysiology position paper: relevance, opportunities, and limitations of experimental models for cardiac electrophysiology research. EP Europace. 2021;23(11):1795-814.

64.   Romito A, Cobellis GJSci. Pluripotent stem cells: current understanding and future directions. 2016;2016.

65.   Singh VK, Saini A, Kalsan M, Kumar N, Chandra RJFic, biology d. Describing the stem cell potency: the various methods of functional assessment and in silico diagnostics. 2016;4:134.

66.   Bindu H, Srilatha BJJSCRT. Potency of various types of stem cells and their transplantation. 2011;1(3):115.

67.   Ilic D, Polak JMJBmb. Stem cells in regenerative medicine: introduction. 2011;98(1):117-26.

68.   Matsa E, Burridge PW, Wu JCJStm. Human stem cells for modeling heart disease and for drug discovery. 2014;6(239):239ps6-ps6.

69.   Bellin M, Casini S, Davis RP, D'aniello C, Haas J, Ward-van Oostwaard D, et al. Isogenic human pluripotent stem cell pairs reveal the role of a KCNH2 mutation in long-QT syndrome. 2013;32(24):3161-75.

70.   Halevy T, Urbach AJJocm. Comparing ESC and iPSC—based models for human genetic disorders. 2014;3(4):1146-62.

71.   Takahashi K, Yamanaka SJc. Induction of pluripotent stem cells from mouse embryonic and adult fibroblast cultures by defined factors. 2006;126(4):663-76.

72.   Yu J, Vodyanik MA, Smuga-Otto K, Antosiewicz-Bourget J, Frane JL, Tian S, et al. Induced pluripotent stem cell lines derived from human somatic cells. 2007;318(5858):1917-20.

73.   Zhang J, Wilson GF, Soerens AG, Koonce CH, Yu J, Palecek SP, et al. Functional cardiomyocytes derived from human induced pluripotent stem cells. 2009;104(4):e30-e41.

74.   Litviňuková M, Talavera-López C, Maatz H, Reichart D, Worth CL, Lindberg EL, et al. Cells of the adult human heart. Nature. 2020;588(7838):466-72.

75.   Onódi Z, Visnovitz T, Kiss B, Hambalkó S, Koncz A, Ágg B, et al. Systematic transcriptomic and phenotypic characterization of human and murine cardiac myocyte cell lines and primary cardiomyocytes reveals serious limitations and low resemblances to adult cardiac phenotype. Journal of Molecular and Cellular Cardiology. 2022;165:19-30.

76.   Machiraju P, Greenway SC. Current methods for the maturation of induced pluripotent stem cell-derived cardiomyocytes. World Journal of Stem Cells. 2019;11(1):33.

77.   Liang W, Gasparyan L, AlQarawi W, Davis DR. Disease modeling of cardiac arrhythmias using human induced pluripotent stem cells. Expert opinion on biological therapy. 2019;19(4):313-33.

78.   Musunuru K, Sheikh F, Gupta RM, Houser SR, Maher KO, Milan DJ, et al. Induced pluripotent stem cells for cardiovascular disease modeling and

precision medicine: a scientific statement from the American Heart Association. Circulation: Genomic and Precision Medicine. 2018;11(1):e000043.

79.   Sayed N, Liu C, Wu JC. Translation of human-induced pluripotent stem cells: from clinical trial in a dish to precision medicine. Journal of the American College of Cardiology. 2016;67(18):2161-76.

80.   Eltahir S, Ahmad KS, Al-Balawi MM, Bukhamsien H, Al-Mobaireek K, Alotaibi W, et al. Lung disease associated with filamin A gene mutation: a case report. Journal of Medical Case Reports. 2016;10(1):1-5.

81.   Bandaru S, Ala C, Zhou A-X, Akyürek LM. Filamin A regulates cardiovascular remodeling. International Journal of Molecular Sciences. 2021;22(12):6555.

82.   Xu Q, Wu N, Cui L, Wu Z, Qiu G. Filamin B: the next hotspot in skeletal research? Journal of Genetics and Genomics. 2017;44(7):335-42.

83.   Sutherland-Smith AJ. Filamin structure, function and mechanics: are altered filamin-mediated force responses associated with human disease? Biophysical reviews. 2011;3(1):15-23.

84.   Sanfilippo C, Di Rosa M. Modulation of myotilin and fylamin C in various muscle diseases: A microarray analysis. Journal of Functional Morphology and Kinesiology. 2016;1(1):90-101.

85.   Zhou A-X, Hartwig JH, Akyürek LMJTicb. Filamins in cell signaling, transcription and organ development. 2010;20(2):113-23.

86.   van der Flier A, Sonnenberg AJBeBA-MCR. Structural and functional aspects of filamins. 2001;1538(2-3):99-117.

87.   Ortiz-Genga MF, Cuenca S, Dal Ferro M, Zorio E, Salgado-Aranda R, Climent V, et al. Truncating FLNC Mutations Are Associated With High-Risk Dilated and Arrhythmogenic Cardiomyopathies. J Am Coll Cardiol. 2016;68(22):2440-51.

88.   Brodehl A, Ferrier RA, Hamilton SJ, Greenway SC, Brundler MA, Yu W, et al. Mutations in FLNC are Associated with Familial Restrictive Cardiomyopathy. Human mutation. 2016;37(3):269-79.

89.   Roldán-Sevilla A, Palomino-Doza J, de Juan J, Sánchez V, Domínguez-González C, Salguero-Bodes R, et al. Missense Mutations in the FLNC Gene Causing Familial Restrictive Cardiomyopathy: Growing Evidence. Circulation: Genomic and Precision Medicine. 2019;12(3):e002388.

90.   Kiselev A, Vaz R, Knyazeva A, Khudiakov A, Tarnovskaya S, Liu J, et al. De novo mutations in FLNC leading to early-onset restrictive cardiomyopathy and congenital myopathy. Human mutation. 2018;39(9):1161-72.

91.	Ahamed H, Subramanian M. Letter by Ahamed and Subramanian Regarding Article "Missense Mutations in the FLNC Gene Causing Familial Restrictive Cardiomyopathy". Circulation: Genomic and Precision Medicine. 2019;12(7):e002587.

92.	Valdes-Mas R, Gutierrez-Fernandez A, Gomez J, Coto E, Astudillo A, Puente DA, et al. Mutations in filamin C cause a new form of familial hypertrophic cardiomyopathy. Nat Commun. 2014;5:5326.

93.	Qin X, Li P, Qu H-Q, Liu Y, Xia Y, Chen S, et al. FLNC and MYLK2 gene mutations in a Chinese family with different phenotypes of cardiomyopathy. International Heart Journal. 2021;62(1):127-34.

94.	Begay RL, Tharp CA, Martin A, Graw SL, Sinagra G, Miani D, et al. FLNC Gene Splice Mutations Cause Dilated Cardiomyopathy. JACC Basic to translational science. 2016;1(5):344-59.

95.	Liebman SW, Palaganas H, Kobany H. A founder mutation in FLNC is likely a major cause of idiopathic dilated cardiomyopathy in Ashkenazi Jews. International Journal of Cardiology. 2021;323:124.

96.	Dungu JN, Langley SG, Hardy-Wallace A, Li B, Barbagallo RM, Field D, et al. Dilated cardiomyopathy: the role of genetics, highlighted in a family with Filamin C (FLNC) variant. Heart. 2021.

97.	Miszalski-Jamka K, Jefferies JL, Mazur W, Glowacki J, Hu J, Lazar M, et al. Novel Genetic Triggers and Genotype-Phenotype Correlations in Patients With Left Ventricular Noncompaction. Circulation Cardiovascular genetics. 2017;10(4).

98.	Ader F, De Groote P, Reant P, Rooryck-Thambo C, Dupin-Deguine D, Rambaud C, et al. FLNC pathogenic variants in patients with cardiomyopathies: Prevalence and genotype-phenotype correlations. Clinical genetics. 2019.

99.	Celeghin R, Cipriani A, Bariani R, Marinas MB, Cason M, Bevilacqua M, et al. Filamin-C variant-associated cardiomyopathy: A pooled analysis of individual patient data to evaluate the clinical profile and risk of sudden cardiac death. Heart Rhythm. 2021.

100.	Kandhari N, Khoury S, Behr ER, Miles C. Cardiac arrest as first presentation of arrhythmogenic left ventricular cardiomyopathy due to Filamin C mutation: a case report. European Heart Journal-Case Reports. 2021;5(11):ytab422.

101.	Gigli M, Stolfo D, Graw SL, Merlo M, Gregorio C, Nee Chen S, et al. Phenotypic Expression, Natural History, and Risk Stratification of Cardiomyopathy Caused by Filamin C Truncating Variants. Circulation. 2021;144(20):1600-11.

102.   Mao Z, Nakamura F. Structure and function of filamin C in the muscle Z-disc. International Journal of Molecular Sciences. 2020;21(8):2696.

103.   Conte G, Piciacchia F, Medeiros-Domingo A, Grego S, Ripellino P, Auricchio A. Filamin C missense variant associated with severe right atrial disease and skeletal myopathy. Journal of Cardiovascular Electrophysiology. 2021;32(10):2777-80.

104.   Shimrit O, Hagith Y, Leonid V, Efrat O, Natalie L, Haike R-W, et al. Reduction in Filamin C transcript is associated with arrhythmogenic cardiomyopathy in Ashkenazi Jews. International Journal of Cardiology. 2020.

105.   Begay RL, Graw SL, Sinagra G, Asimaki A, Rowland TJ, Slavov DB, et al. Filamin C Truncation Mutations Are Associated With Arrhythmogenic Dilated Cardiomyopathy and Changes in the Cell-Cell Adhesion Structures. JACC Clin Electrophysiol. 2018;4(4):504-14.

106.   Augusto JB, Eiros R, Nakou E, Moura-Ferreira S, Treibel TA, Captur G, et al. Dilated cardiomyopathy and arrhythmogenic left ventricular cardiomyopathy: a comprehensive genotype-imaging phenotype study. European Heart Journal-Cardiovascular Imaging. 2019.

107.   Bariani R, Bueno Marinas M, Rigato I, Veronese P, Celeghin R, Cipriani A, et al. Pregnancy in Women with Arrhythmogenic Left Ventricular Cardiomyopathy. Journal of Clinical Medicine. 2022;11(22):6735.

108.   Bariani R, Rigato I, Cason M, Bueno Marinas M, Celeghin R, Pilichou K, et al. Genetic Background and Clinical Features in Arrhythmogenic Left Ventricular Cardiomyopathy: A Systematic Review. Journal of Clinical Medicine. 2022;11(15):4313.

109.   Mestroni L, Sbaizero O. Arrhythmogenic Cardiomyopathy: Mechanotransduction Going Wrong. Am Heart Assoc; 2018.

110.   Bermúdez-Jiménez FJ, Carriel V, Brodehl A, Alaminos M, Campos A, Schirmer I, et al. Novel desmin mutation p. Glu401Asp impairs filament formation, disrupts cell membrane integrity, and causes severe arrhythmogenic left ventricular cardiomyopathy/dysplasia. Circulation. 2018;137(15):1595-610.

111.   Yang Q, Berkman AM, Ezekian JE, Rosamilia M, Rosenfeld JA, Liu P, et al. Determining the Likelihood of Disease Pathogenicity Among Incidentally Identified Genetic Variants in Rare Dilated Cardiomyopathy-Associated Genes. Journal of the American Heart Association. 2022;11(19):e025257.

112.   Brun F, Gigli M, Graw SL, Judge DP, Merlo M, Murray B, et al. FLNC truncations cause arrhythmogenic right ventricular cardiomyopathy. Journal of Medical Genetics. 2020.

113.   Akhtar MM, Lorenzini M, Pavlou M, Ochoa JP, O'Mahony C, Restrepo-Cordoba MA, et al. Association of Left Ventricular Systolic Dysfunction Among Carriers of Truncating Variants in Filamin C With Frequent Ventricular Arrhythmia and End-stage Heart Failure. JAMA cardiology. 2021.

114.   Carruth ED, Qureshi M, Alsaid A, Kelly MA, Calkins H, Murray B, et al. Loss-of-Function FLNC Variants Are Associated With Arrhythmogenic Cardiomyopathy Phenotypes When Identified Through Exome Sequencing of a General Clinical Population. Circulation: Genomic and Precision Medicine. 2022;15(4):e003645.

115.   Hall CL, Akhtar MM, Sabater-Molina M, Futema M, Asimaki A, Protonotarios A, et al. Filamin C variants are associated with a distinctive clinical and immunohistochemical arrhythmogenic cardiomyopathy phenotype. International Journal of Cardiology. 2019.

116.   Hall CL, Gurha P, Sabater-Molina M, Asimaki A, Futema M, Lovering RC, et al. RNA sequencing-based transcriptome profiling of cardiac tissue implicates novel putative disease mechanisms in FLNC-associated arrhythmogenic cardiomyopathy. International Journal of Cardiology. 2019.

117.   Murray B, James CA. Genotype–phenotype Correlates in Arrhythmogenic Cardiomyopathies. Current Cardiology Reports. 2022:1-9.

118.   Fürst DO, Goldfarb LG, Kley RA, Vorgerd M, Olivé M, van der Ven PFJAn. Filamin C-related myopathies: pathology and mechanisms. 2013;125(1):33-46.

119.   Vorgerd M, Van der Ven PF, Bruchertseifer V, Löwe T, Kley RA, Schröder R, et al. A mutation in the dimerization domain of filamin c causes a novel type of autosomal dominant myofibrillar myopathy. 2005;77(2):297-304.

120.   Kley RA, Hellenbroich Y, Van der Ven PF, Fürst DO, Huebner A, Bruchertseifer V, et al. Clinical and morphological phenotype of the filamin myopathy: a study of 31 German patients. 2007;130(12):3250-64.

121.   Fujita M, Mitsuhashi H, Isogai S, Nakata T, Kawakami A, Nonaka I, et al. Filamin C plays an essential role in the maintenance of the structural integrity of cardiac and skeletal muscles, revealed by the medaka mutant zacro. 2012;361(1):79-89.

122.   Chen SN, Lam CK, Wan Y-W, Gao S, Malak OA, Zhao SR, et al. Activation of PDGFRA signaling contributes to filamin C–related arrhythmogenic cardiomyopathy. Science advances. 2022;8(8):eabk0052.

123.   Agarwal R, Paulo JA, Toepfer CN, Ewoldt JK, Sundaram S, Chopra A, et al. Filamin c cardiomyopathy variants cause protein and lysosome accumulation. Circulation Research. 2021;129(7):751-66.

124. Gabbin B. Modeling of a novel filamin-C mutation in restrictive cardiomyopathy using hiPSC-derived cardiomyocytes. University of Applied Sciences Technikum Wien, Vienna. 2020.

125. Tucker NR, McLellan MA, Hu D, Ye J, Parsons VA, Mills RW, et al. Novel mutation in FLNC (filamin C) causes familial restrictive cardiomyopathy. 2017;10(6):e001780.

126. Powers JD, Kirkland NJ, Liu C, Razu SS, Fang X, Engler AJ, et al. Subcellular Remodeling in Filamin C Deficient Mouse Hearts Impairs Myocyte Tension Development during Progression of Dilated Cardiomyopathy. International journal of molecular sciences. 2022;23(2):871.

127. Knyazeva A, Khudiakov A, Vaz R, Muravyev A, Sukhareva K, Sejersen T, et al. FLNC Expression Level Influences the Activity of TEAD-YAP/TAZ Signaling. Genes. 2020;11(11):1343.

128. Zhou Y, Chen Ze, Zhang L, Zhu M, Tan C, Zhou X, et al. Loss of Filamin C Is Catastrophic for Heart Function. Circulation. 2020;141(10):869-71.

129. Chevessier F, Schuld J, Orfanos Z, Plank A-C, Wolf L, Maerkens A, et al. Myofibrillar instability exacerbated by acute exercise in filaminopathy. 2015;24(25):7207-20.

130. Dalkilic I, Schienda J, Thompson T, Kunkel LJM, biology c. Loss of FilaminC (FLNc) results in severe defects in myogenesis and myotube structure. 2006;26(17):6522-34.

131. Ruparelia AA, Zhao M, Currie PD, Bryson-Richardson RJJHmg. Characterization and investigation of zebrafish models of filamin-related myofibrillar myopathy. 2012;21(18):4073-83.

132. Neethling A, Mouton J, Loos B, Corfield V, de Villiers C, Kinnear C. Filamin C: a novel component of the KCNE2 interactome during hypoxia. Cardiovasc J Afr. 2016;27(1):4-11.

133. Maiweilidan Y, Klauza I, Kordeli EJEcr. Novel interactions of ankyrins-G at the costameres: the muscle-specific Obscurin/Titin-Binding-related Domain (OTBD) binds plectin and filamin C. 2011;317(6):724-36.

134. Ader F, Russi M, Tixier-Cardoso L, Jullian E, Martin E, Richard P, et al. Drosophila CRISPR/Cas9 mutants as tools to analyse cardiac filamin function and pathogenicity of human FLNC variants. Biology Open. 2022;11(9):bio059376.

135. Miller DC, Harmer SC, Poliandri A, Nobles M, Edwards EC, Ware JS, et al. Ajmaline blocks INa and IKr without eliciting differences between Brugada syndrome patient and control human pluripotent stem cell-derived cardiac clusters. 2017;25:233-44.

136.   Horani A, Nath A, Wasserman MG, Huang T, Brody SL. Rho-associated protein kinase inhibition enhances airway epithelial Basal-cell proliferation and lentivirus transduction. American journal of respiratory cell and molecular biology. 2013;49(3):341-7.

137.   Martin-Ibanez R, Unger C, Strömberg A, Baker D, Canals J, Hovatta O. Novel cryopreservation method for dissociated human embryonic stem cells in the presence of a ROCK inhibitor. Human reproduction. 2008;23(12):2744-54.

138.   Freshney RI. Culture of animal cells: a manual of basic technique and specialized applications: John Wiley & Sons; 2015.

139.   Feaster TK, Cadar AG, Wang L, Williams CH, Chun YW, Hempel JE, et al. Matrigel mattress: a method for the generation of single contracting human-induced pluripotent stem cell–derived cardiomyocytes. Circulation research. 2015;117(12):995-1000.

140.   Prajapati C, Ojala M, Lappi H, Aalto-Setälä K, Pekkanen-Mattila M. Electrophysiological evaluation of human induced pluripotent stem cell-derived cardiomyocytes obtained by different methods. Stem Cell Research. 2021;51:102176.

141.   Lam MT, Longaker MT. Comparison of several attachment methods for human iPS, embryonic and adipose-derived stem cells for tissue engineering. Journal of tissue engineering and regenerative medicine. 2012;6(S3):s80-s6.

142.   Batalov I, Feinberg AWJBi. Differentiation of cardiomyocytes from human pluripotent stem cells using monolayer culture: supplementary issue: stem cell biology. 2015;10:BMI. S20050.

143.   Kawamura M, Miyagawa S, Miki K, Saito A, Fukushima S, Higuchi T, et al. Feasibility, safety, and therapeutic efficacy of human induced pluripotent stem cell-derived cardiomyocyte sheets in a porcine ischemic cardiomyopathy model. 2012;126(11_suppl_1):S29-S37.

144.   Laflamme MA, Chen KY, Naumova AV, Muskheli V, Fugate JA, Dupras SK, et al. Cardiomyocytes derived from human embryonic stem cells in pro-survival factors enhance function of infarcted rat hearts. 2007;25(9):1015.

145.   Burridge PW, Matsa E, Shukla P, Lin ZC, Churko JM, Ebert AD, et al. Chemically defined generation of human cardiomyocytes. 2014;11(8):855.

146.   Lian X, Zhang J, Azarin SM, Zhu K, Hazeltine LB, Bao X, et al. Directed cardiomyocyte differentiation from human pluripotent stem cells by modulating Wnt/β-catenin signaling under fully defined conditions. 2013;8(1):162.

147. Minami I, Yamada K, Otsuji TG, Yamamoto T, Shen Y, Otsuka S, et al. A small molecule that promotes cardiac differentiation of human pluripotent stem cells under defined, cytokine-and xeno-free conditions. 2012;2(5):1448-60.

148. Wang H, Hao J, Hong CCJAcb. Cardiac induction of embryonic stem cells by a small molecule inhibitor of Wnt/β-catenin signaling. 2010;6(2):192-7.

149. Burridge PW, Thompson S, Millrod MA, Weinberg S, Yuan X, Peters A, et al. A universal system for highly efficient cardiac differentiation of human induced pluripotent stem cells that eliminates interline variability. PloS one. 2011;6(4).

150. Paige SL, Osugi T, Afanasiev OK, Pabon L, Reinecke H, Murry CEJPo. Endogenous Wnt/β-catenin signaling is required for cardiac differentiation in human embryonic stem cells. 2010;5(6):e11134.

151. Tohyama S, Hattori F, Sano M, Hishiki T, Nagahata Y, Matsuura T, et al. Distinct metabolic flow enables large-scale purification of mouse and human pluripotent stem cell-derived cardiomyocytes. 2013;12(1):127-37.

152. Breckwoldt K, Letuffe-Brenière D, Mannhardt I, Schulze T, Ulmer B, Werner T, et al. Differentiation of cardiomyocytes and generation of human engineered heart tissue. 2017;12(6):1177.

153. Parikh SS, Blackwell DJ, Gomez-Hurtado N, Frisk M, Wang L, Kim K, et al. Thyroid and Glucocorticoid Hormones Promote Functional T-Tubule Development in Human-Induced Pluripotent Stem Cell-Derived Cardiomyocytes. Circ Res. 2017;121(12):1323-30.

154. Wardyn JD, Jeyasekharan ADJe. Immunofluorescence. 2001:1-9.

155. Im K, Mareninov S, Diaz M, Yong WH. An introduction to performing immunofluorescence staining. Biobanking. 2019:299-311.

156. Becheva ZR, Gabrovska KI, Godjevargova TIJCP. Comparison between direct and indirect immunofluorescence method for determination of somatic cell count. 2018;72(8):1861-7.

157. George SA, Efimov IR. Optocardiography: a review of its past, present, and future. Current opinion in biomedical engineering. 2019;9:74-80.

158. Sanderson MJ, Smith I, Parker I, Bootman MD. Fluorescence microscopy. Cold Spring Harbor Protocols. 2014;2014(10):pdb. top071795.

159. Shihan MH, Novo SG, Le Marchand SJ, Wang Y, Duncan MK. A simple method for quantitating confocal fluorescent images. Biochemistry and Biophysics Reports. 2021;25:100916.

160. Shum K, Rossi J. SiRNA delivery methods. Methods in Molecular Biology: Springer. 2016.

161.	Ditzel HJ, Tuttolomondo M, Kauppinen S. Design and delivery of SiRNA therapeutics: Humana Press; 2021.

162.	Birmingham A, Anderson E, Sullivan K, Reynolds A, Boese Q, Leake D, et al. A protocol for designing siRNAs with high functionality and specificity. Nature protocols. 2007;2(9):2068-78.

163.	Lu M, Zhang M, Hu B, Huang Y. siRNA Design and GalNAc-Empowered Hepatic Targeted Delivery. Design and Delivery of SiRNA Therapeutics: Springer; 2021. p. 77-100.

164.	Cartwright J. Functional Studies of Genetic Variants in TRPM7 and AKAP9–Two Candidate Genes for Stillbirth: Queen Mary University of London; 2018.

165.	Mahmood T, Yang P-C. Western blot: technique, theory, and trouble shooting. North American journal of medical sciences. 2012;4(9):429.

166.	Sala L, Ward-van Oostwaard D, Tertoolen LG, Mummery CL, Bellin M. Electrophysiological analysis of human pluripotent stem cell-derived cardiomyocytes (hPSC-CMs) using multi-electrode arrays (MEAs). JoVE (Journal of Visualized Experiments). 2017(123):e55587.

167.	Gilchrist KH, Lewis GF, Gay EA, Sellgren KL, Grego S. High-throughput cardiac safety evaluation and multi-parameter arrhythmia profiling of cardiomyocytes using microelectrode arrays. Toxicology and applied pharmacology. 2015;288(2):249-57.

168.	Kussauer S, David R, Lemcke H. hiPSCs derived cardiac cells for drug and toxicity screening and disease modeling: what micro-electrode-array analyses can tell us. Cells. 2019;8(11):1331.

169.	Alayoubi S. Load-dependent electrophysiological and structural cardiac remodelling studied in ultrathin myocardial slices. 2016.

170.	Liu W, Han JL, Tomek J, Bub G, Entcheva E. Simultaneous widefield voltage and interferometric dye-free optical mapping quantifies electromechanical waves in human iPSC-cardiomyocytes. bioRxiv. 2022.

171.	Swift LM, Kay MW, Ripplinger CM, Posnack NG. Stop the beat to see the rhythm: excitation-contraction uncoupling in cardiac research. American Physiological Society Rockville, MD; 2021. p. H1005-H13.

172.	Hamad S, Derichsweiler D, Papadopoulos S, Nguemo F, Šarić T, Sachinidis A, et al. Generation of human induced pluripotent stem cell-derived cardiomyocytes in 2D monolayer and scalable 3D suspension bioreactor cultures with reduced batch-to-batch variations. Theranostics. 2019;9(24):7222.

173.	Du DT, Hellen N, Kane C, Terracciano CM. Action potential morphology of human induced pluripotent stem cell-derived cardiomyocytes

does not predict cardiac chamber specificity and is dependent on cell density. Biophysical journal. 2015;108(1):1-4.

174.   Li W, Luo X, Ulbricht Y, Guan K. Blebbistatin protects iPSC-CMs from hypercontraction and facilitates automated patch-clamp based electrophysiological study. Stem Cell Research. 2021;56:102565.

175.   Jaimes R, McCullough D, Siegel B, Swift L, Hiebert J, McInerney D, et al. Lights, camera, path splitter: a new approach for truly simultaneous dual optical mapping of the heart with a single camera. BMC biomedical engineering. 2019;1(1):1-15.

176.   Hortigon-Vinagre MP, Zamora V, Burton FL, Smith GL. The Use of Voltage Sensitive Dye di-4-ANEPPS and Video-Based Contractility Measurements to Assess Drug Effects on Excitation–Contraction Coupling in Human-Induced Pluripotent Stem Cell–Derived Cardiomyocytes. Journal of Cardiovascular Pharmacology. 2021;77(3):280-90.

177.   Markandeya YS, Kamp TJ. Rational strategy to stop arrhythmias: Early afterdepolarizations and L-type Ca2+ current. Journal of General Physiology. 2015;145(6):475-9.

178.   Kane C, Couch L, Terracciano C. Excitation–contraction coupling of human induced pluripotent stem cell-derived cardiomyocytes. Frontiers in cell and developmental biology. 2015;3:59.

179.   Go A, Srivastava S, Collis L, Coetzee WA, Artman M. Negative inotropic effect of nifedipine in the immature rabbit heart is due to shortening of the action potential. Pediatric research. 2005;57(3):399-403.

180.   Conforti L. Patch-clamp techniques. Cell Physiology Source Book: Elsevier; 2012. p. 369-81.

181.   Hodgkin AL, Huxley AF. A quantitative description of membrane current and its application to conduction and excitation in nerve. The Journal of physiology. 1952;117(4):500.

182.   Neher E, Sakmann B. Single-channel currents recorded from membrane of denervated frog muscle fibres. Nature. 1976;260(5554):799-802.

183.   Sakmann B, Neher E. Patch clamp techniques for studying ionic channels in excitable membranes. Annual review of physiology. 1984;46(1):455-72.

184.   Dallas M, Bell D. Patch clamp electrophysiology: Springer; 2021.

185.   Molleman A. Patch clamping: an introductory guide to patch clamp electrophysiology: John Wiley & Sons; 2003.

186.   Sala L, Yu Z, Ward-van Oostwaard D, van Veldhoven JP, Moretti A, Laugwitz KL, et al. A new hERG allosteric modulator rescues genetic and

drug-induced long-QT syndrome phenotypes in cardiomyocytes from isogenic pairs of patient induced pluripotent stem cells. EMBO molecular medicine. 2016;8(9):1065-81.

187.   Hallas T, Eisen B, Shemer Y, Ben Jehuda R, Mekies LN, Naor S, et al. Investigating the cardiac pathology of SCO2-mediated hypertrophic cardiomyopathy using patients induced pluripotent stem cell–derived cardiomyocytes. Journal of cellular and molecular medicine. 2018;22(2):913-25.

188.   Ether ND, Jantre SR, Sharma DB, Leishman DJ, Bailie MB, Lauver DA. Improving corrected QT; why individual correction is not enough. Journal of Pharmacological and Toxicological Methods. 2022;113:107126.

189.   Muellenbroich C, Kelly A, Acker C, Bub G, Breugmann T, Di Bona A, et al. Novel optics-based approaches for cardiac electrophysiology: a review. Frontiers in physiology. 2021:1971.

190.   Yan P, Acker CD, Loew LM. Tethered bichromophoric fluorophore quencher voltage sensitive dyes. ACS sensors. 2018;3(12):2621-8.

191.   Ahola A, Pölönen R-P, Aalto-Setälä K, Hyttinen J. Simultaneous measurement of contraction and calcium transients in stem cell derived cardiomyocytes. Annals of biomedical engineering. 2018;46(1):148-58.

192.   Hortigon-Vinagre M, Zamora V, Burton F, Green J, Gintant G, Smith G. The use of ratiometric fluorescence measurements of the voltage sensitive dye Di-4-ANEPPS to examine action potential characteristics and drug effects on human induced pluripotent stem cell-derived cardiomyocytes. Toxicological Sciences. 2016;154(2):320-31.

193.   Acker CD, Yan P, Loew LM. Recent progress in optical voltage-sensor technology and applications to cardiac research: from single cells to whole hearts. Progress in biophysics and molecular biology. 2020;154:3-10.

194.   Batchel A. A novel Approach to Dual Excitation Ratiometric Optical Mapping of Cardiac Action Potentials with Di-4-ANEPPS Using Pulsed Excitation. IEEE Transactions on Biomedical Engineering. 2011;58:2120-6.

195.   Cox G. Biological confocal microscopy. Materials Today. 2002;5(3):34-41.

196.   Wójcik-Piotrowicz K, Kaszuba-Zwoińska J, Rokita E, Thor P. Cell viability modulation through changes of Ca2+-dependent signalling pathways. Progress in biophysics and molecular biology. 2016;121(1):45-53.

197.   Harris BJ. Calcium imaging in C2C12 muscle myocytes to examine the impact of calmodulin mutations on cell signaling 2020.

198.   Splawski I, Shen J, Timothy KW, Lehmann MH, Priori S, Robinson JL, et al. Spectrum of mutations in long-QT syndrome genes: KVLQT1, HERG, SCN5A, KCNE1, and KCNE2. Circulation. 2000;102(10):1178-85.

199.   Kemp JM, Whittaker DG, Venkateshappa R, Pang Z, Johal R, Sergeev V, et al. Electrophysiological characterization of the hERG R56Q LQTS variant and targeted rescue by the activator RPR260243. Journal of General Physiology. 2021;153(10):e202112923.

200.   Smetana P, Batchvarov VN, Hnatkova K, Camm AJ, Malik M. Ventricular gradient and nondipolar repolarization components increase at higher heart rate. American Journal of Physiology-Heart and Circulatory Physiology. 2004;286(1):H131-H6.

201.   Rhett JM, Ongstad EL, Jourdan J, Gourdie RG. Cx43 associates with Nav1. 5 in the cardiomyocyte perinexus. The Journal of membrane biology. 2012;245(7):411-22.

202.   Workman A, Marshall G, Rankin A, Smith G, Dempster J. Transient outward K+ current reduction prolongs action potentials and promotes afterdepolarisations: a dynamic-clamp study in human and rabbit cardiac atrial myocytes. The Journal of physiology. 2012;590(17):4289-305.

203.   Tse G. Mechanisms of cardiac arrhythmias. Journal of arrhythmia. 2016;32(2):75-81.

204.   Pfeiffer-Kaushik ER, Smith GL, Cai B, Dempsey GT, Hortigon-Vinagre MP, Zamora V, et al. Electrophysiological characterization of drug response in hSC-derived cardiomyocytes using voltage-sensitive optical platforms. Journal of pharmacological and toxicological methods. 2019;99:106612.

205.   Paci M, Penttinen K, Pekkanen-Mattila M, Koivumäki JT. Arrhythmia mechanisms in human induced pluripotent stem cell–derived cardiomyocytes. Journal of Cardiovascular Pharmacology. 2021;77(3):300-16.

206.   Odening KE, Gomez A-M, Dobrev D, Fabritz L, Heinzel FR, Mangoni ME, et al. ESC working group on cardiac cellular electrophysiology position paper: relevance, opportunities, and limitations of experimental models for cardiac electrophysiology research. EP Europace. 2021;23(11):1795-814.

207.   Rajamohan D, Matsa E, Kalra S, Crutchley J, Patel A, George V, et al. Current status of drug screening and disease modelling in human pluripotent stem cells. Bioessays. 2013;35(3):281-98.

208.   Mathur A, Loskill P, Shao K, Huebsch N, Hong S, Marcus SG, et al. Human iPSC-based cardiac microphysiological system for drug screening applications. Scientific reports. 2015;5(1):8883.

209.   Rowe RG, Daley GQ. Induced pluripotent stem cells in disease modelling and drug discovery. Nature Reviews Genetics. 2019;20(7):377-88.

210.   Parikh SS, Blackwell DJ, Gomez-Hurtado N, Frisk M, Wang L, Kim K, et al. Thyroid and glucocorticoid hormones promote functional T-tubule development in human-induced pluripotent stem cell–derived cardiomyocytes. Circulation research. 2017;121(12):1323-30.

211.   Bell DC, Dallas ML. Using automated patch clamp electrophysiology platforms in pain-related ion channel research: insights from industry and academia. British journal of pharmacology. 2018;175(12):2312-21.

212.   Garg P, Garg V, Shrestha R, Sanguinetti MC, Kamp TJ, Wu JC. Human induced pluripotent stem cell–derived cardiomyocytes as models for cardiac channelopathies: a primer for non-electrophysiologists. Circulation research. 2018;123(2):224-43.

213.   Laurila E, Ahola A, Hyttinen J, Aalto-Setälä K. Methods for in vitro functional analysis of iPSC derived cardiomyocytes—Special focus on analyzing the mechanical beating behavior. Biochimica et Biophysica Acta (BBA)-Molecular Cell Research. 2016;1863(7):1864-72.

214.   Casini S, Verkerk AO, Remme CA. Human iPSC-derived cardiomyocytes for investigation of disease mechanisms and therapeutic strategies in inherited arrhythmia syndromes: strengths and limitations. Cardiovascular drugs and therapy. 2017;31(3):325-44.

215.   Kilpinen H, Goncalves A, Leha A, Afzal V, Alasoo K, Ashford S, et al. Common genetic variation drives molecular heterogeneity in human iPSCs. Nature. 2017;546(7658):370-5.

216.   Wrighton KH. The different flavours of iPS cells. Nature Reviews Genetics. 2017;18(7):394-.

217.   Doss MX, Sachinidis A. Current challenges of iPSC-based disease modeling and therapeutic implications. Cells. 2019;8(5):403.